Impact of BET bromodomain inhibition on *KRAS*-mutated non-small cell lung cancer

Dissertation

zur Erlangung des akademischen Grades

Doctor rerum naturalium

(Dr. rer. nat.)

eingereicht an der

Lebenswissenschaftlichen Fakultät der Humboldt-Universität zu Berlin

von

M.sc Olaf Klingbeil

Präsidentin der Humboldt-Universität zu Berlin

Prof. Dr.-Ing. Dr. Sabine Kunst

Dekan der Lebenswissenschaftlichen Fakultät der Humboldt-Universität zu Berlin

Prof. Dr. Bernhard Grimm

Gutachter/in:

1. Prof. Dr. Ann Ehrenhofer-Murray

2. Dr. habil Bernard Haendler

3. Prof. Dr. Matthias Ocker

Datum der mündlichen Prüfung: 16.12.2016

Acknowledgements

First I would like to thank Dr. Pascale Lejeune for the opportunity to complete my PhD thesis in her group and introducing me to the exciting field of pre-clinical cancer research and drug finding. Also I am very grateful to Dr. habil. Bernard Haendler for numerous fruitful discussions and advice. The support of my mentors was essential all along the three years of my PhD work.

I would like to thank Prof. Dr. Ann Ehrenhofer-Murray from the Humboldt-Universität Berlin, Prof. Dr. Matthias Ocker and Dr. habil. Haendler from Bayer Pharma Berlin for evaluating this work. Also I would like to thank the other members of the "Promotionskommission" Prof. Dr. Ana Pombo (Vorsitzende) and Prof. Dr. Leonie Ringrose from the Humboldt-Universität Berlin for finding the time to participate to my thesis committee.

I am very thankful to Martina Runge for her excellent technical support in the NGS-library preparation and microarray preparation, and to Dr. Ralf Lesche, who provided me with the sequencing and microarray data.

Finally, I would like to thank the members of the Oncology Departments at Bayer Pharma in Berlin, for their support, assistance, work spirit, supportive discussions and inspiration.

Table of content

Table of content

1. Introduction

1.1 Chromatin organization and epigenetics

1.1.1 DNA and chromatin structure

In the mid-twentieth century deoxyribonucleic acid (DNA) was identified to be the source of all genetic instructions. Together with Watson and Crick's concept of the DNA double helix structure (Watson and Crick, 1953), this revolutionized and reshaped the science of biology and gave birth to the new area of Molecular Biology. This understanding also opened up a whole new level of complex questions such as how cells bearing the same genetic build-up can differentiate into very distinctive and functionally varied cell types as found in all pluricellular living organisms.

1.1.2 Information flow in the cell

The central dogma of molecular biology originates from Crick (Crick, 1970; Crick, 1958) who stated that the transfer of information flows from DNA sequence to messenger ribonucleic acid sequence (mRNA) to amino acids sequence. This one way direction of information flow occurs in most living cells, with the exception of some viruses, where both directions are possible. The information is maintained by duplication of the genomic DNA (gDNA) during cell division by a process called replication.

1.1.3 The nucleosome

The human genome consists of long linear DNA pieces called chromosomes, stabilized by telomeres at their ends. Altogether the human genome consist of about 3 billion nucleotides (Pollard et al., 2008). Chromosomes consist of two so-called "sister" chromatids that are joined at the centromere, a protein junction complex. Diploid human cells have 23 pairs of chromosomes, 22 pairs of autosomes and one pair of allosomes, which adds up to 46 chromosomes. The DNA of a human cell is about 2 m long. To fit into the cell nucleus it has to be tightly packed by being wrapped around octamer basic protein complexes called histones (H2A, H2B, H3 and H4) to form disk-shaped nucleosomes. There are 147 DNA base pairs wrapped around one octamer (Khorasanizadeh, 2004; Kouzarides, 2007). The amino terminal ends of the histones (N-terminal tails) of about 30 amino acids and possess important

regulatory functions. In addition, one molecule of histone 1 (H1) binds at the entry and exit of the DNA at the nucleosome (Figure 1). The nucleosome structure strongly influences whether DNA can be accessed by the replication or transcription machinery.
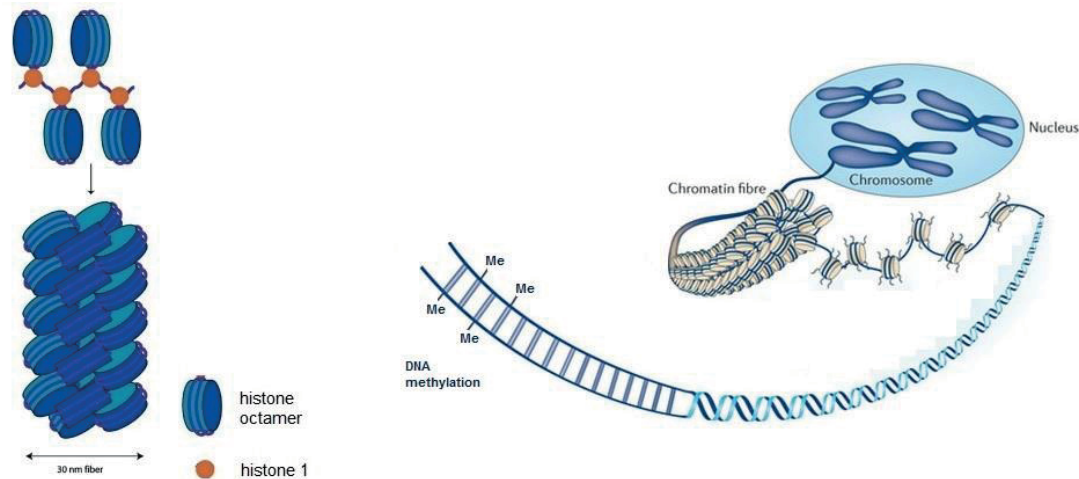
Figure 1: Schematic representation of nucleosome packing: The histone octamer is shown in blue and histone 1 shown in orange. Illustration of chromatin packaging: from an "open" to a condensed structure. Left panel adapted from (Khorasanizadeh, 2004) and right panel adapted from (Arrowsmith et al., 2012).

1.1.4 Heterochromatin and euchromatin

Genomic DNA interacts with histone proteins to form large macromolecule complexes collectively called chromatin. The local state of chromatin is described as either heterochromatin, which is predominantly methylated and has low levels of acetylation at the histones. In this state chromatin is more compact and expression of genes is reduced. The euchromatin state on the other side, which represents the vast majority of the genome, can have highly acetylated and actively transcribed regions as well as inactive regions with low levels of acetylation, methylation and phosphorylation (Jenuwein and Allis, 2001).

1.1.5 Epigenetic gene regulation and the histone code

While bacteria regulate gene transcription at regions upstream of the transcription start site the promoter site using cis-regulatory elements, eukaryotes possess an additional level of gene transcriptional regulation called the "histone code" (Strahl and Allis, 2000). Although this term is widely used, there is not a strict code of underlying histone modification that defines DNA function. Nevertheless the concept of a "histone code" underlines the importance of epigenetic processes such as histone post-translational modifications (PTMs) that can be

written or erased by specialized enzymes and read by dedicated domains, which ultimately influences all DNA-centered processes. The PTMs of histone tails possess important functions such as regulation of chromatin environmental state and of replication, gene transcription and DNA repair. Histone PTMs include acetylation (Allfrey et al., 1964; Parthun, 2007; Sterner and Berger, 2000) and methylation (Shilatifard, 2006; Zhang and Reinberg, 2001) but also ubiquitinylation (Shilatifard, 2006), phosphorylation (Nowak and Corces, 2004) and poly-adenosine diphosphate-ribosylation (Khorasanizadeh, 2004). Several other histone PTMs have additionally been described. It is now widely accepted that epigenetic regulation by reader, writer and eraser enzymes is of high functional importance for cell fate and function (Figure 2).
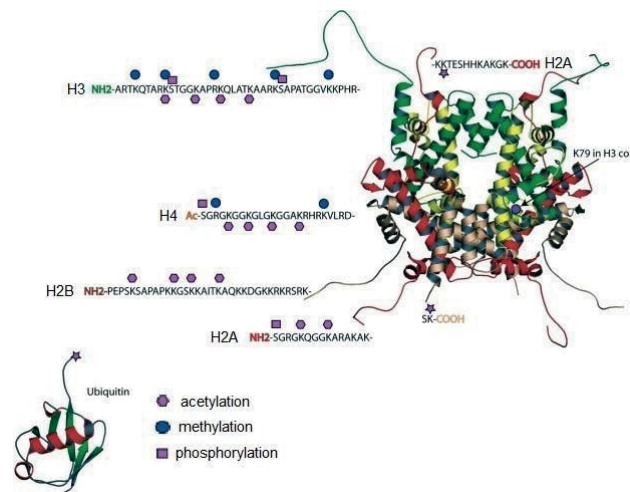
Figure 2: Histone modifications: Different PTMs at various positions of the histone tails and core are shown and marked. Histone H4 is shown in yellow, H3 in green, H2A in red and H2B in gold. Blue circles indicate methylation sites, purple hexagons acetylation sites, purple squares phosphorylation and purple stars ubiquitinylation sites. Adapted from (Khorasanizadeh, 2004).

1.1.5.1 DNA methylation

Another epigenetic modification is DNA methylation. It was first postulated in 1975 as an inheritable epigenetic mark for gene silencing (Holliday and Pugh, 1975; Riggs, 1975). Methylation of the DNA takes place at the 5' carbon atom of cytosine (5mC) predominantly in the context of cytosine followed by a guanidine residue (CpG). CpG-rich regions of about 1 kilo base pairs (kb) length are found in the majority of transcription start site (TSS) of genes. DNA methyltransferases (e.g. DNMT1, DNMT3A and DNMT3B) have been identified to be responsible for the set-up and maintenance of DNA methylation patterns. DNA demethylation

can be a rather indirect process involving removal of the complete methylated base during cell division or DNA repair mechanisms. Enzymes like the methylcytosine dioxygenases ten-eleven translocation (TET) have been found to drive this process (Rawluszko-Wieczorek et al., 2015).

1.1.5.2 Histone variants

During the synthesis phase (S phase) of the cell cycle, chromatin assembles from canonical histones (H2A, H2B, H3 and H4) (Kamakaka and Biggins, 2005). While there are multiple copies of genes coding for the canonical histones, there are also some histone variants (paralogs) that can influence some properties of the nucleosome, when integrated. Histone variant expression is not restricted to S phase and also plays a major role in cell differentiation (Bosch and Suau, 1995; Pina and Suau, 1987; Winston, 2001). There are a number of H1 (e.g. $H1^0$ and H5) (Parseghian and Hamkalo, 2001; Roche et al., 1985) and H2A (e.g. H2A.Z and H2A.X) (Ausio and Abbott, 2002; Redon et al., 2002) variants, while there are no or very little known variants of H2B and H4. There are two major H3 variants (H3.3 and centromeric H3 (CenH3)). Histone variants also play an important role in the cellular DNA damage response (DDR). For instance H2A.X phosphorylation by DDR kinases takes place at DNA double-strand break (DSB) sites (Rogakou et al., 1998) and functions as a marker leading to DSB repair initiation.

1.1.5.3 Histone acetylation

Histones can be acetylated at the ε-nitrogen of lysine (K) residue by enzymes named type-A and type-B histone acetyltransferases (HATs), which use acetyl coenzyme A (acetyl-CoA) as cofactor. Acetylation of histones takes place at histone tails (e.g. H3K27Ac, H4K5Ac, H4K8Ac, H4K12ac and H4K16ac) as well as at histone core elements under cellular stress like DNA damage. (e.g. H3K56ac) (Tjeertes et al., 2009). Acetylation changes the charge of the ε-nitrogen leading to reduced interaction with the negative phosphate backbone of the DNA (Figure 3).

Introduction
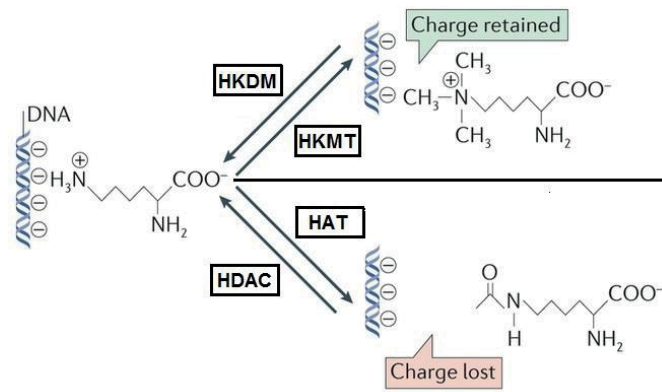
Figure 3: Schematic illustration of lysine DNA interaction: Acetylation of lysine by histone acetyl transferases (HATs) and deacetylation by histone deacetylases (HDACs) can change the charge of the ε-nitrogen of the amino acid residue, leading to changes of the interaction between histone tails and the negatively charged phosphate backbone of DNA. Addition of a methyl group at the ε-nitrogen of lysine by histone lysine methyl transferases on the other hand does not change the charge of lysine. Adapted from (Tessarz and Kouzarides, 2014).

Type-A HATs are a diverse family of enzymes with sequence and conformational structure homology found in the nucleus (Marmorstein, 2001; Sterner and Berger, 2000). Type-B HATs are predominantly located in the cytosol and all share sequence homology (Parthun, 2007). The type-A HATs form 3 families, GNAT, MYST and CBP/p300, and are usually associated with large multi-protein complexes (Yang and Seto, 2007), defining their functional role (Bannister and Kouzarides, 2011). CBP/p300 acetylates H3K27, marking transcriptionally regulatory regions (enhancer). Type-B HATs only acetylate newly synthesized non-nucleosomal histones. The acetylation of histones H3 and H4 is removed during histone maturation and integration into nucleosomes (Parthun, 2007).

The enzymatic counterparts to HATs are the histone deacetylases (HDACs). They are subdivided into four family classes. Class I, II and IV share structural homology and use zinc metal ions to remove the acetyl group from lysine (Hodawadekar and Marmorstein, 2007), while Class III, the sirtuin family, uses nicotinamide adenine dinucleotide (NAD^+) as a cofactor (Frye, 2000; Imai et al., 2000). Histone deacetylation is a rather unselective process and little preference for individual histone lysine residues has been evidenced (22). As removal of acetylation is correlated with more compact DNA and repression of transcription, HDACs are often found in repressive complexes (Bernstein and Schreiber, 2002; Jenuwein and Allis, 2001; Kouzarides, 2007).

Introduction

1.1.5.4 Histone phosphorylation

Phosphorylation of histones can take place at the hydroxyl-residues of serine, threonine or tyrosine, and are dependent on dedicated kinases and phosphatases (Oki et al., 2007). Kinases transfer a phosphate group from adenosine triphosphate (ATP) to the amino acid residue. This changes the charge of the amino acid to a negative state, which influences DNA histone interaction. A few kinases (e.g. ERK2) are known to have DNA binding domains (Hu et al., 2009) by which they can be recruited to the chromatin. Given the high turnover of H3S10P marks by aurora kinase, the phosphatase activity of PP1 phosphatase is probably quite high in the nucleus (Bannister and Kouzarides, 2011). Nevertheless far less is known about histone phosphatases.

1.1.5.5 Histone methylation

Histone methylation predominantly takes place at lysine residues and does not affect the local charge of the histone as opposed to phosphorylation or acetylation (Figure 3). Additionally lysines can get multiple methylation marks from mono- to tri-methylation and arginine can undergo mono- or di-methylation in a symmetric or asymmetric fashion (Bedford and Clarke, 2009), which adds even more complexity to histone methylation (Bannister and Kouzarides, 2011; Lan and Shi, 2009; Ng et al., 2009).

The first histone lysine methyltransferase (HKMT) was found 16 years ago (Rea et al., 2000) and since then many more have been described. Almost all HKMTs identified harbor a catalytic SET domain, which transfers a methyl group from S-adenosylmethionine (SAM) to the ε-nitrogen of lysine. Most of them methylate histone tails, while the DOT1L enzyme lacks a SET domain and methylates H3K79 which is localized in the histone core (van Leeuwen et al., 2002). HKMTs can discriminate between different lysine residues and their methylation states in the cellular context. They are quite specific (Cheng et al., 2005) and can methylate their lysine substrate only to a certain degree (Zhang et al., 2003). HKMTs can exhibit gene repressing functions, one example being the Enhancer of zeste homolog 2 (EZH2) member of the polycomb repressive complex (PRC2), which methylates H3K27 to induce heterochromatin formation and gene suppression. Histone methylation can on the other hand also be associated with gene activation. H3K4 tri methylation (H3K4me3) is a mark of transcriptionally active promoters and H3K4 mono methylation (H3K4me1) additionally marks enhancers. H3K4 is methylated by a complex called COMPASS. There are three

different complexes associated with SET1 consisting of a central SET1-like methyltransferase (SET1A/B, MLL1/2 or MLL3/4) unit surrounded by six to eight other proteins. The COMPASS complex can methylate H3K4 (Cheng et al., 2014), which is a hallmark of transcriptionally active promoters and distal regulatory elements (H3K4me1) (Ernst et al., 2011) resulting from the MLL3/4 complex (repression mark), while H3K4me3 results from MLL1/2 or SET1A/B and is only found near the TSS of active genes (Heintzman et al., 2007). Lysine methylation gets removed by the Lysine-specific demethylase 1 (LSD1) a histone lysine demethylase (HKDM) that was discovered in 2004 (Shi et al., 2004).

LSD1 uses flavin adenine dinucleotide (FAD) as a co-factor to demethylate mono and di methylated lysine (e.g. H3K4me1/2). Like HATs LSD1 functions in large complexes that guide and influences its activity in a context-specific manner. Another class of lysine demethylases was identified later. It is characterized by JmjC-domains (Tsukada et al., 2006) (e.g. jumonji, AT rich interactive domain 2 (JARID2)) and the ability to demethylate tri-methylated lysines (Whetstine et al., 2006).

Besides lysine, arginine residues can also be methylated. Arginine methyltransferases (PRMT) are categorized into two classes: type-I and type-II. Both classes generate mono methylated arginine, but type I generates asymmetric and type II symmetric di methylated arginine (Wolf, 2009). PRMTs transfer the methyl group from SAM to the ω-guanidine group of arginine onto a variety of substrates (Bannister and Kouzarides, 2011), while PRMT 1,4,5 and 6 predominantly methylate histone arginines (Bedford and Clarke, 2009). Methylation of arginine is removed in an indirect way named deamination (Cuthbert et al., 2004; Wang et al., 2004) or directly by the JMJD6 demethylase (Chang et al., 2007; Robinson et al., 2016).

1.2   Histone modification readers

Epigenetic readers are proteins with dedicated domains that specifically recognize epigenetic modifications and enable downstream signaling that influences gene transcription. Such reader domains were initially found in type-A HATs (Dhalluin et al., 1999). Later a large number of different domains capable of recognizing modified histones were identified using techniques based on either fluorescence (Kim et al., 2006), immobilized histones (Stucki et al., 2005) or stable isotype labeling by amino acids in cell culture (SILAC), leading to a comprehensive list of histone-binding proteins (Bartke et al., 2010; Vermeulen et al., 2010).

Introduction

Three major reader domains that can bind to acetylated lysines have been described (Figure 4), namely plant homeodomain (PHD) (Zeng et al., 2010), YEATS (Andrews et al., 2016) and bromo domains (Dhalluin et al., 1999).
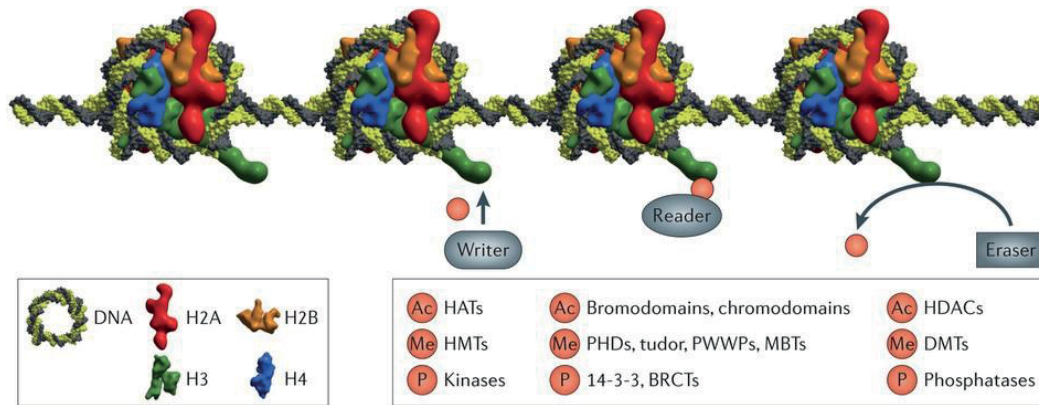
Figure 4: Histone modifications and their readers, writers and erasers: Histone proteins of the nucleosome are shown in red, orange, green and blue (H2A, H2B, H3 and H4) and DNA in yellow/gray. Histone modification reader, writer and eraser proteins of: acetylation (Ac), methylation (Me) and phosphorylation (P) are included. HATs = histone acetyltransferases, HMTs = histone methyltransferases, HDACs= Histone deacetylases, DMTs = demethylases, PHDs = plant homeodomains, PWWPs = Proline-Tryptophane-Tryptophane-Proline domains, MBTs = malignant brain tumor domains, BRCT = carboxy-terminal domain of a breast cancer susceptibility protein. From (Filippakopoulos and Knapp, 2014).

1.2.1 The bromodomain and extra terminal domain family

In the human genome 61 bromodomains (BRDs) present in 46 proteins have been identified. They cluster into eight major classes based on their structural similarity (Figure 5A) (Filippakopoulos and Knapp, 2014). The bromodomain and extra terminal domain (BET) family belongs to the class II. Bromodomains share a conserved left-handed bundle of four alpha helices (αZ, αA, αB, αC) linked by loops of different lengths (ZA and BC) and recognize different acetylated lysines (Figure 5B) (Filippakopoulos et al., 2012).

The BET family includes 4 members: BRDT, BRD2, BRD3 and BRD4 each harboring two bromodomains (BD1 and BD2) and an extra terminal region at the C terminus that interacts with different protein partners (Figure 6). Interestingly, the BD1 or BD2 similarity is higher between the family members than BD1 and BD2 within the same protein (Belkina and Denis, 2012). While BRD2, BRD3 and BRD4 are expressed ubiquitously in human tissues (Loven et al., 2013), BRDT is exclusively found in testis (Gaucher et al., 2012) where it has an important role in spermatogenesis (Berkovits and Wolgemuth, 2013). BRD2, 3 and 4 bind to

Introduction

chromatin genome-wide and are regulators of essential cellular processes including transcription, DNA replication, cell cycle progression and the maintenance of higher-order chromatin structure (Wang et al., 2012).
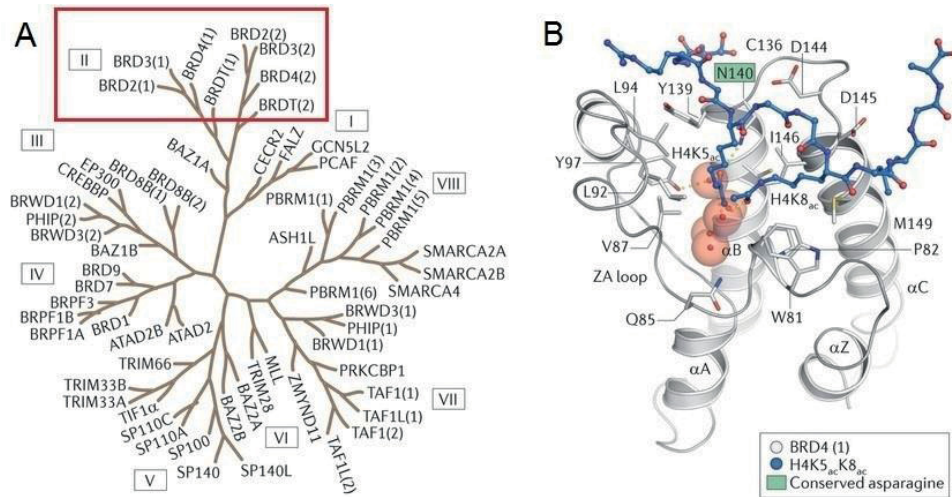
Figure 5: Phylogenetic tree of bromodomain proteins and structural representation of BRD4-BD1 binding to H4K5ac-K8ac peptide. A: Phylogenetic tree showing the eight structurally diverse classes of bromodomains (BDs) and protein names. Red box marks the class II cluster which is found in the bromodomain and extra terminal domain family (BET). Numbers in brackets indicate the BD number within one protein. B: Structural illustration of BRD4 BD1 with its four alpha helices (αZ, αA, αB, αC) linked by loops of different lengths (ZA and BC) in white, and the bound di-acetylated histone 4 peptide (H4K5acK8ac) in blue. The peptide engages the conserved asparagine (N140) which is highlighted in green. Red spheres indicate conserved water molecules forming hydrogen bonds with BD1 (PDB ID: 3UVW). Adapted from (Filippakopoulos and Knapp, 2014).
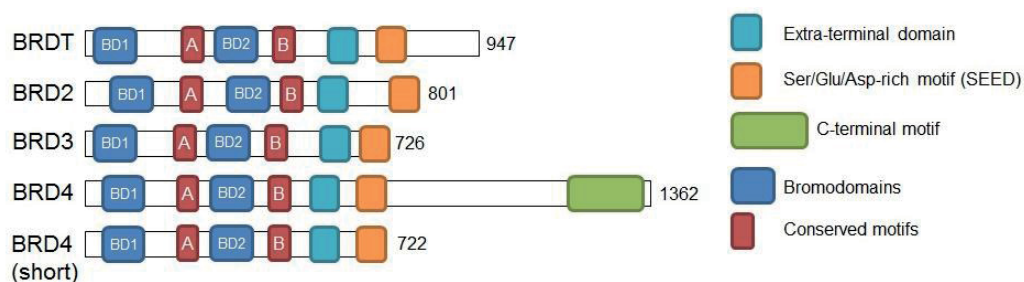
Figure 6: Schematic illustration of bromodomain and extra terminal domain proteins: Boxes delineate the conserved domains of BET family members Bromodomains (BD1/2), motifs A and B, extra terminal domain and SEED motif. For BRD4 the short isoform is additionally shown and for BRD2, 3 and T only the main isoform is shown. Numbers denote the length of each protein.

Introduction

1.2.2   The human cellular BRD4 protein

The bromodomain-containing protein 4 (BRD4) is the best characterized member of the BET family. It was found to bind to a bookmarking histone modification H4K5ac to rapidly re-activate transcription after mitosis (Zhao et al., 2011) and is generally involved in regulating RNA Polymerase II transcriptional activity. Mice knock-out studies show that BRD2 (Gyuris et al., 2009; Shang et al., 2009) and BRD4 (Houzelstein et al., 2002) are each essential for embryonic development. The two bromodomains (BD1 and BD2) which enable BRD4 to bind to acetylated lysines of histones show different preferences. In a SPOT array BD1 shows strong binding to acetylated histone 3 at K4, K9, K27, K36, K115 and K122 and histone 4 at K44, K77, K79 and K91, while BD2 preferentially binds to histone 3 at K18, K36, K37, K56 and histone 4 at K5, K20 and K44 (Filippakopoulos et al., 2012).

It was initially proposed that BRD4 binds to free positive transcription elongation factor-b (P-TEFb) and recruits it to acetylated promoters (Jiang et al., 1998; Wu and Chiang, 2007), while later it was found that BRD4 recruits Mediator protein (Kanno et al., 2014) and transcription factors (Roe et al., 2015) to localize to hyper-acetylated promoter and enhancer regions to initiate transcription of defined downstream genes (Bhagwat et al., 2016). In addition BRD4 was found to interact with JMJD6 a histone arginine demethylase. JMJD6 demethylates repressive dimethyl marks of H4R3 (H4R3me2s) as well as the 5' cap of 7SK snRNA, which leads to destabilization of 7SK snRNA and a release of P-TEFb from the 7SK/HEXIM snRNP inhibitory complex (Figure 7).

Introduction
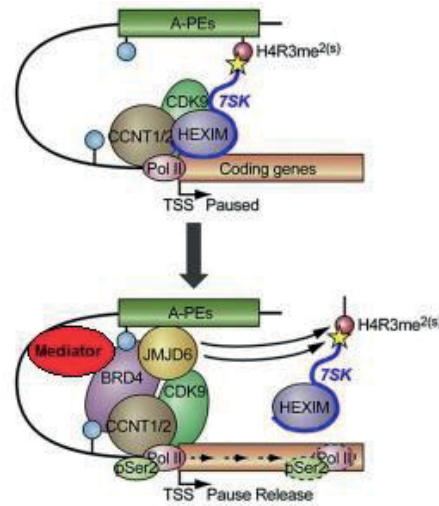
Figure 7: Schematic illustration the BRD4-JMJD6 mediated pause-release model: JMJD6 is recruited to the anti-pause enhancer (A-PE) by BRD4 interacting with histone acetylation, transcription factors or mediator complex. Enzymatic activity of JMJD6 leads to removal of the repressive H4R3me2s mark and decapping of 7SK snRNA, leading to release of P-TEFb (CCNT/1/2 and CDK9) from the inhibitor HEXIM/7SKsnRNA complex and finally to pause-release of polymerase II. Adapted from (Liu et al., 2013).

.

1.2.3 Tissue-specific expression of genes

The mammalian genome codes for around 21.000 genes (Weinberg, 2014), which can be functionally divided into two classes, namely the housekeeping genes and the tissue-specific genes. In a differentiated cell only about 3000-5000 housekeeping genes and 1000 tissue-specific genes are expressed. This implies that the expression of a large number of genes from the genome must be coordinately repressed, while other genes have to be actively expressed at specific time points to guarantee cellular viability and tissue-specific functions (van Nimwegen, 2003).

1.2.4 Transcription factors and gene-regulation in eukaryotes

Transcription factors (TFs) are an essential regulatory unit in the maintenance and state of all living cells (van Nimwegen, 2003). Linage specific TFs are responsible for the earliest event during cellular differentiation (Arner et al., 2015). About 6% of human genes code for TFs, they can be categorized into a few families with similar binding mechanisms. TFs recognize a defined short sequence of around 5-10 nucleotides (sequence motif) in the genome. Such motifs are found in the upstream region of gene promoters and in distal control elements

called enhancer regions. Most TFs interact with co-activators like the mediator complex or co-repressors to regulate the transcription machinery (Pollard et al., 2008).

1.2.5 Gene transcription by RNA polymerase II

Gene transcription in eukaryotic cells is performed by the RNA polymerases. The three RNA polymerases (Roeder and Rutter, 1969, 1970) recognize different promoter regions. RNA polymerase I transcribes rRNA precursors and RNA polymerase III transcribes small non-coding RNAs like transfer RNAs (tRNAs) of typically 76 to 90 nucleotides length, while RNA polymerase II (Pol II) transcribes protein-coding genes to pre-mRNAs. The basal initiation complexes share a conserved core (Vannini and Cramer, 2012) composed of RNA polymerase I/II or III, the TATA box-binding protein (TBP) (Kim and Burley, 1994) and transcription factors TFIIB, TFIIE and TFIIF in the case of RNA polymerase II. Transcription is initiated by recruitment of the RNA polymerase II-TFIIF complex (Chen et al., 2010; Eichner et al., 2010) to the core initiation unit (TFIIB-TBP) bound at the DNA-promoter (Kim et al., 1993a; Kim et al., 1993b) followed by binding of general transcription factors TFIIE and TFIIH to form the pre-initiation complex (PIC) (He et al., 2013). In the presence of nucleoside triphosphates a transcription bubble is produced around the TSS. Conformational changes then lead to positioning of a single strand DNA to the active site of the polymerase serving as a template for the RNA synthesis (Sainsbury et al., 2015).

Transcriptional initiation as well as elongation and termination need to be tightly regulated by the cell. One way to regulate the throughput by Pol II is pausing, which takes place on stimulus-controlled pathway genes and genes involved in development (Jonkers and Lis, 2015). Pol II-pausing can lead to accumulation at the promoter-proximal region around 30-60 nucleotides downstream of the TSS, within the first nucleosome positioned (+1 nucleosome) (Adelman and Lis, 2012; Kulaeva et al., 2013; Kwak and Lis, 2013). This process is dependent on negative elongation factor (NELF) and DRB-sensitivity-induced factor (DSIF). To release Pol II, the P-TEFb complex, which consists of cyclin-dependent kinase 9 (CDK9) and cyclin T1 or cyclin T2 phosphorylates NELF and the carboxy-terminal domain (CTD) at Serine 2 of Pol II and DSIF (Peterlin and Price, 2006). P-TEF-b can associate with eleven-nineteen lysine-rich leukemia (ELL) elongation factors to form the larger super elongation complex (SEC) (Smith et al., 2011). The release of inactive P-TEFb from the inhibitory 7SK/HEXIM snRNP complex is mediated by BRD4, which also interacts with the mediator complex to regulate pre-initiation, initiation and re-initiation in addition to pause-release and

elongation (Figure 7). The CTD undergoes dynamic PTMs (Corden, 2013) that include phosphorylation (Buratowski, 2009) as well as methylation (Dias et al., 2015). The regulation of pause-release seems to be an intricate balance (Jonkers and Lis, 2015) depending on the P-TEFb recruitment, activation and inhibition (Heinz et al., 2015).

Termination of transcription is far less understood. In yeast the transcriptional termination of mRNA coding genes is mainly dependent on cleavage of polyadenylation factor (CPF) and cleavage factor (CF) (CPF-CF) pathway, while the termination of non-coding RNAs depends on the Nrd1-Nab3-Sen1 (NNS) complex.

During the transcription process, pre-mRNAs are modified at their 5' end by addition of a 7-methylguanosine cap and polyadenylation at their 3' end (Bentley, 2014). These modifications are unique for mRNAs and protect them against degradation, thus enhancing translation in the cytoplasmic compartment (Berg et al., 2007; Pollard et al., 2008). The 5' capping of the first nucleotide transcribed necessitates the enzymatic activity of three dedicated proteins, RNA guanylyl triphosphatase (RNGTT), human capping enzyme a guanylyltransferase (hCE) and a RNA methyltransferase (RNMT). The poly(A) tail is added to the 3' of a mRNA after cleaving the precursor mRNA (pre-mRNA) by the cleavage polyadenylation specificity factor (CPSF) (Bienroth et al., 1993) and the polyadenylate polymerase (PAB).

1.3 Methods used to identify genome-wide chromatin interactions

1.3.1 DNase I hypersensitivity sites

Chromatin is packed in nucleosomes which consist of DNA wound around histone octamers. To actively transcribe genes the chromatin has to be in a less compact state. Accordingly, when treating gDNA with a DNA cutting enzyme such as DNase I, the more accessible sites are preferentially cut. Using next generation sequencing (NGS) technologies, DNase I hyper-sensitivity sites (DHSs) can be mapped genome-wide, predicting potential cis-regulatory elements such as TF binding sites. Understanding the role of the non-protein-coding gene regions of the genome is the aim of the ENCODE project (2012; Birney et al., 2007).

Introduction

1.3.2 Chromatin immunoprecipitation

In addition to DHS another powerful tool to examine protein-DNA interactions is the chromatin immunoprecipitation (ChIP) method (Solomon et al., 1988) (Orlando, 2000). Using ChIP together with genome-wide sequencing techniques (ChIP-seq) it is possible to map a target protein of interest to its binding or interaction sites within chromatin. Besides TF binding this also enables to precisely map epigenetic modifications such as histone marks and binding of the mediator complex to identify potential enhancers. Recently this method has been adapted to map the interaction sites of biotin tagged small molecules with chromatin (Chem-seq) (Anders et al., 2014). Nevertheless this assay cannot recapitulate enhancer looping and other conformational properties of the chromatin. For this reason other methods have been developed.

1.3.3 Chromosome conformation capture (3C)

When performing paraformaldehyde-assisted crosslinking, the close proximity interactions such as protein-DNA or DNA-DNA interactions can be preserved. Another method to analyze chromosome conformation is the C- or 3C technology (Hakim and Misteli, 2012). It is used to analyze the conformational organization of chromatin in the cell and has turned into a powerful tool to identify and confirm enhancer-promoter interactions in addition to classical reporter-gene assays.

1.4 Gene editing technologies

Specific experimental manipulation of the genome is crucial to investigate and determine the role of genes in the biological context of disease. Gene editing technologies allow to remove, add or replace specific parts of the genome using nucleases also called "molecular scissors" that introduce specific DNA double strand breaks (DSBs). These include homing meganucleases, zinc finger nucleases (ZFNs), transcription activator-like effector-bases nucleases (TALENs) and the more recently identified and explored clustered regularly interspersed short palindromic repeats (CRISPR)-Cas system. The DSBs at the specific target sites are repaired by one of the host cells recombinational repair mechanisms.

Introduction

1.4.1 DNA DSB repair mechanisms

These mechanisms are either non-homologous end joining (NHEJ), homology directed repair (HDR) or micro-homology mediated end joining (MMEJ). NHEJ repairs a DSB by simply re-ligating the two ends without the need of sequence homology. It is a quite error prone mechanism so that small insertions and deletions are often introduced (Ahnesorg and Jackson, 2007; Moore and Haber, 1996; Pardo et al., 2009). HDR uses a homolog piece of DNA that has to be present in the nucleus to repair a DSB. This repair mechanism is used by the cell during the G2 or S-phase. Similarly to HDR, MMEJ uses a template to repair the DSB.

1.4.2 ZFNs and TALENs

Multiple zinc finger domains (ZFs) that each bind to 3 nucleotides of a target region in the genome fused to the FokI cleavage domain (Kim et al., 1996) can precisely introduce a DSB at the targeted region (Figure 8). ZFNs normally harbor 3-4 ZFs that form an 18-24 nucleotide recognition site that is sufficient to enable unique binding in the genome (Figure 8). Nevertheless ZNFs can have off-target effects that sometimes lead to host cell toxicity (Xiong et al., 2015). Similarly to ZFNs, TALENs can be customized by combining DNA-binding domains that recognize a target sequence. TALENs contain TALE repeats of 33-35 amino acids able to recognize a single base pair via their two hyper variable residues (Figure 8). The custom design of TALENs and ZFNs can be cost- and time-consuming, which limits their use for screening at a larger scale.

Introduction
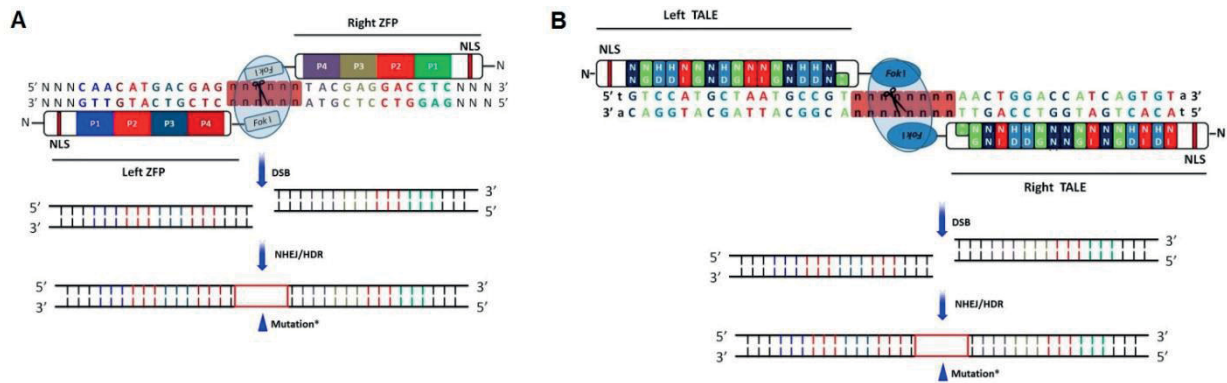
Figure 8: Schematic illustration of ZNF and TALEN structures and target site recognition. A: "ZNF left" and "ZNF right" consist of a nuclear location signal (NLS) at the N-terminus of the protein and 4 individual zinc fingers (P1-P4) that specifically bind to 3 nucleotide target sites and are fused to the FokI cleavage domain. FokI forms a dimer (blue circle) and introduces a DNA double strand break (DSB) that is repaired by the host cell using NHEJ or HDR/MMEJ. B: TALEN consisting of FokI fused to multiple transcription activator-like effectors (TALE) that recognize each a single base pair by their repeat-variable di-residues (RVD) marked in green red or light/dark blue, leading to target specificity target sequence. A and B are adapted from (Xiong et al., 2015).

1.4.3 The CRISPR-Cas system

The CRISPR system is a prokaryotic immune system which protects *Streptococcus thermophilus* and other bacteria from foreign plasmids or bacteriophage virus DNA. It provides an adaptive acquired immunity using exogenous DNA elements to which the bacteria were exposed earlier (Barrangou et al., 2007). The short parts of these elements are integrated into the genome (protospacer) and separated by repetitive elements (direct repeats) close to the *CAS* gene. They are expressed as CRISPR RNAs (crRNAs) that form a stem-loop at the 3' and have a 5' region to target the cas effector complex to interfere with the target sequence. (Marraffini and Sontheimer, 2010). The eukaryotic RNA interference is very different from crRNA interference. It uses distinct protein machineries and recognizes different ribonucleotide species (RNA vs. DNA). As crRNAs can detect DNA (Marraffini and Sontheimer, 2008) self-immunity is prevented as crRNAs discriminate by a 8 nucleotide (nt) repeat sequence at the 5' of the crRNA from outsite the spacer region between target (incomplete binding) and self-DNA (complete binding). The type II CRISPR locus of Streptococcus pyogenes SF370 consists of four genes including the Cas9 nuclease (SpCas9), two crRNAs: one trans-activating crRNA (tracrRNA) and one precursor crRNA (pre-crRNA). These genes have been modified to efficiently work in a mammalian cellular system (Cong et al., 2013). The tracrRNA and crRNA can be fused together to form a single-guide RNA

Introduction

(sgRNA). In contrast to TALENs and ZFNs, the CRISPR-Cas9 system derives its target specificity from a 20 nucleotide long sequence of the sgRNA that directs Cas9 to its target site (Figure 9). The Cas9 nuclease needs a proto-spacer adjacent motif (PAM) region to specifically cut the DNA 3 nucleotides upstream of the PAM (Jinek et al., 2012). The PAM sequence can differ between Cas9 orthologs. This system was used to generate mutant mice in a one-step fashion (Wang et al., 2013) and to perform genome-wide genetic screens (Shalem et al., 2014; Wang et al., 2014). Further advances led to the generation of domain specific mutation screenings that should enable more efficient and faster drug discovery (Shi et al., 2015).
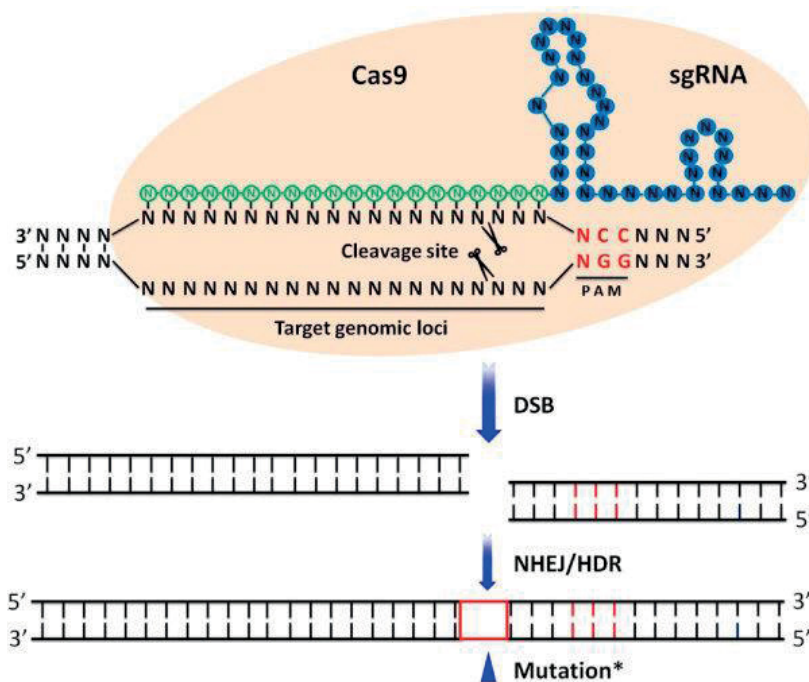
Figure 9: CRISPR-SpCas9 targeting: CRISPR-SpCas9 complex targets genomic locus by Watson-Crick base pairing (green) and cutting at the protospacer adjacent motif PAM region from *Streptococcus pyogenes* (red nucleotides) leading to a double strand break (DSB) that is repaired by cellular repair mechanisms NHEJ or HDR. From (Xiong et al., 2015).

1.5 Cancer epigenetics

Cancer designates diseases originating from uncontrolled cell growth and with the potential to spread to distant parts of the organism.

1.5.1 Hallmarks of cancer

Hanahan and Weinberg introduced the term "Hallmarks of Cancer" to summarize the aberrations that are shared by most cancer types to develop from normal to tumorigenic phenotype (Hanahan and Weinberg, 2000). The hallmarks of cancer originally included six characteristics (sustained proliferative signaling, evading growth suppression, activation of invasion and metastasis, induction of angiogenesis, replicative immortality and resistance to cell death), which were completed by additional features in 2011 (avoiding immune destruction, tumor-promoting inflammation, genome instability and mutations and deregulating cellular energetics) (Hanahan and Weinberg, 2011).

Multiple oncogenic features can be acquired by the cell largely by overexpression or mutation of oncogenes. Some gene functions are needed only during the developmental process of a tumor, while others are needed to maintain the malignant state (tumor drivers). Targeting these tumor driving genes or dependencies is now the rationale for targeted therapy. A number of therapeutics targeting individual hallmarks has been advanced to the clinical stage and many more are in pre-clinical development (Figure 10).

Introduction
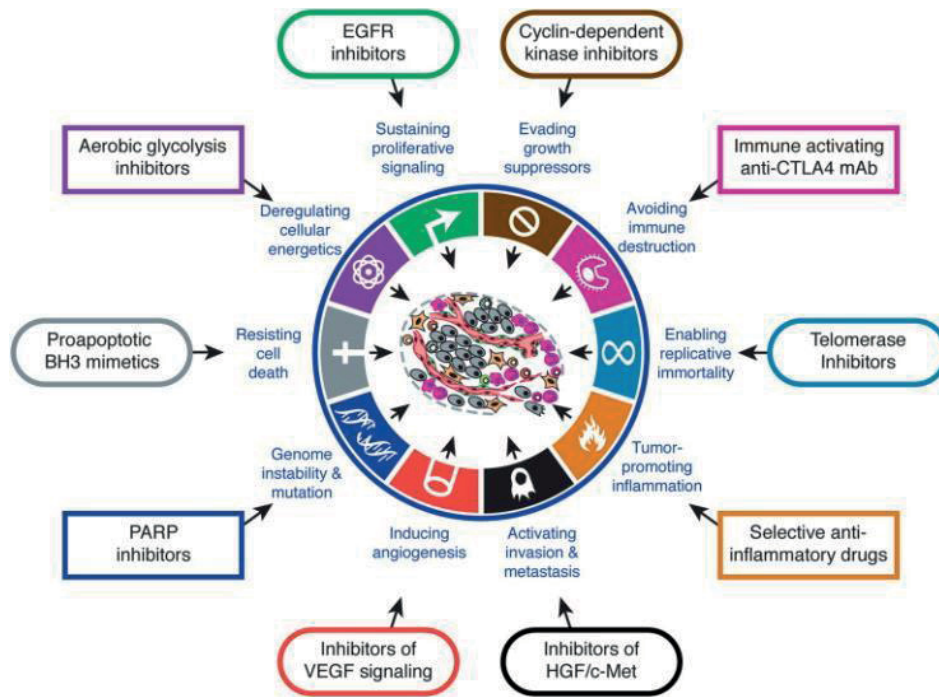
Figure 10: Hallmarks of cancer: A number of agents targeting cancer dependencies have been identified. They include small molecule inhibitors or biomolecules addressing the different hallmarks of cancer: sustaining proliferative signaling, evading growth suppressors, avoiding immune destruction, enabling replicative immortality, tumor-promoting inflammation, activating invasion and metastasis, inducing angiogenesis, genome instability and mutations, resisting cell death and deregulating cellular energetics. Examples are indicated by colored boxes. From (Hanahan and Weinberg, 2011)

1.5.1.1 Resisting cell death

One of the important features of cancer cells is to bypass programmed cell death (apoptosis). During development and tissue maintenance of an organism, apoptosis can be initiated e.g. when cells are damaged or infected by viruses. Cancer cells are able to block the pro-apoptotic signals that can be either extrinsic or intrinsic, by overexpressing anti-apoptotic members of the BCL-2-family or by down-regulation of pro-apoptotic protein members. Extrinsic signals can be mediated by receptor ligand binding and intrinsic signals by e.g. DNA-damage signals. The BCL-2 family can be subdivided into multi domain proteins and BH3-only proteins. The multi domain proteins share four BCL-2 homology domains (BH) 1-4. While Bcl2, BclXL and MCL1 have anti-apoptotic functions BCL-2-antagonist/killer (BAK) and BCL-2-associated X protein BAX act in a pro-apoptotic way.

BAX and BAK are essential to induce outer mitochondrial membrane permeabilization (MOMP). This can be enhanced by BH3-only proteins like BIM and BID that interact with

the binding grove of anti-apoptotic proteins. A number of drugs are currently being developed to inhibit Bcl2 binding to BH3-only proteins. MOMP leads to release of cytochrome C, a trigger of apoptosis. Apoptotic protease activating factor 1 (Apaf-1) binds to cytosolic cytochrome C and forms the apoptosome complex. This complex activates procaspase-9 one of the so-called initiator caspases (Jesenberger and Jentsch, 2002). Caspases are cysteine-aspartic proteases playing a central role in the induction of apoptosis. Initiator caspases-8, -9 and -10 are present in the cytosol in their inactive pro-caspase form and get activated by cleavage of the pro-domain. They then amplify the pro-apoptotic stimulus by activating the downstream effector caspases-3 and-7 (Figure 11A).

In addition the mitochondria-derived activator of caspases (SMAC) is released to inhibit a central negative regulator of apoptosis called the X-linked inhibitor of apoptosis protein (XIAP) which is a member of the inhibitor of apoptosis family (IAP). XIAP binds to active caspases to inhibit their function with its Baculovirus IAP repeat (BIR) domain (Figure 11B). Another negative regulator of caspase activity is the cellular FLICE-like inhibitory protein (c-FLIP) which exhibits high sequence similarity to caspase-8, but lacks the protease domain (Figure 11C). The long isoform of c-FLIP (c-FLIPL) inhibits the activation of pro-caspase-8 by interfering with the dimerization and binding of pro-caspase-8 to FADD (Fas-associated death domain protein) (Hughes et al., 2016). Upon oligomerization of the death receptor after binding of a ligand, FADD binds with its death domains (DD) to the DD of the receptor. Bound FADD recruits pro-caspase-8 by death effector domain (DED) interaction. This triggers self-cleavage of pro-caspase-8 dimers. The active caspases can further initiate the MOMP by BID cleavage or activate downstream caspases like caspase-3 (Kallenberger et al., 2014) (Figure 11A).

Introduction
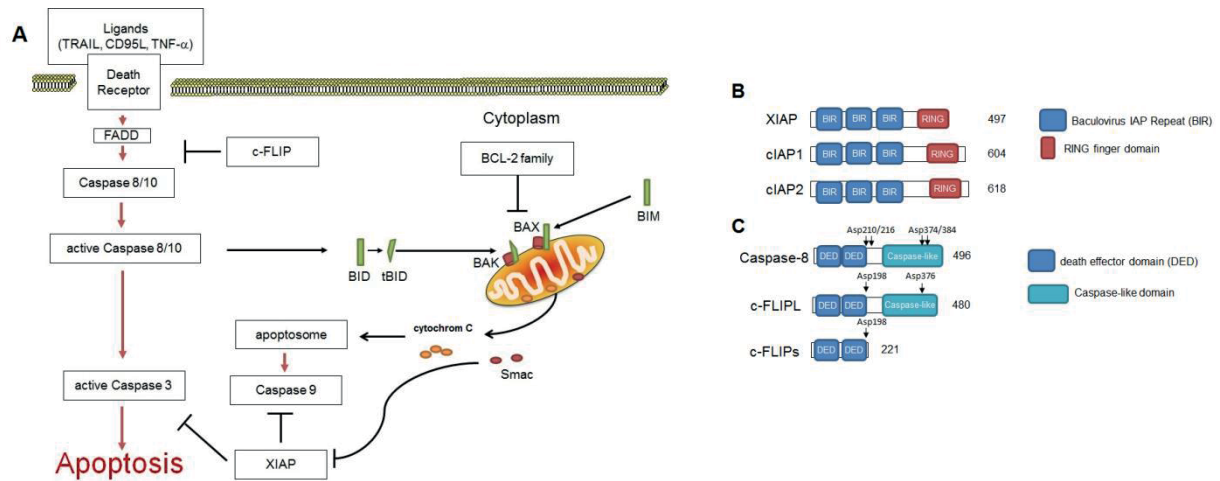
Figure 11: Cellular apoptosis pathway: extrinsic apoptosis pathway is induced by death receptor ligand binding TNF-related apoptosis-inducing ligand (TRAIL), Fas ligand (CD95L) or tumor necrosis factor alpha (TNF-α) leads to activation of caspase-8/10 by FADD. This can be inhibited by c-FLIP. Active caspase-8/10 can further activate the effector caspase 3 or amplify the pro-apoptotic stimulus by cleaving the BH3-only protein BID which leads to BAK/BAK activation. BAX/BAK activation leads to permeabilization of the outer mitochondria membrane and release of cytochrome C and Smac. Smac inhibits XIAP and inhibitor of active caspases 3, 7 or 9. Cytochrom C is bound by Apaf and leads to apoptosome formation that activates Caspase-9. Caspase-9 activates additional caspase 3 leading ultimately to cell apoptosis. B: Schematic illustration of inhibitor of apoptosis protein family (IAP). XIAP, cIAP1/2 harbor three baculovirus IAP repeats (BIR) that can interact with active caspases and a really interesting new gene (RING) zinc finger domain. C: Schematic illustration of Caspase-8a/b isoforms, cellular FLICE like inhibitory protein (c-FLIP) small (s) and large (L) isoforms. Arrows indicate cleavage sites of proteins. Caspase-8 gets cleaved at conserved asparagine residues (Asp/D) leading to protein p18 and p10 that form active caspase-8 homodimer. Caspase activity also leads to cleavage of c-FLIPL at Asp376 and interference with homodimerization of active caspase-8.

1.5.1.2 Myc proto oncogene transcription factor

The Myc transcription factor family consists of c-Myc, N-Myc and L-Myc basic helix loop helix (bHLH) transcription factors. C-Myc forms a heterodimer with MAX to bind to specific e-box consensus sites at gene promoters to regulate gene expression. *MYC* is a proto-oncogene coding for c-Myc which is overexpressed in almost all cancers. Translocation of *MYC* can ultimately lead to the development of cancers such as Burkitt lymphoma and multiple myeloma (MM). The overexpression of c-Myc in normal cells like fibroblasts induces cellular senescence or apoptosis, dependent on the regulatory context of a cell. The predominant induction of apoptosis by high c-Myc levels goes through DNA damage response pathway and p53 tumor suppressor by activation of cyclin-dependent kinase 2

Introduction

(CdK2). In cell with Wrn depletion, a Cdk2 interacting DNA repair protein, high levels of c-Myc induce senescence (Larsson and Henriksson, 2010). Importantly when oncogenes *BRAF* (Zhuang et al., 2008) or *RAS* (Hydbring et al., 2010) are active, c-Myc overexpression suppresses the oncogene-induced senescence. This might explain the proto-oncogenic function of c-Myc in the context of mutated hyper-active RAS. Depletion of c-Myc function in mouse tumor models leads to cell cycle arrest, senescence and tumor regression (Wu et al., 2007). Targeting c-Myc protein directly remains challenging, while targeting the expression of the proto-oncogene has been accomplished by novel drugs like BET inhibitors (Delmore et al., 2011; Zuber et al., 2011; Kandela et al., 2015).

1.5.1.3 *KRAS*-driven non-small cell lung cancer

The kirsten rat sarcoma viral oncogene (*KRAS*) is a mammalian homolog from the RAS gene family, which encode a small GTPases. The guanosine triphosphate (GTP) hydrolase (GTPase) can switch from a GTP-bound active state to a GDP-bound inactive state. The hydrolase activity is enhanced by the RAS GTPase activating protein (GAP), while the exchange of bound-GDP from RAS-GDP is enhanced by RAS-guanine nucleotide exchange factor (RAS-GEF). Interestingly the two other isoforms of RAS (HRAS and NRAS) that are also ubiquitously expressed are mutated at regions that share 100% sequence identity. These point mutations can lead to hyper-activation of RAS. The mutation takes place at three hotspot positions. The most common mutation is found at codon 12 or 13 in the P-Loop of KRAS. This domain interacts with the substrate (GTP) and RAS-GAP. Mutation at codon 12 or 13 leads to reduced RAS-GAP interaction resulting in a hyper-activated form of KRAS. The amino acid at position 61 stabilizes the transition state of GTP during hydrolysis, while mutation reduces the energetic state and decreases GTPase activity (de Castro Carpeno and Belda-Iniesta, 2013). RAS activity influences a number of important cellular functions including cell cycle, survival, growth and endocytosis (de Castro Carpeno and Belda-Iniesta, 2013) (Figure 12).

Introduction
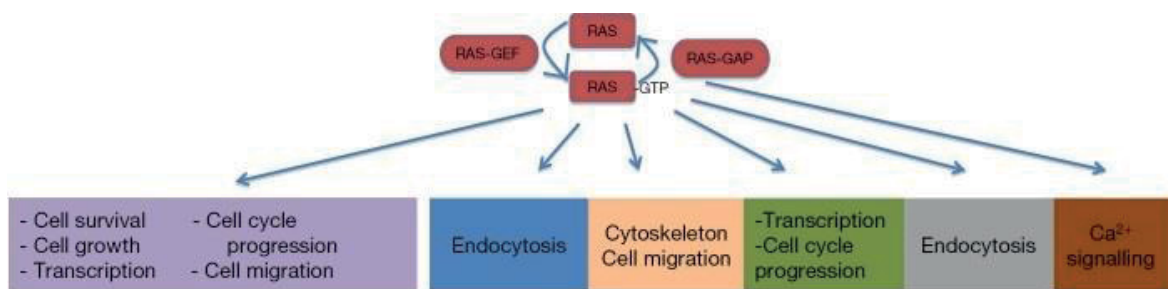
Figure 12: RAS activity influences a number of important cellular functions. The activity of RAS regulated by its GTP binding regulates a number of important cellular functions including cell survival, growth, cycle progression and migration. Proteins controlling the state of RAS are RAS-guanine nucleotide exchange factor (RAS-GEF) and RAS GTPase activating protein (RAS-GAP) that enhances the hydrolase activity. Adapted from (de Castro Carpeno and Belda-Iniesta, 2013).

KRAS is the most commonly mutated gene (25-30%) in non-small cell lung cancer (NSCLC). Other common mutations that can drive NSCLC have been identified and drugs addressing these addictions are in clinical development (Figure 13), but until recently there was no direct targeted therapy for *KRAS* mutations. A recently identified small molecule inhibitor (VSA9) was shown to specifically inhibit the G12C mutation by binding KRAS[G12C]-GDP covalently, but is not effective in other mutations such as types like KRAS[G12D] or KRAS[G12A] (Table 1).

Table 1: Lung adenocarcinoma mutation specificity of *KRAS* adapted from (Prior et al., 2012)

KRAS	codon 12: GGT					
DNA change	-C-	T--	-A-	C--	A--	-T-
amino acid change	G12A	G12C	G12D	G12R	G12S	G12V
number	106	545	222	27	59	279
% of total	8	41	17	2	4	21
KRAS	codon 13: GGC					
DNA change	-C-	T--	-A-	C--	A--	-T-
amino acid change	G13A	G13C	G13D	G13R	G13S	G13V
number	1	43	31	1	1	1
% of total	0	3	2	0	0	0
KRAS	codon 61: CAA					
DNA change	G--	--C/T	A--	-T-	-C-	-G-
amino acid change	Q61E	Q61H	Q61K	Q61L	Q61P	Q61R
number	0	11	1	5	0	2
% of total	0	1	0	0	0	0

Introduction
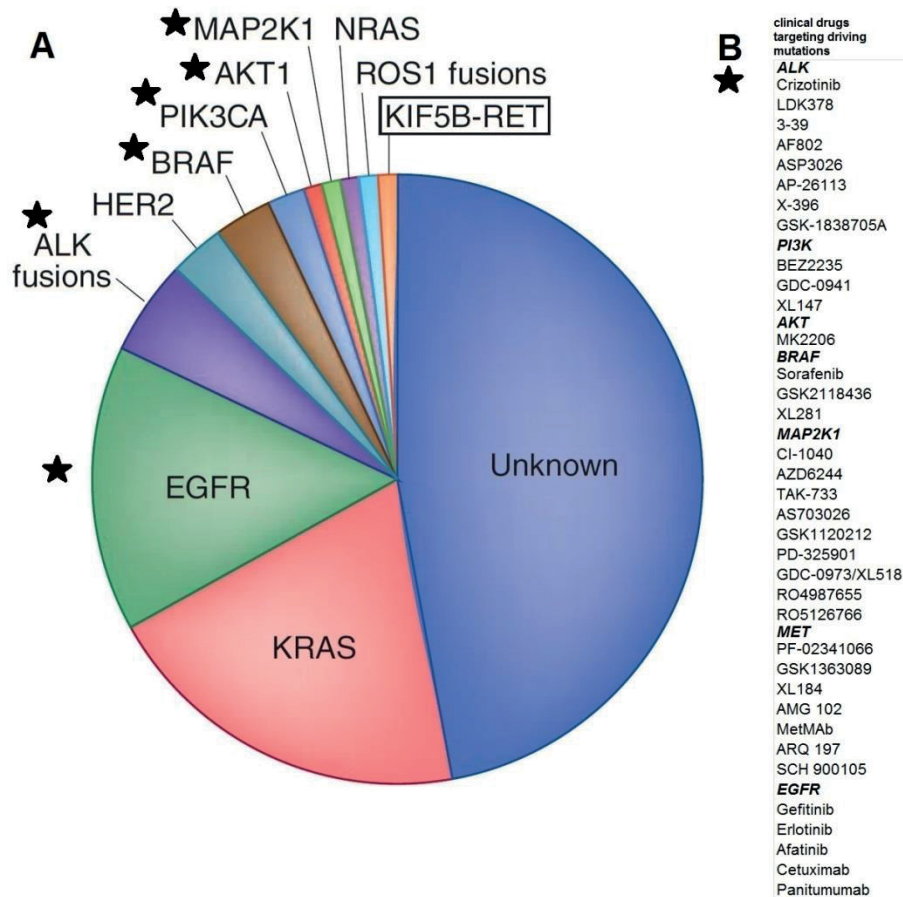
Figure 13: Driving mutations of non-small cell lung cancer: A: Identified driving mutations in NSCLC. KRAS = kirsten rat sarcoma viral oncogene, EGFR = epidermal growth factor receptor, ALK = anaplastic lymphoma kinase, HER2 = human epidermal growth factor receptor 2, BRAF = v-Raf murine sarcoma viral oncogene homolog B, PIK3CA = Phosphatidylinositol-4,5-bisphosphate 3-kinase catalytic subunit alpha, AKT1 = v-akt murine thymoma viral oncogene homolog 1, MAP2K1 = mitogen-activated protein kinase kinase 1, NRAS = neuroblastoma rat sarcoma viral oncogene, ROS1 = v-ros avian UR2 sarcoma virus oncogene homolog 1, KIF5B-RET = kinesin family member 5B - rearranged during transfection (receptor tyrosine kinase) adapted from (Pao and Hutchinson, 2012). B: Stars highlight targets with oncogenic driving mutations in NSCLC for which drugs are currently in the clinic or in clinical development. Database search performed mid 2010 adapted from (Pao and Girard, 2011).

1.5.2 BET inhibitors as novel epigenetic drugs to target cancer

Modification of the epigenetic code, can lead to changes of gene regulation, which ultimately have different cellular phenotypes or outcomes. Deregulation of driving genes or tumor suppressors by changes of HDAC expression was the first epigenetic mechanism identified to cause major changes in cancer (Barneda-Zahonero and Parra, 2012; Lee et al., 2012; Magnaghi-Jaulin et al., 1998). It led to the clinical development and approval of targeted approaches against epigenetic modulator proteins using small molecule inhibitors (Barneda-

Introduction

Zahonero and Parra, 2012; Bolden et al., 2006; Filippakopoulos and Knapp, 2014; Garber, 2007). Besides the HDAC inhibitors Vorinostat and Romidepsin another group of inhibitors addressing a different epigenetic protein family, DNMTs, 5-azacytidine and 5-aza-2′-deoxycytidine, was approved by the food and drug administration (FDA) for the treatment of some rare cancer types. Following the promising clinical results of these first generation epigenetic drugs, a number of other potential epigenetic drug targets belonging to the writer, eraser of reader families were studied in detail. For several of them, potent and selective inhibitors were identified which led to the initiation of early clinical studies (Gelato et al., 2016; Heyn and Esteller, 2012). They include inhibitors of the BET family which includes BRD2, 3 and 4 (Figure 14A). The potential of BET inhibition was first demonstrated in the context of a rare, aggressive cancer type, NUT midline carcinoma (NMC) which results from a gene rearrangement leading to a fusion protein between BRD3 or BRD4 with the nuclear protein in testis (NUT) (Figure 14B). BET inhibitors targeting this chimeric protein have shown promising anti-tumor activity in pre-clinical NMC models (Filippakopoulos et al., 2010) and more recently in early clinical trials (Stathis et al., 2016). The oncogenic effect is dependent on the BRD3 or BRD4 function to bind to acetylated histones and the recruitment of HATs by the NUT fusion part. This leads to hyper-acetylation of enhancers and up-regulation of the c-Myc proto-oncogene transcription factor and to inhibition of cell differentiation (French, 2014). By mimicking acetylated lysine, BET inhibitors competitively bind to BET bromodomains and thereby prevent the interaction with chromatin (Alekseyenko et al., 2015; Filippakopoulos and Knapp, 2014; Filippakopoulos et al., 2010).
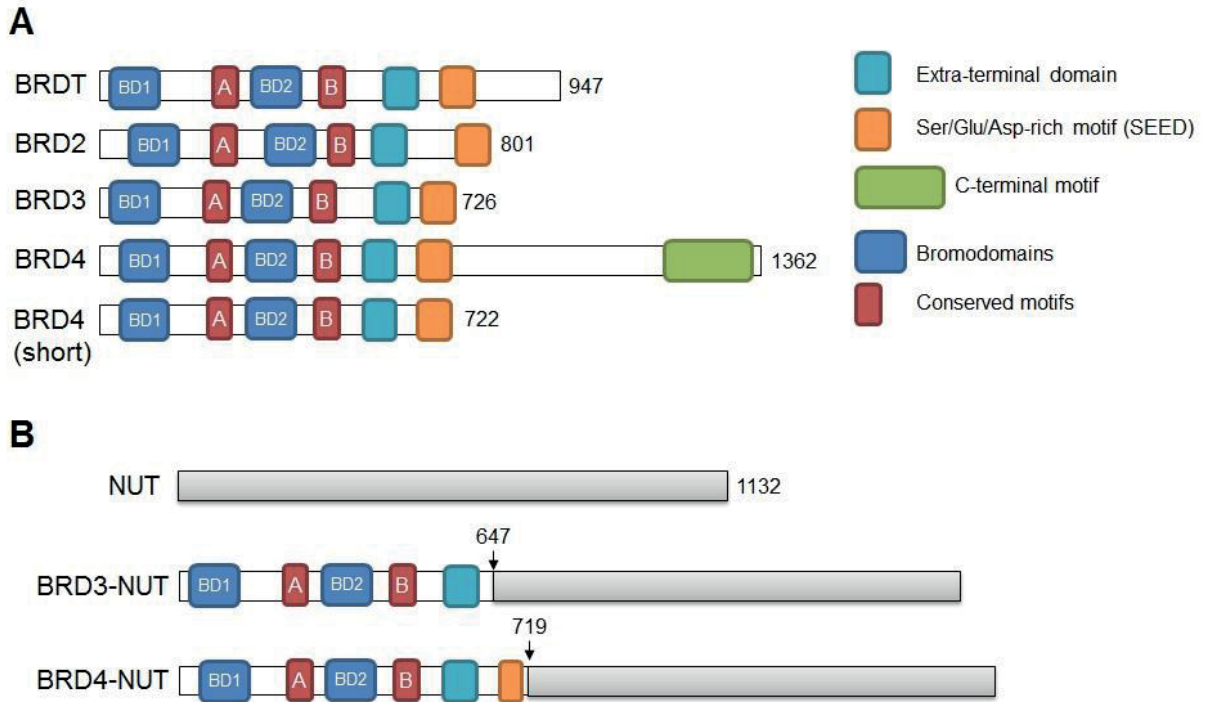
Figure 14: Schematic illustration of bromodomain and extra terminal domain proteins and NUT fusions: A: Boxes delineate the conserved domains of BET family members Bromodomains (BD1/2), motif A and B, extra terminal domain and SEED motif. For BRD4 the short isoform is shown and for BRD2, 3 and T only the main isoform is shown. Numbers denote numbers of amino acids. B: Nuclear protein in testis (NUT) protein and BRD3, 4 fusions are shown. Arrow shows the amino acid at which NUT is fused to BRD3, 4.

The beneficial effect of BET inhibition was thereafter found to extend to other cancer types with the help of JQ1, a potent and selective tool compound, and of other pan-BET inhibitors (e.g. I-BET762 and OTX-015) in a large number of pre-clinical models of hematological and solid tumors (Table 2). This strongly supports that BRD4 plays a major role in a number of different cancers and that its inhibition is an attractive strategy for cancer treatment. Several BET inhibitors are now being evaluated in clinical trials addressing hematological and solid tumors.

Introduction

Table 2: Cancer indications of pre-clinical models in which BET inhibitors showed activity

Cancer type	Reference	BET inhibitor used in the study
acute lymphoid leukemia	(Da Costa et al., 2013; Ott et al., 2012)	JQ1
acute myeloid leukemia	(Rathert et al., 2015; Shen et al., 2015; Zuber et al., 2011)	JQ1
B-cell lymphoma	(Boi et al., 2015; Trabucco et al., 2015)	JQ1;OTX-015
Burkitt's lymphoma	(Mertz et al., 2011; Tolani et al., 2014)	JQ1
mantle cell lymphoma	(Sun et al., 2015)	JQ1
leukemia stem cells	(Fong et al., 2015)	JQ1
multiple myeloma	(Chaidos et al., 2014; Delmore et al., 2011)	JQ1;IBET-151;IBET-762
T-cell acute lymphoid leukemia	(Loosveld et al., 2014)	JQ1
breast cancer	(Sengupta et al., 2015b)	JQ1
Ewing sarcoma	(Hensel et al., 2016)	JQ1
glioblastoma	(Cheng et al., 2013)	JQ1
Merkel-cell carcinoma	(Shao et al., 2014)	JQ1
medulloblastoma	(Bandopadhayay et al., 2014; Henssen et al., 2013; Tang et al., 2014; Venkataraman et al., 2014)	JQ1
melanoma	(Segura et al., 2013)	JQ1
Merkel cell carcinoma	(Sengupta et al., 2015a)	JQ1
neuroblastoma	(Henssen et al., 2016; Puissant et al., 2013)	JQ1;OTX-015
NUT- middle line carcinoma	(Filippakopoulos et al., 2010)	JQ1
non-small cell lung cancer	(Lockwood et al., 2012; Shimamura et al., 2013)	JQ1
osteosarcoma	(Baker et al., 2015)	JQ1

Introduction

Cancer type	Reference	BET inhibitor used in the study
ovarian carcinoma	(Baratta et al., 2015)	JQ1
pancreatic cancer	(Kumar et al., 2015; Sahai et al., 2014)	JQ1
prostate cancer	(Asangani et al., 2014; Wyce et al., 2013)	JQ1
small cell lung cancer	(Lenhart et al., 2015)	JQ1
thyroid cancer	(Mio et al., 2016)	JQ1;IBET-762
uveal melanoma	(Ambrosini et al., 2015)	JQ1

Interestingly, some kinase inhibitors are also potent inhibitors of BRD4, examples include the PLK1 inhibitor BI2536 and the JAK2 inhibitor TG101209 (Ciceri et al., 2014). They bind to the bromodomain pocket and mimic acetyl-lysine like the known BET inhibitors do (Ember et al., 2014). This suggests that the anti-tumor activity of some clinical or approved kinase inhibitors is to a certain degree due to BRD4 inhibition.

Following the initial positive results with JQ1 in NMC, activity of this compound was also shown in models of hematological malignancies (Delmore et al., 2011; Zuber et al., 2011) driven by the c-Myc oncogene. Since then the activity of BET inhibitors has been mainly attributed to down-regulation of c-Myc (Delmore et al., 2011; Kandela et al., 2015; Zuber et al., 2011) or N-Myc (Henssen et al., 2016; Puissant et al., 2013) expression. Later the regulation of other oncogenes by BRD4 was evidenced. However, in lung cancer recent studies provided rather controversial results about the involvement of c-Myc in the response to JQ1 (Lockwood et al., 2012; Shimamura et al., 2013) which is why we initiated a comprehensive program to understand the role of BRD4 in this indication.

2. Research outline

The BET family member BRD4 is indispensable for major cellular functions such as cell proliferation, transcriptional regulation and DNA damage repair. The bromodomains of BRD4 facilitate an interaction with acetylated lysines found in chromatin and in transcriptional regulators. This interaction can be inhibited by blocking the bromodomain binding pocket with small molecule inhibitors. BET inhibitors exhibit potent anti-tumor activity in a wide range of tumors due to transcriptional down-regulation of major oncogene drivers. Nevertheless this anti-tumor activity can be quite diverse within one indication and a number of resistant models always exist. The goal of this study was to characterize the anti-tumor activity of BET inhibitors in pre-clinical models of *KRAS*-mutated NSCLC to identify the drivers of anti-tumor activity and to find combination partners that re-sensitize resistant cells to BET inhibitors.

The results have the potential to advance the understanding of the mechanism of the anti-tumor activity of BET inhibitors in *KRAS*-mutated NSCLC, an indication with yet unmet medical need, and to find attractive combination partners that might improve the clinical efficacy of BET inhibitors.

3. Materials and Methods

3.1 Materials

3.1.1 Equipment and materials

Table 3: Equipment and materials.

Name	Company
2100 bioanalyzer	Agilent Technologies
37 °C incubator Hera cell 150i	Thermo Scientific
6, 96-well culture plate clear	TPP
7900HT Fast Real-Time PCR System	Applied Biosystems
8, 12, 16-channel pipettes	Thermo Scientific
96, 384-well culture plate white	Perkin Elmer
Bioruptor	Diagenode
Cell culture flasks (25, 75, 162, 225, 300 cm²)	TPP
Cell incubator	Thermo Scientific
Centrifuge 5417R	Eppendorf
Centrifuge Heraeus Multifuge 3SR+	Thermo Scientific
Centrifuge RC 5C Plus	Sorval
Countess cell counter	Invitrogen
Covaris S220 device	Covaris
FACSCanto II	BD biosciences
iBlot	Invitrogen
Intelli mixer tube rotator	Sky Line
Inverted Zeiss Axio Observer, Z1 LSM710 microscope	Zeiss
Menzel Coverglasses	Menzel
Nanodrop 2000	Thermo Scientific
Nunc Glass Base Dish 27mm	Thermo Scientific
NuPAGE 4-12% Bis-Tris Gel	Life technologies
Odyssey Fc	Licor
Parafilm M	Pechiney Plastic Packaging
Pipet filter tip (10µl, 2000µl, 1000µl)	Eppendorf
Pipet filter tip (10µl, 2000µl, 1000µl)	Thermo Scientific
Pipetboy acu	Integra Biosciences
Pipettes	Eppendorf
Precellysis 24	Bertin technolgies
Precision wipes	Kimtech Science
Reaction tubes (0.5ml, 1.5ml, 2ml)	Eppendorf
ReadyAgarose Wide Mini gels (8, 12, 20 wells)	Bio-Rad
Stripette (5, 10, 25, 50 ml)	Corning
Tecan M1000	Tecan

Materials and Methods

Name	Company
Thermomixer Comfort	Eppendorf
Thermomixer Comfort	Eppendorf
UV light viewer	Biostep
Victor X3	Perkin Elmer
X cell sure lock electrophorese chamber	Invitrogen

3.1.2 Chemicals, reagents and kits

Table 4: Chemicals, reagents and kits

Name	Company
16% Formaldehyde solution methanol free	Thermo Scientific
Agilent DNA 12000 reagents	Agilent Technologies
Ampicillin	Sigma Aldrich
BCA assay	Thermo Scientific
Bovine serum albumin (BSA)	Sigma Aldrich
CD95L (FasL)	Adipogen
Complete & Complete mini protease inhibitor	roche
Cycloheximid	Sigma Aldrich
DAPI (4',6-Diamidino-2-Phenylindole, Dihydrochloride)	Biotinum
DiaMag protein A coated magnetic beads	Diagenode
DMEM/Hams' F12 (1:1)	Biochrom
DMSO (Dimethyl Sulfoxide)	Sigma Aldrich
DNA chips for Agilent 2100 bioanalyzer	Agilent Technologies
DNA ladder low and high range, 1kb Plus	Invitrogen
Dynabeads M-280 Sheep anti-rabbit IgG	Invitrogen
Dynabeads MyOne Streptavidin T1	Invitrogen
EDTA	Sigma Aldrich
EGTA	Bio world
EndoFree Plasmid Maxi Kit	Qiagen
Ethanol	Sigma Aldrich
Fetal calf serum	Biochrom
Glycerol	Sigma Aldrich
Glycerol 99.5%	Alfa Aesar
HEPES 1M	Biochrom
HEPES pH 7.5	Applichem
Hyclone pure water	GE Healthcare
Hygromycin B	Biochrom
iBlot gel transfer stacks nitrocellulose	Life Technologies
Isopropanol	Acros organics
iz-Trail	Adipogen
Kanamycin	Sigma Aldrich
LiCl	Sigma Aldrich
Lipofectamine LTX plus	Life Technologies

Materials and Methods
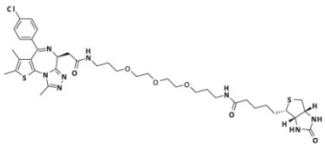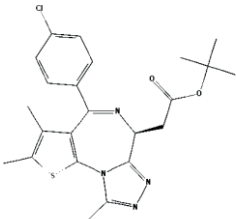
Name	Company
Matrigel	BD Bio
MEM Earle's	Biochrom
Methanol	Millipore
MgCl$_2$*6H$_2$O	Alfa Aesar
mircoTUBE AFA Fibre Pre-Slit	Covaris
M-PER	Thermo Scientific
NaCl	Sigma Aldrich
NaCl 5M	Sigma Aldrich
NaCl solution 0.9%	Baxter
Na-deoxycholate	Sigma Aldrich
NaOH 2M	Sigma Aldrich
Non-essential amino acids	Biochrom
NP-40 alternative	Calbiochem
NuPAGE 4-12% Bis-Tris Gels mini & midi	Life Technologies
NuPAGE LDS sample buffer	Life Technologies
NuPAGE MOPS SDS Running buffer 20X	Life Technologies
NuPAGE Sample Reducing Agent (10X)	Life Technologies
Oligofectamine	Invitrogen
Opti-MEM	Invitrogen
Paraformaldehyde	Sigma Aldrich
PIPES	Sigma Aldrich
Ponceau's solution	Fluka
Precellys-Ceramic Kit	peqlab
Precision Plus Protein Dual Color Standard	BioRAD
Prolong (R) Gold Antifade Reagent	Cell Signaling Technology
Proteinase K	Sigma Aldrich
Puromycin	Santa Cruz Biotechnology
QIAquick PCR purification kit	Qiagen
QIAshredder	Qiagen
Re-Blot Plus Strong	Millipore
RIPA Lysis and Extraction Buffer	Thermo Scientific
RNase A	Invitrogen
RNeasy Plus Mini Kit	Qiagen
RPMI-1640	Biochrom
RT² First Strand Kit	Qiagen
RT² SYBR green ROX qPCR Mastermix	Qiagen
S.O.C. medium	Invitrogen
SDS 10%	Sigma Aldrich
SDS powder	Sigma Aldrich
Sodium acetate pH 5.0	Thermo Scientific
Sucrose	Sigma Aldrich
SuperScript III First-Strand Synthesis Supermix	Invitrogen
SuperSignal West Femto Maximum sensitivity substrate	Thermo Scientific

Materials and Methods
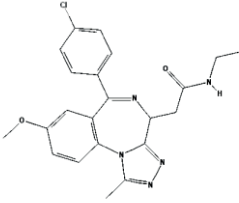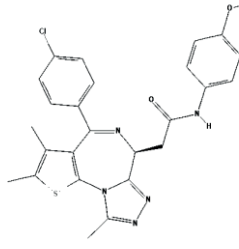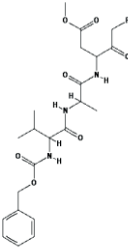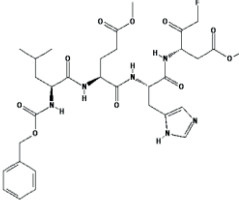
Name	Company
TaqMan Fast Advanced Master Mix	Applied Biosystems
TNF alpha	Adipogen
TPX vials	Diagenode
TRIS-HCl	Gibco
Triton X-100	Sigma Aldrich
Tryptan Blue staining 0.4%	Invitrogen
Tween 20	Sigma Aldrich
Ultra Pure Water	Biochrom
Vectashield Mounting medium for fluorescence	Vector Laboratories
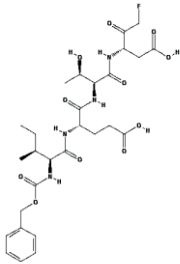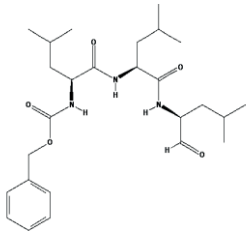
3.1.2.1 Chemical compounds

Table 5: Pharmacological inhibitors and chemical compounds

Name	Structure	PubChem CID/Ref.:	Purchased from
Bio-JQ1(S) (pan-BET inhibitor)		(Anders et al., 2014)	Bayer compound repository
JQ1(S) (pan-BET inhibitor)		46907787	Bayer compound repository

Materials and Methods

Name	Structure	PubChem CID/Ref.:	Purchased from
I-BET762 (pan-BET inhibitor) clinical development		52934829	Bayer compound repository
OTX-015 (pan-BET inhibitor) clinical development		9936746	Bayer compound repository
pan-Caspase inhibitor Z-VAD-FMK (carbobenzoxyvalyl-alanyl-aspartyl fluoromethyl ketone)		5737	Promega
Caspase-9 inhibitor Z-LEHD-FMK (carbobenzoxyleucyl-glutamyl-histidyl-aspartyl fluoromethyl ketone)		10032582	BD Biosciences

Name	Structure	PubChem CID/Ref.:	Purchased from
Caspase-8 inhibitor Z-IETD-FMK (carbobenzoxyisoleucyl-glutamyl-threonyl-aspartyl fluoromethyl ketone)		9852146	BD Biosciences
Intra-strand DNA linker Cisplatin cis-diaminedichloroplatinum (CDDP)		2767	Sigma Aldrich
Proteasome inhibitor MG-132		462382	Sigma Aldrich

3.1.3 Buffers and solutions

TBS – tris buffered saline: 20 mM Tris-HCl [pH 7.4], 500 mM NaCl

PBS – phosphate buffered saline: 0.137 M NaCl, 2.7 mM KCl, 8 mM Na_2HPO4, 1.8 mM KH_2PO_4 [pH 7.4]

TBS-T and PBS-T: TBS or PBS, 0.1% (v/v) Tween-20

Materials and Methods

TE buffer: 10 mM Tris-HCl [pH 8.0], 1 mM EDTA

10x PIPES buffer: 1.5 g PIPES (100 mM), 2 mL 2 M NaOH, 48 mL H_2O

10x Sucrose/MgCl₂ buffer: 3 M Sucrose, 30 mM $MgCl_2*6H_2O$

Cytoskeleton (CSK) buffer: 10 mM PIPES, 300 mM Sucrose, 100 mM NaCl, 3 mM $MgCl_2*6H_2O$

Detergent washout buffer 1: CSK Buffer, 0.1% (v/v) Triton X-100

Detergent washout buffer 2: CSK Buffer, 0.5% (v/v) Triton X-100

Western blot (WB) blocking solution: 5% non-dry fat milk powder (w/v) in PBS or TBS.

Immunofluorescence blot blocking solution: 10% normal goat serum (v/v) in PBS, 0.3% (v/v) Triton X-100.

ChIP lysis buffer 1: 50 mM HEPES [pH 7.3], 140 mM NaCl, 1 mM EDTA, 10% glycerol, 0.5% NP-40, 0.25% Triton X-100, 1 tablet protease inhibitors complete (per 50 mL).

ChIP sonication buffer:, 50 mM Tris-HCl [pH 7.5], 140 mM NaCl, 1 mM EDTA, 1 mM EGTA, 1% Triton X-100, 0.1%-0.75% (w/v) SDS, 0.1% Na-deoxycholate (w/v), 1 tablet protease inhibitors complete (per 50 mL).

ChIP sonication buffer high salt:, 50 mM Tris-HCl [pH 7.5], 500 mM NaCl, 1 mM EDTA, 1 mM EGTA, 1% Triton X-100, 0.1% SDS, 0.1% Na-deoxycholate (w/v), 1 tablet protease inhibitors complete (per 50 mL).

ChIP Li washing buffer: 20 mM Tris [pH 8.0], 1 mM EDTA, 250 mM LiCl, 0.5% NP-40, 0.5% Na-deoxycholate

ChIP washing buffer: 10 mM Tris-HCl [pH7.5], 0.1 mM EDTA

ChIP elution buffer-ChIP: 50 mM Tris-HCl [pH 8.0], 10 mM EDTA, 1% SDS

ChIP elution buffer-Chem: 50 mM Tris-HCl [pH 8.0], 10 mM EDTA, 10% SDS

Materials and Methods

RIPA buffer: 25 mM 50 mM Tris-HCl [pH 7.6], 150 mM NaCl, 1% NP-40, 1% Na-deoxycholate (w/v), 0.1% SDS

Western blot (WB) lysis buffer: RIPA buffer, 100U/mL Benzonase, 5 μM EDTA, 1x Halt Protease and Phosphatase Inhibitor Cocktail (Protase inhibitors: Aprotinin, Bestatin, E-64, Leupeptin and Phosphatase inhibitors (Sodium Fluoride, Sodium Orthovanadate, Sodium Pyrophosphate, β-glycerophosphate)

M-PER buffer: proprietary detergent in 25 mM bicine buffer [pH7.6]

Chromatin separation buffer: M-PER buffer, 5 μM EDTA, 1x Halt Protease and Phosphatase Inhibitor Cocktail.

3.1.4 Human cell lines

All cell lines used in this study were purchased from the American Type Culture Collection (ATCC) or the *Deutsche Sammlung von Mikroorganismen und Zellkulturen GmbH* (DSMZ). The H441 cell line was from the Bayer cell stock and has been authenticated by finger-printing at the DSMZ. Cells were maintained in RPMI 1640 or DMEM/F12 supplemented with 10% (v/v) FCS. Non-essential amino acids were added in the case of DV90. IMR-90, Wi38 and HFF-1 cells were cultured in MEM Earle's Medium with 10% FCS.

Table 6: Human cell lines used in this study with corresponding culture media and source of origin

Name of cell line	Culture medium	Culture medium supplement	Tissue type	Origin
DV90	RPMI-1640	10% FCS+ NEA	NSCLC	DSMZ
NCI-H1373	RPMI-1640	10% FCS	NSCLC	ATCC
LCLC97TM1	RPMI-1640	20% FCS	NSCLC	DSMZ
NCI-H1792	RPMI-1640	10% FCS	NSCLC	ATCC
SKLU-1	RPMI-1640	10% FCS	NSCLC	ATCC
NCI-H2122	RPMI-1640	10% FCS	NSCLC	ATCC

Name of cell line	Culture medium	Culture medium supplement	Tissue type	Origin
NCI-H441	RPMI-1640	10% FCS	NSCLC	authenticated at DMSZ
NCI-H23	RPMI-1640	10% FCS	NSCLC	ATCC
A549	DMEM/Hams' F12 (1:1)	10% FCS	NSCLC	DSMZ
NCI-H460	DMEM/Hams' F12 (1:1)	10% FCS	NSCLC	ATCC
NCI-H358	RPMI-1640	10% FCS	NSCLC	ATCC
NCI-H2347	RPMI-1640	10% FCS	NSCLC	ATCC
NCI-H2030	RPMI-1640	10% FCS	NSCLC	ATCC
Wi38	MEM Earle's	10% FCS	normal lung fibroblast	ATCC
IMR-90	MEM Earle's	10% FCS	normal lung fibroblast	ATCC
HFF-1	MEM Earle's	10% FCS	normal foreskin fibroblast	ATCC

3.1.5 Mouse strains

Mouse strains used in this study were FOX chase severe combined immunodeficiency (SCID) mice (CB17/Icr-Prkdc^{scid}/IcrIcoCrl) purchased from Charles River Germany.

3.1.6 Bacterial strains and media

The *Escherichia coli* (*E. coli*) strain used for plasmid amplification and purification was XL1-Blue competent cells (Stratagene). *E.coli* bacteria were cultured and grown in LB (Luria Bertani) liquid medium or solid medium produced in the Quality Control Biology department of Bayer Pharma.

LB Medium liquid: 0.5% NaCl, 1% Bacto-Pepton, 0.5% Yeast extract

LB Medium solid: 0.5% NaCl, 1% Bacto-Pepton, 0.5% Yeast extract, 1.7% Bacto-Agar

3.1.7 Oligonucleotides

3.1.7.1 TaqMan Probes

Table 7: TaqMan gene expression assays and RT²-array used in this study

Gene symbol	Name	Reference
MYC	c-Myc proto-oncogene	Hs00905030_m1
FLIP	FLICE like inhibitor protein	Hs00153439_m1

XIAP	X-linked inhibitor of apoptosis protein	Hs00745222_s1
FOSL1	Fos-related antigen 1	Hs04187685_m1
BRD4	Bromodomain-containing protein 4	Hs01006453_m1
BRD3	Bromodomain-containing protein 3	Hs00201284_m1
BRD2	Bromodomain-containing protein 2	Hs01121986_g1
PPIA/	Cyclophilin A	4326316E
Human Apoptosis PCR Array 384HT		PAHS-30127

3.1.7.2 ChIP qRT-PCR primers

Table 8: ChIP qRT-PCR primer used in this study

Gene symbol	location	Company
XIAP	hXIAP NM_001167.2 at -10kb from TSS	Qiagen
XIAP	hXIAP NM_001167.2 at -2kb from TSS	Qiagen
XIAP	hXIAP NM_001167.2 at +1kb from TSS	Qiagen
XIAP	hXIAP NM_001167.2 at +8kb from TSS	Qiagen
FLIP	hFLIP NM_003879.4 at -2kb from TSS	Qiagen
FLIP	hFLIP NM_003879.4 at +1kb from TSS	Qiagen

3.1.7.3 Small interfering RNA (siRNA)

Table 9: siRNAs used in this study

Gene symbol	Reference	Company
Control siRNA	1027281	Qiagen
FLIP	L-003772-00-0010	GE Dharmacon
XIAP	L-004098-00-0010	GE Dharmacon

3.1.8   Reagents and antibodies
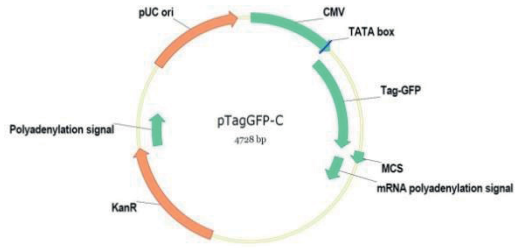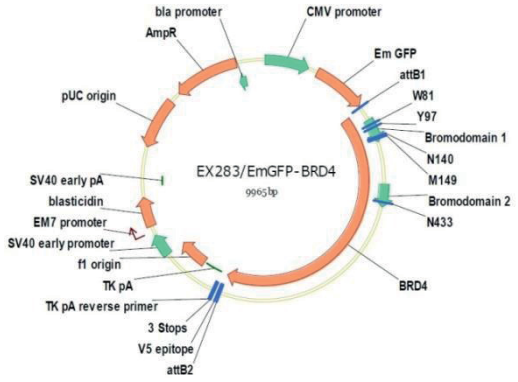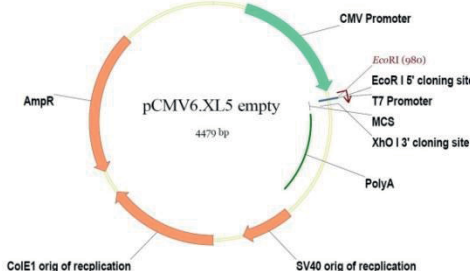
3.1.8.1 Plasmids
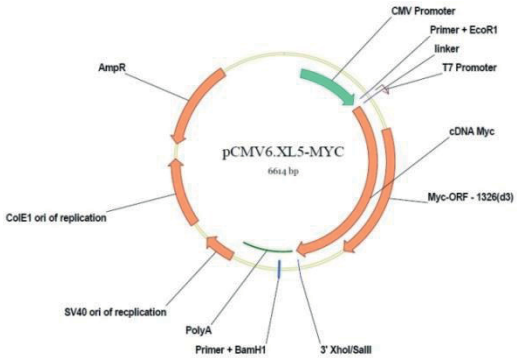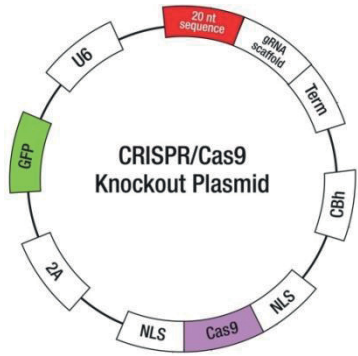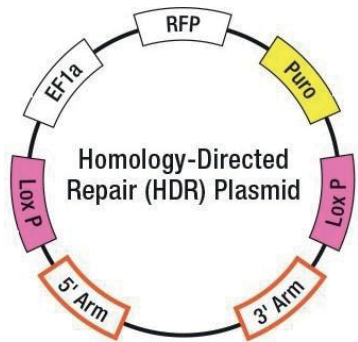
Human MYC cDNA construct was purchased from OriGene (pCMV6.XL5, pCMV6.XL5-MYC) and Tag-GFP construct from Evrogen (pTagGFP-C). CRISPR knockout plasmid pools of 2-3 guide RNAs (BAX-KO-GFP, BAK-KO-GFP) were purchased from Santa Cruz Biotechnology that derived guide sgRNA sequences from a CRISPR Knock-out (GeCKO) v2 library (Ran et al., 2013; Shalem et al., 2014).

Materials and Methods

Corresponding CRISPR homology directed repair (HDR) plasmids were purchased from Santa Cruz Biotechnology (BAX-HDR-RFP-Puro, BAK-HDR-RFP-Puro). HDR plasmid overhang arms for the 5' and 3' for the specific cutting sites were designed and synthesized by Santa Cruz Biotechnologies. 5' and 3' arms are flanking LoxP sites and selection marker gene cassettes for red fluorescent protein (RFP) and puromycin resistance gene.

Table 10: Plasmid vectors used in this study or used to produce stable cell lines presented in this study

Name	Source	Plasmid map
pTagGFP-C	Evrogen	
pcDNA6.2/N-EmGFP-BRD4	Structural Genomics Consortium (Oxford)	
pCMV6.XL5 (PCMV6XL5)	Origene	

Materials and Methods

Name	Source	Plasmid map
pCMV6.XL5-MYC (SC112715)	Origene	
CRISPR/Cas9 knockout Plasmids: BAX-KO-GFP BAK-KO-GFP	Santa Cruz Biotechnology	
Homology-directed repair (HDR) Plasmids: BAX-HDR-RFP-Puro BAK-HDR-RFP-Puro	Santa Cruz Biotechnology	

3.1.8.2 Antibodies

Antibodies and beads used for Immunoblotting and Chromatin immunoprecipitation (ChIP) antibodies are listed in tables 9-12.

Table 11: Primary antibodies used for western blot staining

Antibody	Company	Concentration
Mouse-anti-c-Myc	Abcam (ab32)	1 µg/ml

Materials and Methods

Antibody	Company	Concentration
Rabbit-anti-FOSL1	Cell signaling (#5281)	1 µg/ml
Mouse-anti-c-FLIP	Enzo Life Sciences (7F10)	1 µg/ml
Rabbit-anti-BCL-XL	Cell signaling (#2764)	1 µg/ml
Rabbit-anti-Mcl1	Cell signaling (#5453)	1 µg/ml
Rabbit-anti-BCL2	Cell signaling (#2870)	1 µg/ml
Rabbit-anti-c-IAP1	Cell signaling (#7065)	1 µg/ml
Rabbit-anti-c-IAP2	Cell signaling (#3130)	1 µg/ml
Rabbit-anti-Survivin	Cell signaling (#2808)	1 µg/ml
Rabbit-anti-XIAP	Cell signaling (#2045)	1 µg/ml
Rabbit-anti-BID	Cell signaling (#2002)	1 µg/ml
Rabbit-anti-BAX	Cell signaling (#5023)	1 µg/ml
Rabbit-anti-BAK1	Cell signaling (#12105)	1 µg/ml
Rabbit-anti-PARP	Cell signaling (#9542)	1 µg/ml
Rabbit-anti-LKB1	Cell signaling (#27D10)	1 µg/ml
Rabbit-anti-p53	Cell signaling	1 µg/ml
Rabbit-anti-p21	Cell signaling	1 µg/ml
Rabbit-anti-GAPDH	Abcam (ab9485)	0.5 µg/ml
Rabbit-anti-β-ACTIN	Abcam (ab8227)	0.125 mg/ml

Table 12: Primary antibodies used for ChIP

Antibody	Company
Rabbit-anti-BRD4	Bethyl Laboratories (A301-985A)
rabbit IgG	Sigma Aldrich (R2004-5X1MG)
Rabbit-anti-H3K27Ac	Abcam (ab4729)
Rabbit-anti-H3K4me1	Diagenode (C15410194)
Rabbit-anti-H3K4me3	Diagenode (C15410003)
Rabbit-anti-MED1	Bethyl Laboratories (A300-793A)
Rabbit-anti-Pol2	Santa Cruz Biotechnologies (sc-899X)

Table 13: Antibodies used for immunofluorescence

Antibody	Company	Concentration
Rabbit-anti-BRD4	Abcam (ab128874)	3.63 µg/mL
Mouse- anti-tubulin-Alexa Fluor 488 conjugate	Abcam (ab195887)	2.5 µg/mL

Materials and Methods

Table 14: Secondary conjugate antibodies used for western blot staining immunofluorescence

Antibody	Company	Concentration
Anti-rabbit-HRP	invitrogen (656120)	0.1 µg/ml
Anti-mouse-HRP	Santa Cruz Biotechnologies (sc-2005)	0.2 µg/ml
Anti-rabbit-Alexa Fluor 647	Thermo Fisher Scientific (A-21245)	4 µg/mL

3.1.9   Software

Table 15: Software and scripts used in this study

Name	Version	Company/link
bamToGFF	-	Bradner laboratory
Bdg2bw	-	https://gist.github.com/taoliu/2469050
bedGraphToBigWig	-	https://gist.github.com/2469050
bedTools	2.26.0	Quinlan laboratory
Bowtie	2	Langmead laboratory
DAVID	6.7	https://david.ncifcrf.gov/home.jsp
EndNote	X4	Thomas Reuters
Excel	2010	Microsoft
FACSDiva software	8.0.1	BD
GraphPad Prism	6	GraphPad Software
GSEA	2.2	Broad Institute
IGV	2.3.81	Broad Institute
Illustrator	CS5	Adobe
Image Studio	5.2	Li-Cor
Magellan	7.2	Tecan
Model-bases Analysis for ChIP-seq	2	Liu laboratory
Nanodrop	2000	Fisher Scientific
Peakanalyzer	1.4	Bertone laboratory
PerkinElmer Manager	2030	PerkinElmer
Powerpoint	2010	Microsoft
ROSE	-	Young laboratory
RQ Manager	1.21	Applied Biosystems
SAMtools	1.3.1	www.htslib.org/
SDS	2.4	Applied Biosystems
SeqPlots	1.10.2	http://github.com/przemol/seqplots
Word	2010	Microsoft

Materials and Methods

3.2 Methods

3.2.1 Cell lines and culture conditions

3.2.1.1 Thawing of cryo-conserved cell lines

Cells were frozen in 90% fetal calf serum (FCS) and 10% dimethyl sulfoxid (DMSO) before storing in liquid nitrogen gas-phase at around -270 °C (cryo-conservation). Thawing of cell lines was done at 37 °C before transfer into pre-warmed appropriate culture medium containing FCS. Cells were centrifuged at 300 g to separate them from residual DMSO. Cells were re-suspended and transferred into a 75 cm² culture flask (T75) which was cultured in an incubator at 37 °C, 5% CO_2 and >80% humidity (incubation). Culture medium was replaced after 24 h. Cells were passaged when reaching 80-90% confluence.

3.2.1.2 Passaging of cells

Cells were grown in the incubator until 80-90% confluence was reached. To detach adherent cells, the culture media was removed, cells were washed once with magnesium and calcium free phosphate-buffered saline (DPBS) and treated with trypsin 0.25% / ethylenediaminetetraacetic acid (EDTA) solution at 37 °C. Detachment of cells was ensured using a microscope. Detached cells were re-suspended in culture media containing FCS to quench trypsin activity. Cells were counted and viability was determined by mixing 10 µL of cell suspension with 10 µL trypan blue and subjected to the automated counting system Countess. Cell suspension was then diluted and re-seeded into a new culture flask for the maintenance of the cell line or to culture plates, flasks or plates to perform subsequent experiments.

3.2.2 Determination of cell doubling time and optimal seeding density for viability assays

To optimize conditions for cell viability assays and drug testing, cell doubling time and optimal cell seeding number were determined. Cells were seeded at 1,000, 2,000, 3,000, 4,000, 6,000 and 10,000 cells/well in 50 µL. Cells were seeded in 6 replicate wells per cell density on a 96-well plate. After 24 h (day 0) incubation, 50 µL culture medium containing 0.1% DMSO were added. The ATP content of each well which is representative of the number

of viable cells was determined using CellTiter-Glo One Solution (CTG) every 24 h for 4 subsequent days starting on day 0. In accordance to the manufacturer's instructions 100 µL CTG were added to 100 µL cell suspension. The plates were equilibrated at room temperature (RT) for 20 min prior to addition of CTG at RT and subsequent sealed before incubation for 15 min at RT on a shaker at 500 rpm, to ensure complete lysis of the cells. The luminescence signal was determined on a plate reader (VictorX3) using a protocol of an intensity count of 1 second per well.

The cell doubling time (Dt(x)) in hours was determined by dividing log(2) by the cell line specific calculated slope of the logarithmic signal increase per day (x) multiplied by 24. The cell density that still showed log-growth on day 3-4 and not reaching a plateau was considered as the optimal cell number.

$$Dt(x) = \frac{\log(2)}{x} * 24$$

$$x: \frac{\log(signal\ increase)}{day}$$

3.2.3   Drug treatment and determination of cell viability

Cells were seeded at the pre-optimized density which was between 1000-2000 cells/50 µL/well in the 96-well plate format, on the day before treatment. On day 0, cells were treated with 50 µL of medium containing 0.1% DMSO or 0.1% DMSO and small molecule inhibitor. The 2x drug concentrated medium was generated by adding 1 µL of serial diluted drug in DMSO to 500 µL culture media. The final drug concentration range was between 10-8.5 and 10-5 mol/L (M) with half log fold steps. The cells were cultured in presence of drug or vehicle for 72 h. The on-plate positive control wells were treated with 1 µM MG-132, a proteasome inhibitor toxic to most cell lines. On day 3 post-treatment the cell viability was assessed in triplicate using CTG assay according to the manufacturer's instructions as described above (3.2.2).

Values were normalized to 100%, which was equivalent to the average of the negative control DMSO and to 0%, which was equivalent to the average of the positive control MG-132.

Materials and Methods

$$V(x) = \frac{(x - \text{blank}) - (\text{postiv control} - \text{blank})}{(\text{negative control} - \text{blank}) - (\text{positiv control} - \text{blank})}$$

$$Viability\ in\ \%{:}\ V(x) * 100\%$$

The cellular half-inhibitory concentrations of each inhibitor (IC_{50}) values were calculated using a non-linear regression model in GraphPad Prism 6 calculating an IC_{50} and a Hill Slope value that can be used to calculate IC_x. Resulting IC_{50} values were expressed as an average of two or three independent experiments.

$$S(x) = (\text{postiv control} - \text{blank}) + \frac{(\text{negative control} - \text{blank})}{1 + \left(\frac{10^{\log IC_{50}}}{10^x}\right)^H}$$

$$IC_x = \left(\frac{x}{100 - x}\right)^{1/H} * IC_{50}$$

$$S(x){:}\ Varibale\ slope\ sigmoidal\ equation$$

$$H{:}\ Hill\ Slope$$

3.2.4 Drug combination and synergy calculation

3.2.4.1 Drug combination with cisplatin

A549 cells were seeded at pre-optimized density of 350 cells/well in 384-well plate format on the day before treatment and cultured in presence of drug or vehicle for 72h. The drug combination ratio (R) between JQ1 and cisplatin is described as R_a for JQ1 and R_b for cisplatin. R_a to R_b ratios generated by mixing 10 mM stock solutions of JQ1 and cisplatin ratios R1-5: 1) 0.8/0.2; 2) 0.6/0.4; 3) 0.4/0.6; 4) 0.2/0.8; 5) 0.1/0.9. Starting from the stock ratios the final drug ratio concentration ranged from $10^{-8.5}$ to 10^{-5} mol/L (M). The dilution was made in half log fold steps. The twofold drug concentrated medium was generated by adding 1 µL of serial diluted drug in DMSO to 500 µL culture media. On-plate positive control wells were treated with 1 µM MG-132. Values were normalized to 100%, which was equivalent to the average of the negative control DMSO and to 0%, which was equivalent to the average of the positive control MG-132. Viability was assessed in duplicate using CellTiter-Glo One

Materials and Methods

Solution (CTG) assays according to the manufacturer's instructions as described above (3.2.2).

Combined drug effects were calculated by the combination-index (CI) analysis. The CI values were calculated from a range of drug ratios (R) and the corresponding IC50 values.

$$CI_1 = \frac{(R_{1a}) \times IC_{50} \text{ combination}}{IC_{50} \text{ JQ1}} + \frac{(R_{1b}) \times IC_{50} \text{ combination}}{IC_{50} \text{ cisplatin}}$$

[$R_{[1-5]}$ (R_a(JQ1)/R_b(cisplatin)): 0.8/0.2; 0.6/0.4; 0.4/0.6; 0.2/0.8; 0.1/0.9]

IC_{50} values were calculated using non-linear regression model in GraphPad Prism 6. The resulting IC_{50} and CI values were expressed as the average of two independent experiments.

3.2.4.2 Drug combinations with TRAIL ligand

Cells were seeded in 96-well plates at 4000 cell/well/45 µL density 24 h prior to combination treatment (day-1). On day 0 cells were treated with 45 µL of 2x small molecule containing media. Final concentrations of JQ1 ranged from 0.5-2.5 µM. After 2 h of incubation at 37 °C wells were subjected to 100 µL 10x concentrated 0.1% BSA-PBS containing diluted TRAIL ligand. Final TRAIL concentrations ranged from 0.01-1,000 ng/mL. After 24 h the viability of the cells was determined using the CTG assay as described above (3.2.2).

3.2.5 Cell cycle analysis

Cell lines growing in exponential phase were detached and 100,000 – 200,000 cells were seeded in 1 mL culture media in six-well plates. After 24 h in the incubator, the seeding medium was removed and replaced with 2 mL BET inhibitor or DMSO vehicle containing culture medium and incubated for 18 h. Cells were then subjected to 10 µM EdU, a cell permeable nucleotide analog that gets incorporated into the DNA during synthesis (S)-phase, and further incubated for 6 h before staining. Cells were washed once with cold PBS and detached using Trypsin/EDTA solution, and medium and washing buffer were collected. Cells were re-suspended in the collected culture medium and washing buffer, and filtered through a 70- µm mesh cap of a flow cytometry tube. Cells were spun down at 300 g using a centrifuge.

Medium was removed and cells were washed with 3 mL 1% BSA containing PBS and then centrifuged at 300 g. Washing solution was removed and cell pellet was re-suspended in 100 µL fixative solution containing formaldehyde from Click-iT EdU Alexa Fluor 647 Flow Cytometry Assay Kit. Cells were incubated in fixation solution for 15 min in the dark at RT and washed with 3 mL 1% BSA containing PBS and centrifuged at 300 g. Washing buffer was removed and 100 µL saponin-based buffer (1% BSA in PBS) was used to permeabilize the cells. EdU Click-it staining solution containing 10 µL copper sulfate, 438 µL PBS, 50 µL reaction buffer additive and 2.5 µL Alexa Fluor 647 azide per sample was prepared and added. Cells were stained for 30 min at RT in the dark, washed with 3 mL saponin-based buffer after and centrifuged at 300 g. Washing buffer was removed and cells were re-suspended in saponin-based buffer containing 1 µg/mL 4′,6-Diamidin-2-phenylindol (DAPI) for 1 h at 4 °C in the dark to stain the DNA. EdU$^+$ and EdU$^-$ populations were determined and separated by DNA content using a FACS-Canto II Flow Cytometry system and BD FACSDiva software. FACS analysis enabled the separation of EdU$^+$ S-Phase population and EdU$^-$ subG1, G1 and G2/Mitosis (M) populations.

3.2.6   Annexin V/PI staining

3.2.6.1 Annexin V/PI staining of BET inhibitor treated cells

Cell lines growing in exponential phase were detached and 300,000 cells were seeded in 1 mL culture media in six-well plates. After 24 h in the incubator seeding medium was removed and replaced with 2 mL of 0.5 µM or 2.5 µM BET inhibitor or DMSO vehicle containing culture media and incubated for 48 h. Cells were washed once with cold PBS and then detached using Trypsin/EDTA solution. Medium and washing buffer were collected. Cells were re-suspended in collected culture medium and washing buffer, and filtered through a 70- µm mesh cap of a flow cytometry tube. Cells were spun down at 300 g using a centrifuge. Medium was removed and cells were washed with 2 mL PBS and then centrifuged at 300 g. Washing solution was removed and the cell pellet was re-suspended in 300 µL binding buffer from FITC Annexin-V Apoptosis Detection kit I. 100,000 cells were stained in 100 µL binding buffer containing 5 µL PI solution and 5 µl Annexin V-FITC solution for 15 min in the dark at RT. Viable (Annexin V$^-$/PI$^-$), early apoptotic (Annexin V$^+$/PI$^-$), late apoptotic (Annexin V$^+$/PI$^+$) and necrotic population (Annexin V$^-$/PI$^+$) were determined by a flow cytometer.

Materials and Methods

3.2.6.2 Annexin V/PI staining of JQ1 and death ligand combination

Cells growing in exponential phase were detached and 300,000 cells were seeded in 1 mL culture media in six-well plates. After 24 h in the incubator seeding media was removed and replaced with 2 mL of 1 µM JQ1 or DMSO vehicle containing culture media and pre-incubated for 2 h before addition of TRAIL for 24 h at 10 ng/mL or 100 ng/mL final concentration. Cells were stained as described above (3.2.6.1) and analyzed by a flow cytometer.

3.2.6.3 Annexin V/PI staining of JQ1 and death ligand combination rescue

H1373 cells growing in exponential phase were detached and 300,000 cells were seeded in 1 mL culture media in six-well plates. After 24 h in the incubator seeding medium was removed and replaced with 2 mL of JQ1 or DMSO vehicle containing culture media and pre-incubated for 2 h before addition of TRAIL for 24 h at 10 ng/mL final concentration together with a final concentration of 20 µM Caspase-8 (z-IETD-FMK), Caspase-9 (z-LEHD-FMK) or pan-Caspase inhibitor (z-VAD-FMK). Cells were stained as described above (3.2.6.1) and analyzed by a flow cytometer.

3.2.6.4 Annexin V/PI staining of BET inhibitor and cisplatin combination

A549 cells growing in exponential phase were detached and 200,000 cells were seeded in 1 mL culture medium in six-well plates. After 24 h in the incubator seeding medium was removed and replaced with 2 mL of culture media containing 1 µM JQ1 or DMSO vehicle in combination with 20 µM cisplatin and incubated for 48h. Cells were stained as described above (3.2.6.1) and analyzed by a flow cytometer.

3.2.7 Western blot

Culture medium was removed from cells. Cells were washed in cold PBS, and then lyzed using WB lysis buffer (radioimmunoprecipitation assay (RIPA) buffer containing Halt Protease and Phosphatase inhibitor mixture and 100 U/mL Benzonase. Tumor tissues samples were disrupted in tubes containing ceramic beads and WB lysis buffer at 5000 rpm for 15 s using the Precellys 24 system. Lysates were incubated at 4 °C overnight and clarified by centrifugation at 13,000 x g for 10 min. To determine the protein concentration the Pierce

Materials and Methods

BCA Protein Assay kit was used. For that 1 µL of total lysate was added to 199 µL of 1x BCA staining solution, a mixture of 1 part solution A and 25 parts solution B, and incubated for 1 h at 37 °C. Absorbance was determined at 562 nm wavelength. An on-plate BSA protein standard with a concentration range from 0,069 - 4.41 µg was used to determine the amount of protein in the total cell lysates. Equivalent amounts of lysate were denatured in 1x LDS sample buffer together with 1x sample reducing agent and denatured at 70 °C for 10 min. The lysates were loaded on SDS gels together with 10 µL of protein marker (Precision Plus Protein Dual Color Standard) and run at 100-120 mA for 1 h. Proteins were blotted on Nitrocellulose membrane using the iBLOT protein transfer system at program 3 for 9 min. Membrane was stained and checked using Ponceau S solution for 2 min and washed with water for 5 min to confirm successful protein transfer. Membranes were blocked in 5% non-dry fat milk containing PBS or TBS for 30 min at RT on a rocking plate. Primary antibody incubation was done in 5% non-dry fat milk containing PBS or TBS at 4 °C overnight. Membranes were washed 5 times for 5 min with PBS or TBS containing 0.1% tween 20 (PBS-T or TBS-T). Horseradish peroxidase (HRP)-conjugated secondary antibody was diluted in 5% non-dry fat milk containing PBS or TBS for 1 h and washed 5 times for 5 min with PBS-T or TBS-T. Membranes were developed using HRP substrate (SuperSignal West Femto Maximum sensitivity substrate) by mixing luminol enhancer solution and peroxide buffer 1:1 and adding it onto the membrane followed by detection of the signal on an Odyssey Fc imaging system.

3.2.8 RNA extraction

Cells were seeded at 100,000-300,000 cells/well in a 6-well culture plate on the day before treatment. Total RNA was extracted using the RNeasy Plus Mini kit. Culture medium was removed from cells. Cells were washed with cold PBS, and then lysed using 350 µL of guanidine-isothiocynate and 2 M DTT-containing high salt RLT Plus Buffer. Lysate was transferred to QIAshredder tubes and centrifuged for 2 min at 13,000 g for homogenization. Samples were frozen at -80 °C or RNA extraction was performed directly afterwards. Lysates were passed through gDNA Eliminator spin column to eliminate genomic DNA from the sample. 350 µL of 70% ethanol were added to provide optimal conditions for the RNA to bind to the silica membrane of the RNeasy spin column. Samples were transferred to the RNeasy spin column and centrifuged for 1 min at >10,000 g. The flow through was discarded and 700 µL washing Buffer RW1 were added and passed through the column by centrifugation (1 min

at 13,000 g). The RNA was washed twice with 500 µL RPE and the flow through was discarded. The column was moved to a new collection tube and centrifuged for additional 2 min at 13,000 g to dry the membrane. RNA was eluted from the column by using 50 µL RNase-free water and centrifugation for 1 min at 13,000 g. RNA was kept on ice and concentration was determined using the spectrophotometer NanoDrop 2000 system.

3.2.9   Gene expression analysis

3.2.9.1 TaqMan

Total RNA of cells was extracted using the RNeasy Plus Mini kit as described above (3.2.8). Total RNA was transcribed to cDNA using SuperScript III First-Strand Synthesis Supermix. The cDNA was synthesized from 500 – 1000 ng of total RNA. 0.5 µL of TaqMan Gene Expression assay was mixed with 1 µL cDNA, 3.5 µL H_2O and 5 µL TaqMan Fast Advanced Master Mix and transferred into a 384 well plate. A number of different TaqMan Gene Expression assays were used to determine expression of target genes (Table 7). The 384-well plates were centrifuged for 1 min at 500 g to spin down the reaction mixes. The plates were then kept in the dark at 4 °C until measurement in the HT7900 system using the following PCR protocol: 95 °C for 20 s, 40 cycles of 95 °C for 1 s followed by 60 °C for 20 s. The relative gene expression was calculated with the ΔΔCt method, using the average threshold for PPIA (peptidylprolyl isomerase A) to normalize gene expression between samples. All samples were measured in triplicate.

<u>ΔΔCt method</u>

1. $\Delta Ct = Ct_{target\ gene} - Ct_{housekeeping\ gene}$
2. $\Delta\Delta Ct = \Delta Ct_{treatment\ sample} - \Delta Ct_{control\ sample}$
3. $\Delta\Delta Ct = \Delta Ct - Ct$
4. $fold\ expression = 2^{-\Delta\Delta Ct}$

3.2.9.2 Apoptosis PCR array

Total RNA of cells was extracted using the RNeasy Plus Mini kit as described above (3.2.8). The cDNA was synthesized from 1000 ng total RNA using RT² First Strand Kit. It was added to 1048 µL H2O and 1150 µL 2x RT² SYBR Green ROX qPCR Mastermix. The cDNA qPCR

Materials and Methods

Mastermix was transferred into a Human Apoptosis PCR Array 384HT plate containing 384 specific primer pairs each being pre-coated in separate single wells. The plates were then kept in the dark at 4 °C until measurement. The following qRT-PCR protocol was run: 95 °C for 10 min, 40 cycles of 95 °C for 15 s followed by 60 °C for 60 s on the HT7900 system and the Ct values were determined using SDS software. Relative expression was calculated with the ΔΔCt method (3.2.9.1), using the average threshold for the human housekeeping genes B2M, GAPDH, HPRT1 and RPLP0 to normalize gene expression between samples.

3.2.9.3 Genome-wide expression profiling using microarray

The genome-wide expression data were generated by the Target Discovery Department at Bayer Pharma as described before (Hernando et al., 2016). In brief: total RNA was extracted from 200,000 human NSCLC DV90 cells seeded into six-well culture plates on the day before treatment. RNA was extracted from 4-5 replicate wells. Cells were treated with DMSO or the corresponding IC_{50} (135 nM) or IC_{90} (785 nM) dose of JQ1 in DV90 cells. RNA was extracted using RNeasy Kit. 250 ng of total RNA were amplified using the Affymetrix GeneChip WT PLUS Reagent Kit in accordance to the manufacturer's manual ("Target Preparation for GeneChip Whole Transcript (WT) Expression Arrays"). The Affymetrix Human Gene 2.1 ST 96-array plates were hybridized with 3 μg of fragmented and labeled single-strand cDNA. Microarrays were processed in accordance to the manufacturer's manual and scanned on an Affymetrix GeneTitan instrument. Data can be accessed at the gene expression omnibus (GEO) database (GSE75960).

3.2.10 Chromatin immunoprecipitation (ChIP) experiments

3.2.10.1   ChIP-sequencing (seq)

3.2.10.1.1   Optimization of DNA shearing conditions

Besides optimal immunoprecipitation conditions it is critical to optimize the DNA shearing conditions to produce the right fragment size for downstream applications like next generation sequencing techniques. The optimal fragment size of the DNA is around 150-900 base pairs (bps) length. The shearing conditions were optimized for the human NSCLC cell lines DV90 and H1373. To find the optimal conditions, 6×10^7 cells were detached by removing the culture medium through washing with cold PBS and addition of 5 ml Trypsin/EDTA to the

Materials and Methods

300 cm² culture flasks. Harvested cells were cross-linked using 1% methanol-free formaldehyde containing PBS for 10 min at RT before adding 1.25 M glycine containing PBS for 5 min at RT. The cells were lysed using 10 mL cold ChIP lysis buffer 1 on ice for 10 min split into separate tubes with an equivalent of 10^6 cells per tube each and centrifuged for 5 min at 2,000 g and 4 °C. The nucleus pellet was lysed using sonication buffer with ChIP sonication buffer containing either 0.1% or 0.75% SDS. The chromatin samples were transferred to 1.5 mL TPX vials. The samples were kept on ice and sonicated in an ice cold water bath in the Bioruptor with 1, 2 or 3 rounds of 7 cycles of 30 sec on / 30 sec off at highest intensity. Sheared chromatin was cleared by centrifugation for 10 min at 13,000 g and 4 °C. Crosslinking was reversed by adding 1 µL 5 M NaCl and incubating the samples at 65 °C overnight. 1 µL RNase was added to each sample and incubated for 1 h at 37 °C followed by addition of 1 µL proteinase K and 1 h incubation at 50 °C. Samples were then purified using the QIAquick PCR purification kit in accordance to the manufacturer´s manual. Buffer PB was added to each sample at 500 µL together with 10 µL of 3 M sodium acetate pH 5.0 to lower the pH for optimal DNA silica-membrane column binding conditions. The mixture was passed through the column by centrifugation at 13,000 g for 1 min. DNA was washed on the column using 750 µL of washing buffer Buffer PE followed by centrifugation at 13,000 g for 1 min. Residual buffer was removed by additional centrifugation at 13,000 g for 1 min after discarding the flow through. DNA was eluted by addition of 50 µL DNase/RNase free H2O and centrifugation for 1 min at 13,000 g. DNA was handled on ice and concentration was determined using the spectrophotometer NanoDrop 2000 system. Samples were diluted between two- to tenfold to adjust the DNA concentration to a range of 5-50 ng/ µL.

Samples were analyzed on 2100 bioanalyzer using the DNA1200 Assay. Gel-dye mix was generated by adding 25 µL DNA dye concentrate to the DNA gel matrix and mixed for 10 s. Gel-dye mix was spin-filtered at 1,500 g and 9 µL were transferred to a DNA chip and distributed on the chip with equal pressure for 30 sec using a syringe. 5 µL DNA marker were loaded on all 12 sample wells. DNA ladder was at a volume of 1 µL on the chip followed by 1 µL of the sheared purified DNA samples (5-50 ng). The 6 shearing optimization samples were measured in duplicates. The analysis showed that for both cell lines DV90 and H1373 2 rounds of 7 cycles of 30 sec on / 30 sec off at highest intensity together with 0.75% SDS containing ChIP sonication buffer yielded the optimal fragment size of DNA (150-900 bps) for ChIP-seq experiments. These conditions were therefore chosen to perform chromatin preparation at a larger scale.

Materials and Methods

3.2.10.1.2 ChIP-seq and Chem-seq sample preparation

Human NSCLC cells DV90 and H1373 were seeded into 15 x 300 cm² flasks. Cells were grown until they reached about 80-90% confluence and then harvested. Cells were detached by removing the culture medium, washing with cold PBS and adding 5 ml Trypsin/EDTA to each 300 cm² culture flasks. Harvested cells were cross-linked using 1% methanol-free formaldehyde containing PBS for 10 min at RT before adding 1.25 M glycine containing PBS for 5 min at RT. The cells were lysed using 10 mL cold ChIP lysis buffer 1 on ice for 10 min and centrifuged for 5 min at 2,000 g and 4 °C. The nucleus pellet was lysed using sonication buffer with ChIP sonication buffer containing either 0.75% SDS. The chromatin of an equivalent of 10^7 cells in 300 µL buffer was transferred to each 1.5 mL TPX vials. The samples were kept on ice and sonicated in an ice-cold water bath in the Bioruptor with 2 rounds of 7 cycles of 30 sec on / 30 sec off. Sheared chromatin from the same preparation was cleared by centrifugation for 10 min at 13,000 g and 4 °C and pooled after that. An equivalent of 6 x 10^7 cells was used as input for each IP. The 1.8 mL sheared chromatin was added to 7.2 mL ChIP sonication buffer without SDS to reduce the SDS concentration to 0.15% (w/v). 285 µL Dynabeads were incubated with either 12 µg of targeting antibody (Table 12) or 100 µM of biotin tagged BET inhibitor JQ1 (bio-JQ1) in the case of streptavidin Dynabeads on a rotator for 2 h at 4 °C prior addition to diluted ChIP samples. Samples were then incubated at 4 °C overnight on an overhead rotator at 15 rpm. Bound beads from the samples were collected using a magnetic rack. Beads were washed three times with 300 µL using ChIP shearing buffer containing 0.1% SDS. Samples were next washed with 300 µL of ChIP sonication buffer high salt followed by washing with 300 µL ChIP Li washing buffer. Samples were washed once more with 300 µL ChIP washing buffer before eluting samples using 100 µL of ChIP elution buffer-ChIP for antibody bound beads or 50 µL ChIP elution buffer-Chem in the case of bio-JQ1 bound beads. After elution 450 µL ChIP elution buffer-chem without SDS were added to Chem-seq samples. Input samples were prepared by using 1% input sample (18 µL) of sheared material and adding 82 µL ChIP sonication buffer without SDS. Crosslinking was reversed by adding 3.2 µL/100 µL sample of 5 M NaCl and incubating the samples at 65 °C overnight. 1 µL/100 µL sample of RNase A was added to each sample and incubated for 1 h at 37 °C followed by addition of 1 µL/100 µL sample of proteinase K and 1 h incubation at 50 °C. Samples were then purified using the QIAquick PCR purification kit in accordance to the manufacturer's manual. Buffer PB was added at a volume of 500 µL to each sample together with 10 µL of 3 M sodium acetate pH 5.0 to lower the pH for optimal DNA

silica-membrane column binding conditions. The mixture was passed through the column by centrifugation at 13,000 g for 1 min. DNA was treated using 750 µL of washing buffer Buffer PE followed by centrifugation at 13,000 g for 1 min. Residual buffer was removed by additional centrifugation at 13,000 g for 1 min after discarding the flow through. DNA was eluted by addition of 30 µL DNase/RNase free H2O and centrifugation for 1 min at 13,000 g. DNA was kept on ice and its concentration was determined using the spectrophotometer NanoDrop 2000 system. Samples were diluted between two- and tenfold to adjust the DNA concentration to a range of 5-50 ng/ µL.

3.2.10.1.3   ChIP-seq and Chem-seq sample library preparation and sequencing

The downstream processing of samples was performed by the Target Discovery Department at Bayer Pharma including quality control, library preparation and genome-wide sequencing. In brief, samples were analyzed on a 2100 bioanalyzer using the DNA high sensitivity assay described above (3.2.10.1.1). Concentration was determined using High Sensitivity DNA Kit. End repair and phosphorylation, ligation of TrueSeq index adaptor and amplification before subjection to sequencing (HiSeq Sequencing System) were done in accordance to the TrueSeq® ChIP Sample Preparation Guide (illumine).
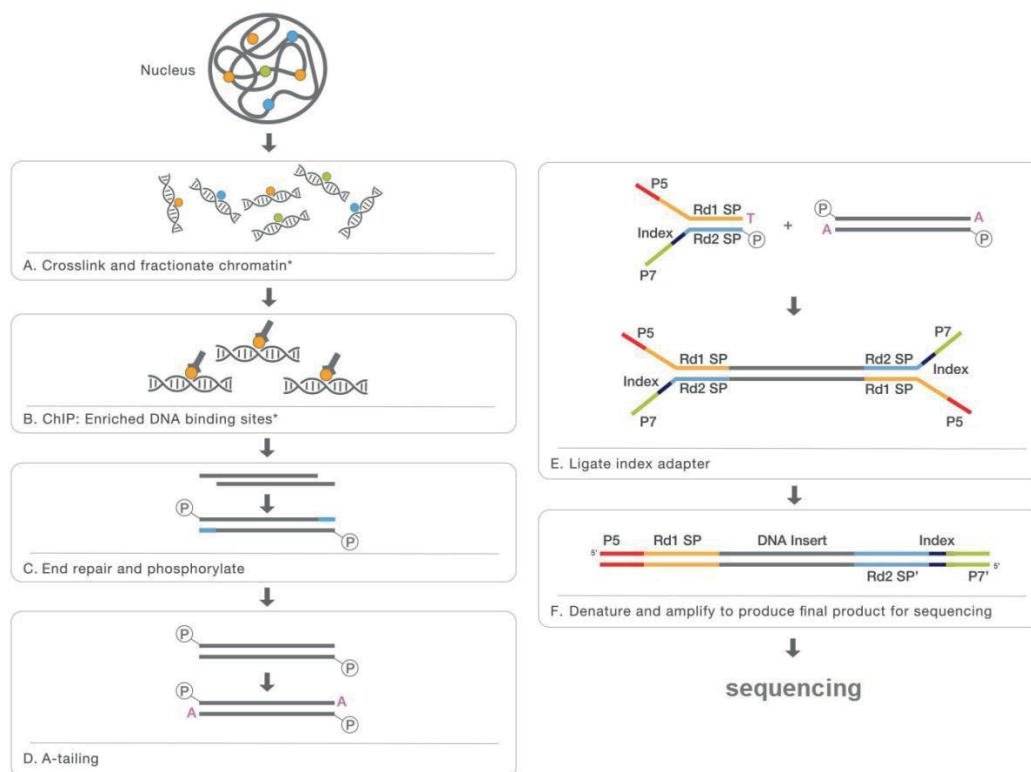
Figure 15: ChIP sequencing sample preparation: Including crosslinking of chromatin in the nucleus (A), chromatin immuoprecipitation/binding of biotin compound and enrichment of sheared DNA fragments (B) and library preparation steps end repair and phosphorylation (C), A-tailing (D), ligation of TruSeq index adaptors (E) and amplification of adaptor-sample DNA sequences (F). Process C-F was performed by the Target Discovery Department at Bayer Pharma. Adapted from (http://www.illumina.com).

3.2.10.2 ChIP quantitative real time-polymerase chain reaction (qRT-PCR)

Cells were seeded in 300 cm² culture flasks and treated with 500 nM JQ1 or DMSO vehicle for 6 h. Cells were washed and fixed with 1% formaldehyde containing PBS for 10 min at RT before adding 1.25 M glycine containing PBS for 5 min at RT. Cells were washed twice using cold PBS, harvested, snap-frozen and stored at -80 °C. $6x10^7$ cells were lysed using 5 mL cold ChIP lysis buffer 1 on ice for 10 min. Samples were centrifuged at 2,000 g for 5 min at 4 °C. Chromatin was isolated using 260 µL ChIP sonication buffer containing 0.1% SDS and transferred to Adaptive Focused Acoustics (AFA) fibre microtubes. Chromatin was sheared using a Covaris S220 device (10% duty cycle, intensity 5, cycle/burst 200) for 12 min at 20 W. Immunoprecipitation was performed using 3 µg of anti-BRD4 or non-specific IgG rabbit antibody. Antibodies were bound to magnetic beads coated with protein A at 4 °C for 2 h using a tube rotator at 25 rpm. Bound beads were washed 3 times with 300 µL ChIP sonication buffer containing 0.1% SDS, one time with ChIP sonication buffer high salt containing 500 mM NaCl, one time with ChIP LiCl washing buffer, one time with ChIP washing buffer. Bound complexes were eluted in 100 µL ChIP elution buffer-ChIP at 65 °C for 10 min. Crosslinking was reversed overnight at 65 °C in a thermixer followed by protein and RNA digestion using 1 µL proteinase K and 1 µL RNase A. DNA purification was performed using the QIAquick PCR Purification Kit. The qRT-PCR was performed mixing 1 µL ChIP sample, 3 µL H2O, 1 µL primers (Table 8) 5 µL 2x Maxima SYBR Green ROX qPCR Mastermix on a 384-well plate on the HT7900 system. The qRT-PCR protocol was run (95 °C for 10 min, 40 cycles of 95 °C for 15 s followed by 60 °C for 60 s) on the HT7900 system and the Ct values were determined using RQ manager software. Relative occupancy of BRD4 at the promoter target sites was calculated relative to the input control using the percent input method.

Materials and Methods

Percent input method

1. $Ct\ input\ _{(100\%)} = Raw\ Ct\ input\ _{(2\%)} - (\log_2(100) - 1)$
2. $Input\ _{(IP)} = 2^{Ct\ input\ _{(100\%)} - Ct\ input\ _{(IP)}}$
3. $Percent\ input\ _{(IP)} = 100\ x\ input\ _{(IP)}$

3.2.11 Plasmid amplification using bacteria culture and maxi preparation

For bacterial transformation competent XL1.blue cells were thawed on ice. 60 µL of bacteria were used for each transformation and were transferred to a 1.5 mL reaction tubes and 1 µL of β-mercapto-ethanol was added. Cells were mixed and incubated for 10 min on ice. 100 ng of the corresponding plasmid were added to the cells and incubated on ice for 1 h. Bacteria were heat-shocked at 42 °C in a thermomixer for 45 sec and after that transferred to ice for 2 min. 240 µL of 37 °C pre-warmed S.O.C medium were added and bacteria were incubated for 1 h at 37 °C and 500 rpm on a thermomixer. Bacterial suspension was then transferred to an agar plate containing the antibiotic (100 µg/mL for ampicillin and 50 µg/mL for kanamycin) addressed by the resistance cassette transferred by the plasmid used for transformation. Plates were incubated at 37 °C overnight. Resistant colonies were picked and incubated in 1 mL liquid LB medium containing the appropriate antibiotic for 6 h at 37 °C and 1000 rpm on a thermomixer. Medium was transferred to 200 mL liquid LB media containing the appropriate antibiotic for overnight incubation at 37 °C and 225 rpm shaking. Amplified plasmids were harvested using the EndoFree Plasmid Maxi kit in accordance to the manufacturer's manual.

3.2.12 BRD4 washout experiments

3.2.12.1 Chromatin separation assay

Cells were seeded at 1-2 x 105 cells/well in a 6-well plate on the day before treatment. On the day after, cells were treated with a dose range of JQ1 (0.01 µM – 5 µM) for 24 h. Culture medium was removed from cells. Cells were washed in cold PBS, and then lysed using WB lysis buffer (Mammalian protein extraction reagent (M-PER) buffer containing Halt Protease and Phosphatase inhibitor mixture). Lysates were incubated at RT for 10 min and chromatin and chromatin-bound factors were removed by centrifugation at 13,000 x g for 10 min. Protein concentrations were determined and equivalent amounts of the cytosolic chromatin-unbound fraction were subjected to western blot analysis as described (3.2.7).

Materials and Methods

3.2.12.2   BRD4-GFP overexpression washout experiment

Glass base dishes were incubated with culture media 1/20 matrigel basement at 37 °C for 1 h in the incubator to coat the glass bottom. H1373 cells were seeded in 1 mL culture medium at a density of 200,000 per well onto coated 27 mm-glass base dishes. Cells were transfected with 2 µg BRD4-GFP plasmid (pcDNA6.2/N-EmGFP-BRD4) (Table 10) using Lipofectamine LTX 24 h before washout. Plasmid was diluted in 150 µL Opti-MEM and 2 µL Plus Reagent was added. Lipofectamine LTX transfection reagent (10 µL) was diluted in 150 µL Opti-MEM and added to the diluted plasmid. After gentle mixing the mixtures were combined and incubated for 5 min. 250 µL were drop wise transferred to the H1373 cell covered with 2 mL FCS containing culture media. 24 h after transfection H1373 cells were inspected under the microscope to ensure expression of GFP in the cells. Cells were treated with 1 mL of 1 µM JQ1 or DMSO control containing culture medium for 2 h in the incubator. Culture medium was removed from the cells which were then washed in 1 mL PBS once. The detergent washout buffer 1 and CSK buffer were freshly prepared and kept at 4 °C. Cells were washed once with 700 µL cold CSK buffer. CSK buffer was then removed, 700 µL detergent washout buffer 1 were added and dishes were incubated for 5 min at 4 °C. Detergent washout buffer 1 was removed and cells were covered with 500 µL PBS containing 4% formaldehyde for fixation. Cells were fixed for 15 min at RT. After fixation cells were washed twice with 500 µL PBS and covered with 1 mL PBS containing 1 µg/mL DAPI and incubated for 1 h in the dark at 4 °C. The washout of BRD4-GFP was assessed using a laser scanning microscope and imaging was processed using Zeiss software.

3.2.12.3   BRD4 endogenous immunocytochemistry and washout experiment

The 4-well-chamber slides were incubated with culture media 1/20 matrigel basement at 37 °C for 1 h in the incubator to coat the glass surface. H1373 and A549 cells were seeded in 0.5 mL culture medium at a density of 50,000 per well onto coated 4well-chamber slides. One day after seeding H1373 cells were treated with 0.5 mL of 1 µM JQ1 or DMSO control containing culture medium for 2 h in the incubator. Culture medium was removed from the cells which were then washed in 0.5 mL PBS once. The Detergent washout buffer 1 and CSK buffer were freshly prepared and kept at 4 °C. Cells were washed once with 350 µL cold CSK buffer. CSK buffer was removed and 350 µL Detergent washout buffer 2 were added and dishes were incubated for 8 min at 4 °C. Detergent washout buffer 2 was removed and cells

were covered with 0.5 mL ice-cold methanol for fixation. Methanol fixation was chosen as PFA fixation led to unspecific staining of the anti-BRD4 antibody. Cells were fixed for 8 min on ice. After fixation cells were washed twice with 500 µL PBS. Cells were blocked using 350 µL of Immunofluorescence blot blocking solution for 45 min at RT. Cells were stained with 300 µL Immunofluorescence blot blocking solution containing 1/100 diluted anti-BRD4 antibody and 1/200 diluted anti-tubulin conjugated antibody (

Table 13) for 1 h at RT in the dark. Staining solution was removed and cells were washed 4 times with 500 µL PBS. Cells were then stained with 300 µL Immunofluorescence blot blocking solution containing 1/500 diluted anti-rabbit conjugated antibody for 30 min in the dark at RT. Chambers were removed from the slide and stained cells were covered with one drop ProLong Gold Antifade Reagent containing 1 µg/mL DAPI followed by addition of cover glass. Slides were kept in the dark overnight to dry. The washout of endogenous BRD4 was assessed using a laser scanning microscope at 630x magnitude and imaging was processed using Zeiss software.

3.2.13 Transfection of cell lines with small interfering RNAs (siRNAs)

For siRNA knockdown 200,000 cells per 6-well were seeded on the day before transfection with ON-TARGETplus-SMARTpool siRNAs using Oligofectamine Transfection Reagent, according to the manufacturer's instruction. Then culture medium was removed and cells were washed with culture medium without FCS. Washing medium was removed and 800 µL of FCS free medium were added to each 6-well. 5 µL of 20 µM siRNA stock solution (100 pmol) were diluted in 175 µL Opti-MEM. Oligofectamine of 4 µL volume was diluted in 15 µL Opti-MEM and incubated for 10 min at RT. Oligofectamine mixture and Oligonucleotide mixture were combined and incubated for 20 min at RT. Mixture containing complexes were transferred dropwise to the cells at a volume of 200 µL. Cells were incubated for 4 h in the incubator at 37 °C before 500 µL culture medium containing 3x the normal FCS concentration were added.

3.2.14 Gene knockout using CRISPR-Cas9 and HDR dependent selection

For CRISPR knockout 100,000 cells per 6-well were seeded on the day before transfection. Cells were transfected with 1-3 µg of CRISPR KO plasmid pool and equal amount of corresponding HDR plasmid pool (Table 10) using Lipofectamine LTX 24 h before selection of stable knockout clones. Plasmids were diluted in 150 µL Opti-MEM and 2-6 µL Plus

Reagent was added. Lipofectamine LTX transfection reagent of 5-10 µL volume was diluted in 150 µL Opti-MEM and added to the diluted plasmids. After gently stirring the mixtures were combined and incubated for 5 min. The transfection mixture containing formed complexes of 250 µL volume was transferred drop wise to the cells covered with 2 mL FCS containing culture medium. One day after transfection cells culture medium was removed and replaced with culture media containing 1-3 µg/mL puromycin. The selection media was replaced every second day. Selection was ensured using a microscope.

Cells were co-transfected as described above using pooled CRISPR-Cas9 knockout (KO) plasmids and homology-directed DNA repair (HDR) plasmids, corresponding to the cut sites generated in the coding region of the target gene by the CRISPR/Cas9 KO plasmids. HDR of the cell leads to integration of the CMV promoter driven puromycin resistance cassette and red fluorescent protein (RFP) (Table 10). Stable knockout cells were selected using previously optimized doses of puromycin dihydrochloride and cultured for 2 weeks. Stable gene knockout was confirmed by western blot.

3.2.15 *MYC* overexpression rescue experiments

For the *MYC* overexpression rescue 300,000 H1373 cells per 6-well were seeded on the day before transfection. Cells were co-transfected as described above using a human c-Myc cDNA construct or empty control vector and TagGFP construct (Table 10) using Lipofectamine LTX 24h before treatment with JQ1. About 5 µg of c-Myc cDNA construct or empty vector plasmid and 1 µg of TagGFP construct were diluted in 150 µL Opti-MEM and 6 µL Plus Reagent were added. Lipofectamine LTX transfection reagent of 10 µL volume was diluted in 150 µL Opti-MEM and added to the diluted plasmids. After gentle stirring the mixtures were combined and incubated for 5 min. The transfection mixture containing formed complexes of 250 µL were transferred drop wise to the cells covered with 2 mL FCS containing culture medium. One day after transfection cell culture medium was removed and replaced with culture media containing 500 nM JQ1 or DMSO control. After 24 h cells were stained using EdU-staining kit and DAPI, and then analyzed as described above (3.2.5).

3.2.16 In vivo mouse studies

All experiments were performed in accordance to the German Animal Welfare Law. Animals were housed following institutional guidelines of Bayer Pharma AG.

Materials and Methods

Six to eight weeks old female SCID mice from Charles River were acclimated for at least seven days before tumor cell injection.

3.2.16.1 Subcutaneous xenograft mouse model H1373

H1373 tumor cells growing exponentially in cell culture were detached using trypsin/EDTA, resuspended in culture media and cell number and viability was determined. The right number of viable cells was calculated and cells were washed in PBS and re-suspended in cold matrigel/culture media without FCS mixture (1:1). H1373 tumor cells were inoculated subcutaneous (s.c.) into the right flank of the mice (3×10^6 cells/mouse in 0.1 mL).

For intra peritoneal (i.p.) injection, JQ1 was dissolved in 30% 2-hydroxypropyl-beta-cyclodextrin (HP-β-CD) in water, pH6 and applied daily with a volume of 10 mL/kg.

3.2.16.2 Subcutaneous xenograft mouse model A549

A549 tumor cells were prepared as described above and inoculated s.c. in female SCID mice at 3×10^6 cells/mouse in 0.1 mL matrigel. Tumor growth was assessed twice a week using a caliper and tumor volume was calculated as described below (3.2.19.1). Tumor bearing mice were randomized before start of treatment. Mouse body weight was determined at least twice a week. For i.p. injection, JQ1 was dissolved in 20 or 30% 2-hydroxypropyl-beta-cyclodextrin (HP-β-CD) in water, pH5-6 and applied daily with a volume of 10 mL/kg. Cisplatin was diluted in NaCl 0.9% pH4-5 and applied 5 times daily intra venouse (i.v.) with a volume of 10 ml/kg or i.p..

3.2.16.3 Evaluation of antitumor efficacy

Tumor growth was assessed using a caliper and tumor volume was calculated using the empiric formula for calculation of tumor volume.

$$tumor\ volume = \frac{length \times width^2}{2}$$

Tumor-bearing mice were randomized before start of treatment. Mouse body weight was determined at least twice a week. Treated over control ratio (T/C) was calculated as mean

Materials and Methods

tumor weight of the treated group divided by mean tumor weight of the vehicle control group at the end of the study (%T/C ≤42% was declared active in agreement with NCI criteria).

$$(\%)\frac{T}{C} = \frac{\frac{1}{n}\sum_{i=1}^{n} X_{i(treated)}}{\frac{1}{n}\sum_{j=1}^{n} X_{j(vehicle)}} \times 100\%$$

Tumor volumes were $\log_{10}$ transformed for statistical analysis. For in vivo experiments One-way analysis of variance (ANOVA) with Sidak's correction for multiple comparisons or two-tailed t-test from GraphPad Prism 6.0 was used. Adjusted p values are indicated using * for p < 0.05, ** for p < 0.01, *** for p < 0.001.

3.2.17 Bioinformatics

3.2.17.1   Gene expression profiling of DV90 NSCLC and gene set enrichment analysis

Cells were treated with DMSO or JQ1 before RNA was extracted and profiled with Affymetrix HuGene-2.1ST arrays as described above (3.2.9.3). Data are available at the GEO database (GSE75960). Probe set intensities were condensed to meta-probe set levels in Genedata Expressionist 9.0 using Robust Multi-array (RMA) algorithm followed by LOWESS normalization. A 2 group t-test was used to compare each treatment condition: 4 h IC_{50} (135 nM) or IC_{90} (785 nM) and 24 h treatment period with JQ1 with the 4 h or 24 h DMSO control group. The resulting p-values were corrected for multiple testing using Benjamini-Hochberg correction (BH-q). Genes with a BH-q value < 0.05 were considered to be significantly altered by the treatment. Additionally a cut-off level of a $\log_2$ (fold change) of ± 0.5 was used to define a list of significantly differentially expressed genes.

3.2.17.2   Gene set enrichment analysis of JQ1-treated DV90 NSCLC expression profile

For the standardization the median value for each gene across replicates (n = 4-5) from DV90 micro-array expression profiling was taken. Gene set enrichment analysis (GSEA) (http://www.broadinstitute.org/gsea) was used to determine enrichment of genes down-regulated by JQ1 treatment in DV90 cells. To test which gene sets were associated with a given phenotype (here 24h of IC_{50} JQ1 treatment), all current gene sets from the Molecular

Signatures Database were used (Msigdb.v5.0). Gene sets enrichment calculates whether a given gene set is enriched at the top or the bottom of a given ranked gene list. The ranked list here consists of all genes identified by expression profiling with the Affymetrix HuGene-2.1ST array and Affymetrix HuGene-2.1st annotation. Duplicate gene identifiers were removed leaving the probe set identifiers with the highest expression. The list was ranked by the difference between expression of DMSO control and JQ1 treated cells. The resulting enrichment score (ES) quantifies the degree of overrepresentation of given gene from a gene set at the top or bottom of the list. A p-value is estimated on the base of the empirical permutation test based on the phenotype. The ES is further normalized to the variation depending on the set size resulting in a normalized enrichment score (NES). The corresponding false discovery rate (FDR) is calculated based on a permutation test, testing a null hypothesis on the distribution of all gene sets used for the given NES. The resulting plots indicate a NES for each gene in an enriched list on the left for the DMSO phenotype or the right for the JQ1 treatment phenotype. Most gene sets locate either on the left or on the right are significantly enriched when the normalized p-value was $p < 0.05$ and $FDR < 0.1$.

3.2.17.3   Patient expression profile analysis using gene set enrichment analysis

Publicly available mRNA expression profiles of lung adenocarcinoma patients - accessible from GEO database (GSE32863) (Selamat et al., 2012) were used. The datasets were accessed by loading the data into Genedata Expressionist and robust spline normalized prior to $\log_2$ transformation. Datasets from patients with defined *KRAS* mutation status were exported and analyzed using GSEA as described above (3.2.17.2). The analyzed gene sets were all Hallmark gene sets (h.all.v5.0). The rank gene list was defined by the difference of expression levels between the average of *KRAS* mutant (n= 21) and the average of *KRAS* wild-type patient (n= 36) expression profiles. Core enrichment profile for the "Hallmark Myc gene signature" was generated using the GSEA tool.

3.2.17.4   Processing of FASTQ ChIP sequencing files

Sequencing data were provided by the Target Discovery Department at Bayer Pharma. The provided FASTQ file containing the raw sequencing reads were aligned using Genedata Refiner Genome integrated script Bowtie (version 2). Bowtie is a high performance alignment tool designed to perform multiple alignments of next generation sequencing data to a

reference genome. The FASTQ files were aligned to the human genome hg19, sorted and indexed using SAMtools. Model-bases Analysis for ChIP-seq (MACS2) software was used on the aligned paired-end reads of ChIP and input samples as a reference to call peaks from enriched regions. Broad peaks from histone marks were called using MACS2 broad mode. The cutoff used for broad and regular peaks was q < 0.1. MACS2 was used to generate bedGraph files containing fragment pileup per million reads. Log likelihood ratio (logLR) of treatment vs. input control samples tracks were generated using MACS2 bdgcmp command. LogLR subtracts the background noise from the treatment samples signal based on a dynamic Poisson model. Pseudocount of 0.00001 was added to avoid $\log_{10}(0)$ during logLR calculation. Files were sorted using bedSort (bedTools v2.26.0)

In order to transform bedGraph files to bigwig bedGraphToBigWig script was used. It uses a combination of slopBed (bedTools) and bedClip (bedTools) together with the chromosome size from the hg19 genome (http://hgdownload.cse.ucsc.edu/goldenPath/hg19/) to remove the section expanding beyond chromosome range, followed by conversion to BigWig using bdg2bw script. ChIP-seq tracks were generated using IGV software. Heatmaps and line plots were generated using seqplots software.

3.2.17.5 Super-enhancer annotation and ranking

Rank ordering of super-enhancers (ROSE) script (Loven et al., 2013; Whyte et al., 2013) was used to generate stitched enhancers and to separate super-enhancers from typical enhancers. Therefore ROSE stitches putative enhancers of close proximity, no farther than 12.5 kb, from one another. Putative enhancers were H3K27Ac$^+$ peaks identified from ChIP-seq datasets as described above. The 2.5 kb region around the TSS of genes was excluded. The bamToGFF script is used to calculate the read density of the ranking BAM file (MED1) and the control BAM file (whole cell lysate input control) in units of reads-per-million-mapped per bp (rpm/bp). Finally the stitched enhancers were sorted by signal (ranking BAM density – control BAM density) into two groups, namely super-enhancers and typical enhancers. Super-enhancers were annotated to their closest coding gene using PeakAnalyzer v1.4. PeakAnalyzer annotation was done using the Homo_sapiens.GRCH37.64gtf as a reference. Even though this method is not very accurate in assigning typical enhancers to their genes (Mora et al., 2015) it has been shown to be quite accurate in case of super-enhancer assignment (Whyte et al., 2013).

3.2.18 Statistical analyses

For statistical analyses of experiments, One-way analysis of variance (ANOVA) with Sidak's correction for multiple comparisons or two-tailed t-test from GraphPad Prism 6.0 or GeneData Expressionist was used. Adjusted p values are indicated using * for $p < 0.05$, ** for $p < 0.01$, *** for $p < 0.001$.

4. Results

4.1 BET inhibitors show differential anti-tumor activity in a panel of NSCLC cell lines

BET inhibitors are active in a wide range of tumor types (Table 2). Nevertheless their anti-tumor activity can be quite diverse, even within a defined cancer indication. Recent studies have proposed the transcriptional deregulation of oncogenes like *GLI* (Tang et al., 2014), *FOSL1* (Lockwood et al., 2012), *MYCN* or *MYC* (Delmore et al., 2011; Zuber et al., 2011) by BET inhibitors to be a critical factor for the anti-tumor activity in a number of indications including lung cancer (Lockwood et al., 2012; Shimamura et al., 2013). A number of mouse models recapitulating the development and growth of malignant tumors are available to study cancer biology. Among these, the *KRAS*-driven mouse model has become the golden standard to study NSCLC. This genetically engineered mouse model (GEMM) harbors a lox-STOP-lox KRASG12D cassette in the second exon of the endogenous *KRAS* gene. Time- and tissue-specific expression of the CRE-recombinase introduced by adenovirus transduction leads to mutation of the *KRAS* gene in lung epithelial cells and formation of tumors. Recently the inhibition of c-Myc transcription factor by its engineered dominant-negative form Omomyc, provided evidence that c-Myc function was essential for continuous growth and survival of *KRAS*-driven tumors in the GEMM (Soucek et al., 2013).

4.1.1 Human *KRAS* mutant adenocarcinomas are enriched for the hallmark c-Myc target gene signature

The expression profiles of adenocarcinomas from patients with defined *KRAS* status (publically available at GEO database (GSE32863)) were compared to evaluate the enrichment of hallmark gene sets (3.2.17.2). Gene set enrichment revealed that the *KRAS*-mutated NSCLC patient population (n=21) had a significant enrichment of c-Myc hallmark target genes compared to patients with wild-type *KRAS* (n=36) with a normalized enrichment score (NES) of 1.72 (Figure 16A). *KRAS* signature, which served as a control, was also enriched in the *KRAS* mutant population (Figure 16B). In addition the *KRAS* mutant patient population had significantly increased *MYC* expression levels, which would explain the enrichment of its target genes (Figure 16C).

Results
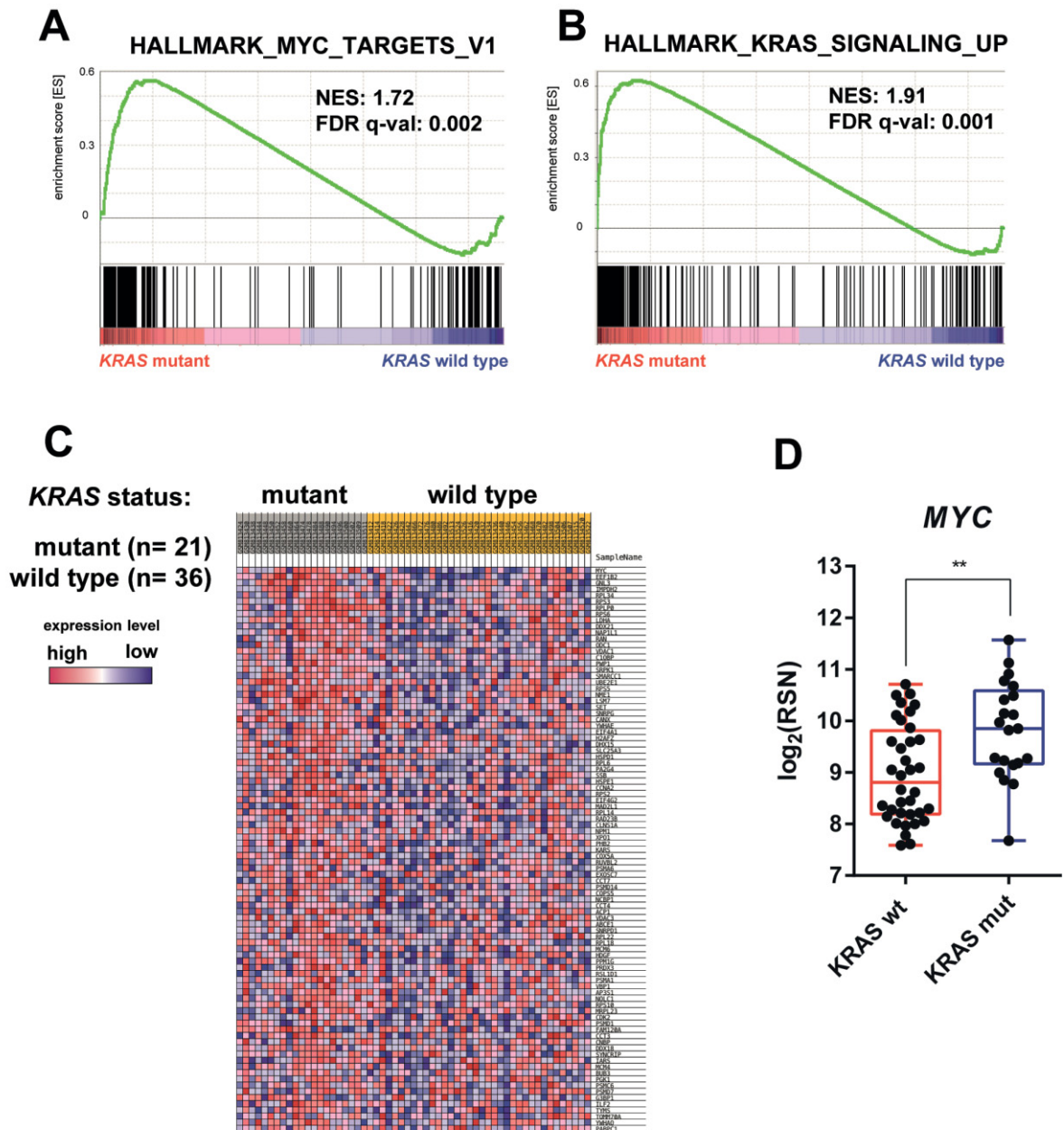
Figure 16: Gene set enrichment analysis comparing expression profiles of *KRAS* mutant and wild-type adenocarcinomas from GEO database (GSE32863). A, B: Enrichment plots indicating the enrichment score of HALLMARK_MYC_TARGETS_V1 and HALLMARK_KRAS_SIGNALING_UP gene sets comparing *KRAS* mutant (n=21) and *KRAS* wild-type (n=36), Normalized enrichment score (NES) and the corresponding false discovery rate (FDR). C: Heatmap of core enriched genes from the HALLMARK_MYC_TARGETS_V1 gene set comparing *KRAS* mutant and *KRAS* wild-type samples. The color code indicates the relative expression levels of the genes listed on the right and ranked by position in the overall rank list (red = high expression to blue = low expression). *KRAS* mutant samples names are highlighted in grey and *KRAS* wild-type in yellow. D: Plot showing the expression of *MYC* after Robust Spline normalization (RSN) and log$_2$ transformation. Dots indicate the expression of the individual patient samples within the *KRAS* wild-type (wt) and *KRAS* mutant (mut) populations. ** p > 0.01 unpaired parametric two-tailed t-test.

Results

Following this observation, the first aim of this work was to evaluate and characterize the effect of BET inhibitors on a number of defined *KRAS* mutant NSCLC cell lines *in vitro,* as BET inhibitors potently reduce the growth of *MYC*-dependent malignancies like MM and acute myeloid leukemia (AML) (Delmore et al., 2011; Zuber et al., 2011).

4.1.2 Determination of cellular half-inhibitory concentrations of BET inhibitors in a panel of NSCLC cell lines

To investigate the effects of the pan-BET inhibitors JQ1 and I-BET762 on cell growth and cell viability, a panel of 12 *KRAS*-mutated NSCLC cell lines were seeded at optimal cell density (3.2.2) and treated for 72 h with different doses of BET inhibitors ($10^{-8.5}$ M to 10^{-5} M). The cellular half-inhibitory concentration (IC_{50}) served as an indicator to identify distinct subgroups of cell lines that were either particularly sensitive or resistant to BET inhibition (Figure 17A). The BET inhibitors JQ1 and I-BET762 showed a similar activity pattern in the 12 cell lines tested, providing evidence that the effect seen was target dependent. However, i*n vitro* JQ1 showed an overall higher activity compared to I-BET762. The growth of the cell lines DV90, H1373 and LCLC97TM1 was particularly sensitive towards BET inhibition with IC_{50} values of 106 nM, 154 nM and 405 nM for JQ1 and 139 nM, 350 nM and 752 nM for I-BET762 respectively. The NSCLC cell lines showed overall a low mutation frequency of additional oncogenic drivers known in this tumor type, with the exception of a *HER2* mutation in DV90 cells, a *MEK1* and *PIK3CA* mutation of H460 cells and a *NRAS* mutation in H2347 (Figure 17B). Interestingly the mutation status of the p53 tumor suppressor gene was independent from the sensitivity towards BET inhibition, while another tumor suppressor *Liver kinase B1* (*LKB1*) was frequently mutated in the less sensitive cell lines H23, A549, H460 and H2030. This was in accordance with a recent study demonstrating that *KRAS/LKB1* double mutant cells were less sensitive to BET inhibition (Shimamura et al., 2013). Co-occurring genetic alterations of *KRAS* and the *LKB1* tumor suppressor gene leads to a more aggressive type of lung cancer and define a major subgroup of *KRAS*-mutated NSCLC (18-32%) (Ji et al., 2007; Skoulidis et al., 2015).

Results

Figure 17: Determination of the cellular half inhibitory concentration (IC_{50}) of BET inhibitors in 12 *KRAS*-*mutated* NSCLC cell lines. A: $Log_{10}IC_{50}$ from cell viability assays using *KRAS* mutant NSCLC cell lines after 72 h treatment with JQ1 or I-BET762. The data are represented as the mean IC_{50} of 2 or 3 independent experiments. B: Mutation status from the Cancer Cell Line Encyclopedia (CCLE) and Catalogue of Somatic Mutations in Cancer (COSMIC) databases of the tested NSCLC cell lines sorted by JQ1 sensitivity.

It was then evaluated whether the cell lines which were most sensitive to BET inhibition were also the fastest growing ones. No big differences in terms of growth rate was observed when comparing the cell doubling time *in vitro* at three different cell densities and still growing exponentially after 4 days, except for two cell lines growing significantly faster (A549 Dt= 25.3h; H460 Dt= 18.3h) and 2 others growing significantly slower (H2347 Dt= 40.3h; H358 Dt= 37.7h) (Figure 18A). The sensitivity to BET inhibition was not dependent on the respective basal growth rate of the cell lines.

Gene expression patterns of cancer cell lines can differ significantly, dependent on their genetic and epigenetic status. Gene expression of the BET family (*BRD2, BRD3* and *BRD4*) was therefore compared between the 12 cell lines, normalized to the expression of the stem cell derived normal human lung fibroblast cell line WI38 and to the expression of early passage primary fibroblast cells IMR-90. *BRD2*, *BRD3* and *BRD4* are ubiquitously found in human cells (Loven et al., 2013) and there were only slight differences in their expression levels (Figure 18B), in line with their essential cellular functions including transcriptional regulation, DNA replication, cell cycle progression and maintenance of higher-order chromatin structure (Jung et al., 2015; Wang et al., 2012).

Results
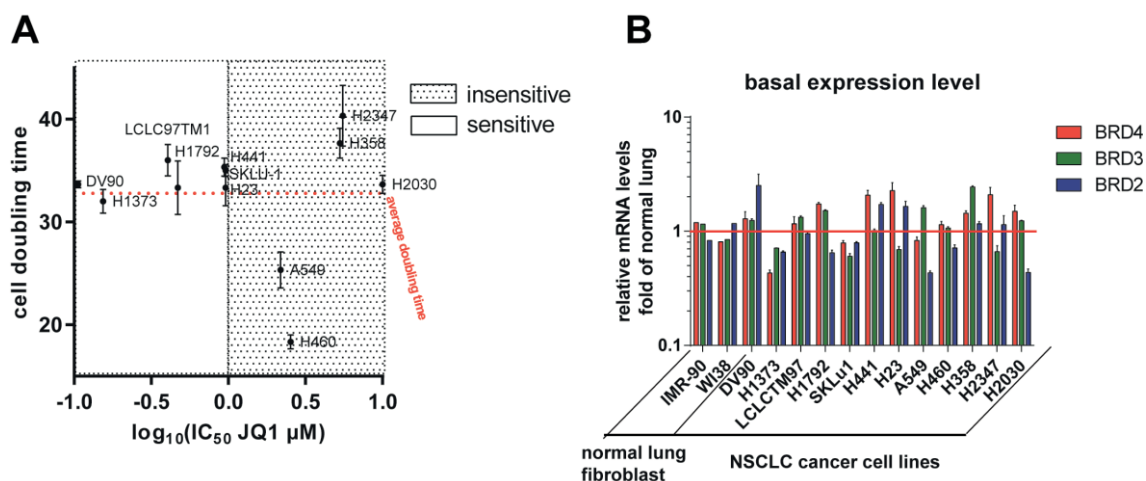
Figure 18: Correlation of JQ1 sensitivity and cell doubling time or basal expression of *BRD2*, *3* or *4*. A: Plot showing the cell doubling time of the 12 NSCLC cell lines test. JQ1 sensitive cells (< 1 µM) and insensitive cells (> 1 µM) against the $\log_{10}IC_{50}$ of JQ1 from the 72h cell viability assay are highlighted. The average doubling time of all 12 NSCLC cell lines is indicated in red. Data represent mean ± SEM. B: Relative expression of the 12 NSCLC cell lines. Basal expression of *BRD2*, *BRD3* and *BRD4* was calculated using ΔΔCt method normalized on the endogenous housekeeping gene cyclophilin A (*PPIA*) and normal lung fibroblast expression. Error bars denote SEM (n=3).

4.1.3   Analysis of functional BRD4 inhibition and resulting cellular phenotypes

4.1.3.1 Cell cycle distribution analysis and determination of apoptosis after BET inhibition

To further characterize the effect of BET inhibitors on the cellular phenotype a cell cycle distribution assay was performed using a flow cytometry EdU staining assay. EdU is a nucleotide analog that gets incorporated into the genomic DNA during the synthesis (S) phase of the cell. EdU can be specifically stained and used, together with the DNA content stained by DAPI, to determine the cell cycle phases of the cell.

In both sensitive and resistant cell lines the cell cycle distribution was determined after 24 h of treatment with the BET inhibitors JQ1, OTX-015 or I-BET762. H1373 and DV90 cells showed a dose-dependent shift from S phase towards G0/G1-population upon treatment (Figure 19A, B), with a stronger effect in H1373 compared to DV90 cells.

Results
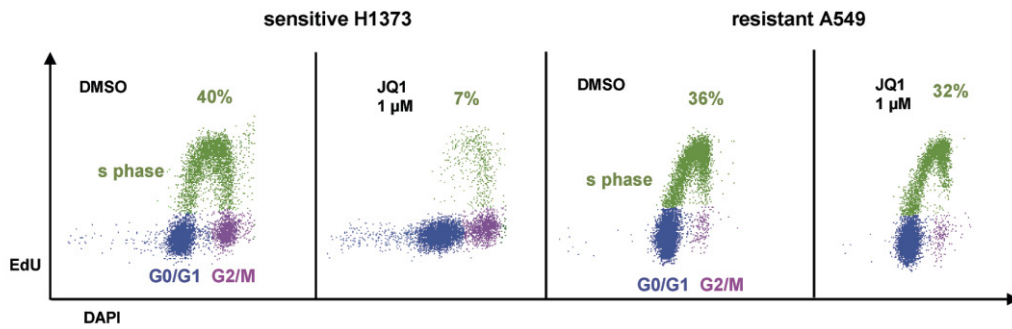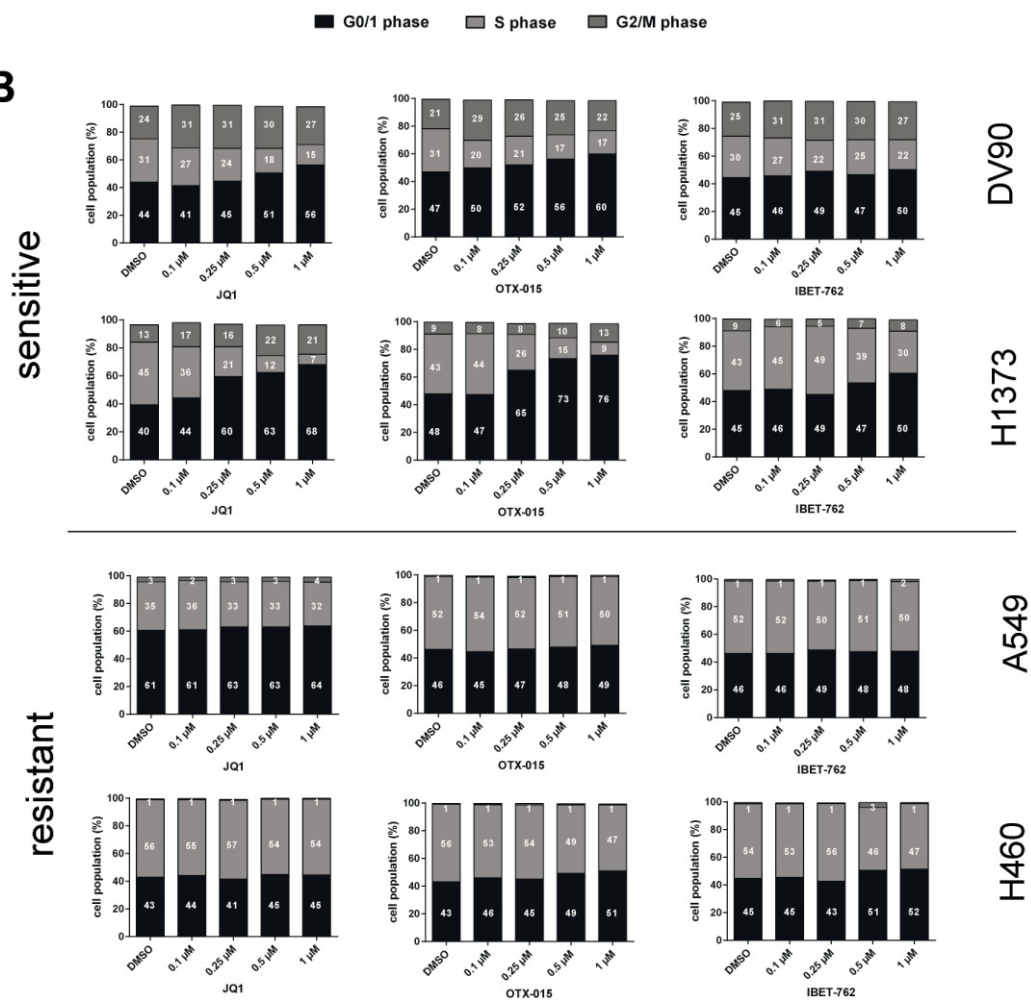
Figure 19: Cell cycle distribution analysis of two sensitive cell lines H1373, DV90 and two insensitive cell lines A549 and H460 after BET inhibitor treatment. A: Representative cell cycle distribution of viable H1373 or A549 cells 24 h after 1 μM JQ1 treatment. The S-phase cell population is shown in green, G0/G1 in blue and G2 in purple. B: Cell cycle analysis of sensitive DV90 and H1373 and resistant A549 and H460 cells following 24 h of JQ1, OTX-015 or I-BET762 treatment. Data are shown as the mean (n=2) for JQ1.

Results

Additionally, induction of programmed cell death was determined in H1373, DV90, H460 and A549 cells. Dose-dependent induction of apoptosis after 48 h of JQ1 or OTX-015 treatment was observed in sensitive DV90 and H1373 cells but not in resistant A549 and H460 cells, irrespective of the p53 status of the cells (Figure 20). Interestingly, in sensitive cell lines, the induction of apoptosis was stronger in DV90 compared to H1373 cells, suggesting that the predominant response in DV90 cells is induction of apoptosis, while in H1373 it is primarily cytostatic. It is noteworthy that both DV90 and H1373 cells were quite sensitive towards detachment from the culture surface and re-suspension, a procedure needed for flow cytometer analysis, which explains the higher apoptotic rates of DMSO control samples.
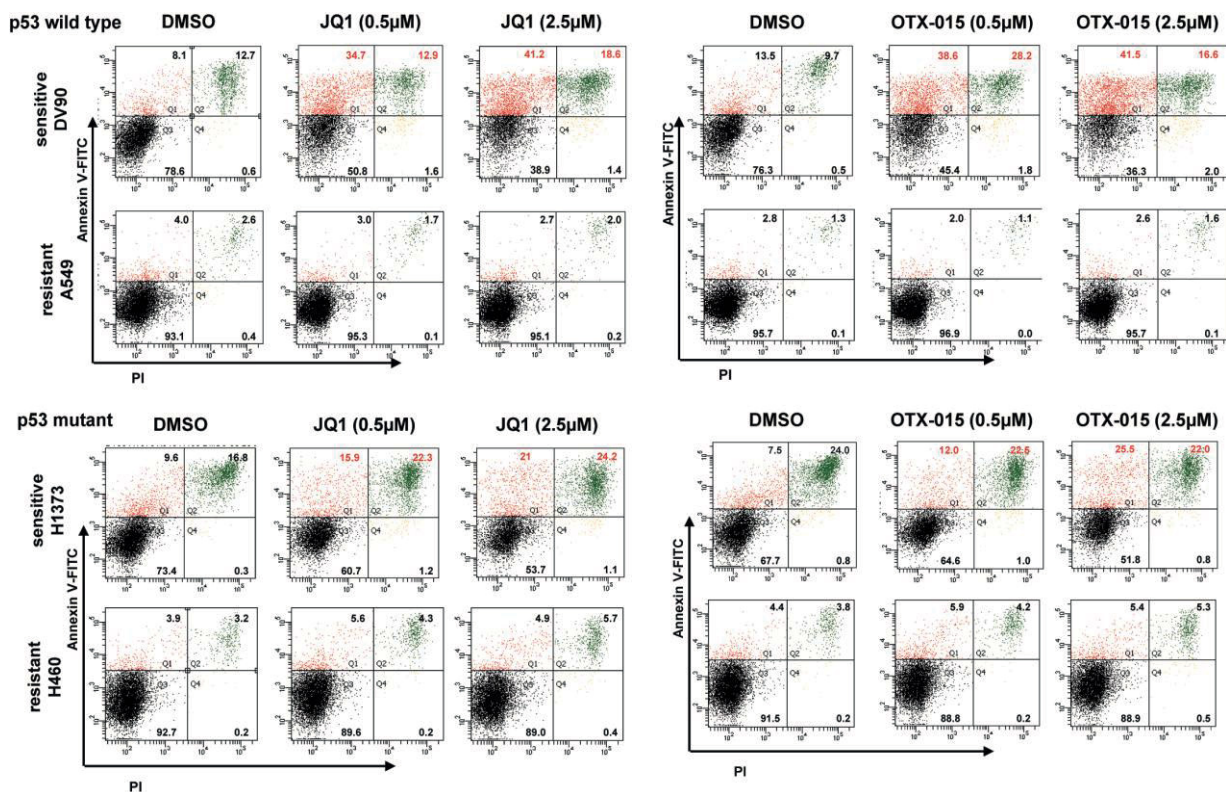
Figure 20: Analysis of apoptosis in two sensitive cell lines H1373, DV90 and two insensitive cell lines A549 and H460 after BET inhibition. Flow cytometry results showing percentage of viable and apoptotic cells of H1373 and H460 cells after JQ1 or OTX-015 treatment for 48 h followed by AV-FITC and PI staining. AV-positive only population (red: early apoptotic), AV/PI- double positive population (green: late apoptotic), AV/PI negative population (black: viable) and PI positive only (yellow: necrotic).

Results

4.1.3.2 Functional analysis of BET inhibition in the cellular context

BET inhibitors are competitive binders of the bromodomain pockets and interfere with BET – chromatin interactions. In order to investigate the cellular function of BET inhibitors in removing BRD4 from chromatin of the cell, H1373 cells were treated with 1 µM of JQ1 24h post transfection with a pcDNA6.2 plasmid overexpressing N-EmGFP-BRD4. Expression of BRD4-GFP was visually confirmed using microscopy. The unbound BRD4 was washed out of the nucleus using a detergent buffer containing Triton X-100 and PIPES (3.2.12.2). Cells were then fixed using paraformaldehyde and counterstained with DAPI in PBS before visualization using microscopy. BRD4-GFP was localized only in the nucleus, as seen by the overlap of DAPI and BRD4-GFP. In the DMSO-treated control, nuclei still containing BRD4-GFP were observed, while no BRD4-GFP could be detected in the nuclei of JQ1-treated cells after the washout was performed (Figure 21).
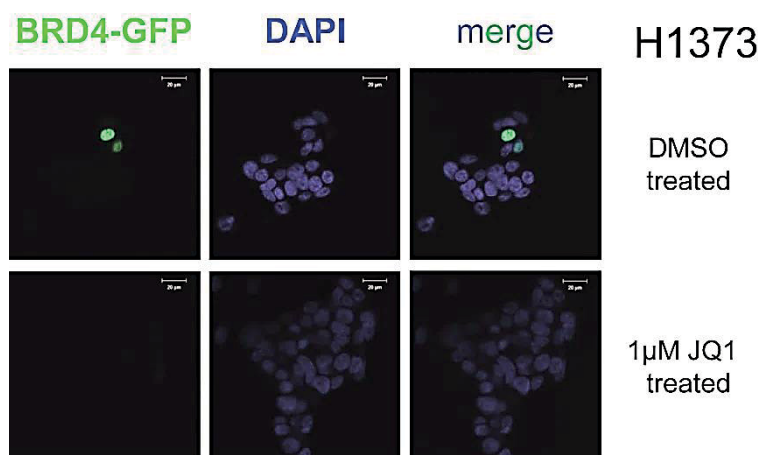
Figure 21: Chromatin-unbound washout experiment of BRD4-GFP overexpression plasmid transfected H1373 cells. H1373 cells were transfected with N- terminal tagged BRD4 full-length overexpression plasmid 24 h prior treatment with 1 µM JQ1 and chromatin-unbound washout using Detergent washout buffer 1 before fixation using para-formaldehyde and DAPI counter staining (3.2.12.2). Fluorescence was visualized using microscopy and 500-fold magnification. White bar indicates 20 µm.

While most small molecules can penetrate into the cells by passing the cellular membrane without active transport, cancer cells have been described to export small molecules actively by transporters like P-glycoprotein or Multidrug-Resistance-Protein-1 (MDR-1) and thereby acquiring resistance to chemotherapy. To investigate whether the differential response of the different cell lines was linked to a reduced intracellular function of JQ1, endogenous BRD4

Results

was washed out after treatment of sensitive H1373 cells and insensitive A549 cells. Similar to the BRD4-GFP fusion, the endogenous BRD4 was strongly removed by the washout detergent when cells were treated with 1 µM JQ1 2 h before the washout (3.2.12.2). To be noted that harsher washout conditions were needed (3.2.12.3). Potentially due to the stronger interaction of the native form compared to the BRD4-GFP fusion protein , even though it was taken care of adding GFP at the N terminal site in order to maintain the interactions of the extra-terminal domain and the C terminal motif (Figure 6). JQ1 was able to reduce BRD4 chromatin interaction in sensitive H1373 cells and insensitive A549 cells (Figure 22).
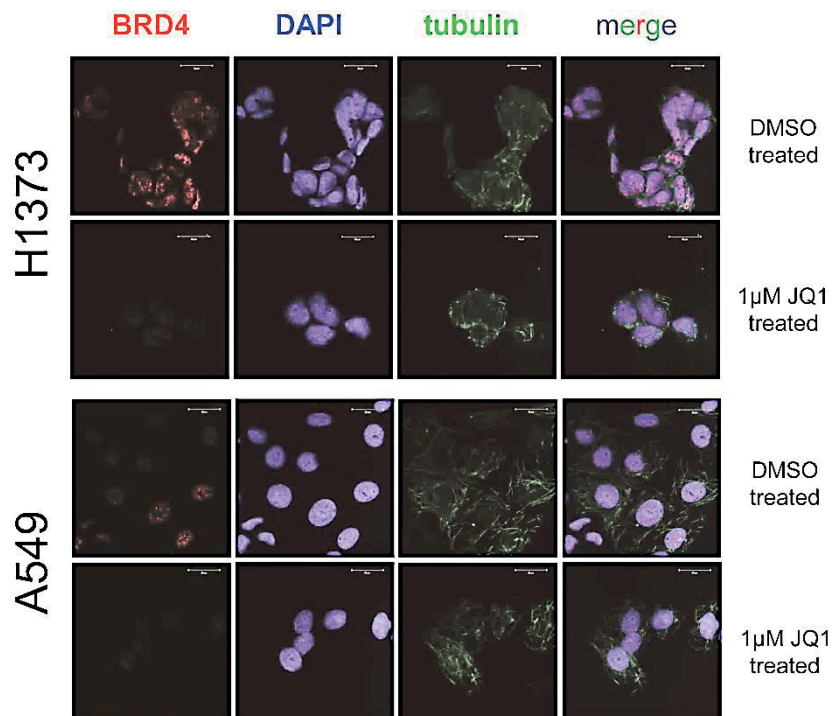
Figure 22: Washout experiments of chromatin-unbound endogenous BRD4 after JQ1 treatment of sensitive H1373 cells and insensitive A549 cells. H1373 cells were treated with 1 µM JQ1 for 2 h and chromatin-unbound washout using Detergent washout buffer 2 before fixation using Methanol and stained with primary BRD4 antibody, alexa 488-conjugated tubulin antibody and DAPI (3.2.12.3). Fluorescence was visualized using microscopy and 630-fold magnification. White bar indicates 20 µm.

To confirm this finding, a chromatin separation assay was used to separate the chromatin-bound fraction from the chromatin-unbound and cytosolic fractions. Sensitive DV90 and H1373 cells and insensitive H2030 cells were treated with varying doses of JQ1 (0.01 µM – 5 µM) for 24 h followed by complete lysis of the cells using M-PER buffer containing protease inhibitor and centrifugation (3.2.12.1). Chromatin free lysates were analyzed using western

Results

blot staining for BRD4 and GAPDH loading control. In all 3 cell lines JQ1 treatment led an increase of chromatin-unbound BRD4 in a dose-dependent manner. In DV90 cells a low level of BRD4 was chromatin-unbound even in the DMSO control, but increasing doses of JQ1 led to an even higher unbound fraction (Figure 23). The effective removal of BRD4 from the chromatin by JQ1 was seen in all 3 cell lines and was independent of the anti-proliferative activity of the compound.
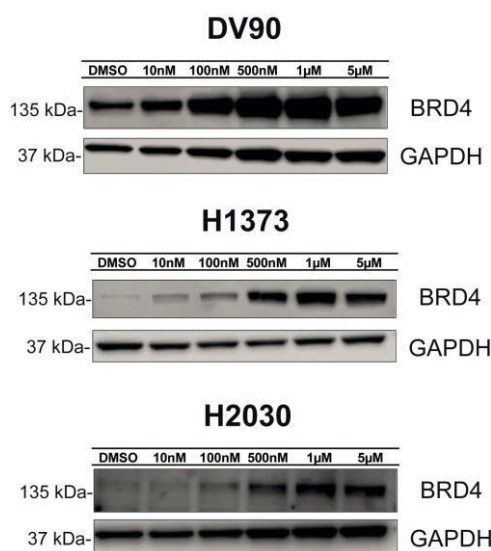
Figure 23: Western blot analysis of chromatin-unbound BRD4 after JQ1 treatment of sensitive DV90, H1373 cells and insensitive H2030 cells. For the separation of chromatin-bound and chromatin-unbound/cytoplasmic fraction DV90, H1373 and H2030 cells were treated with varying doses of JQ1 24 h before lysis using M-PER-Buffer containing protease inhibitor. Equal amounts of lysate were analyzed using western blot.

It is therefore assumed that the differential cellular response to BET inhibition might depend on gene regulatory changes defined by the epigenetic state of the cells. To follow up on this the effect of BET inhibition on gene expression was examined in a genome-wide transcription study of the sensitive DV90 cells.

4.1.4 Analysis of whole transcript profiling of JQ1 treated sensitive DV90 cells

To fully analyze the transcriptional changes induced by BET inhibition, the whole transcript of DV90 was profiled after treatment with IC_{50}, IC_{90} dose of JQ1 or DMSO control for 4 h and 24 h in 4-5 replicates using micro-array technology (data provided by the Target Discovery Department at Bayer Pharma) (3.2.9.3). This enabled the characterization of early

Results

transcriptional responses and secondary downstream transcriptional responses due to the cell response phenotype e.g. apoptosis or cell cycle arrest. The expression profiles after JQ1 treatment (IC_{50} (135 nM) and IC_{90} (785 nM)) were compared with the corresponding each DMSO control treatment samples and a 2 group test (t-test) was used to compare the expression of the control and treated samples. The genes with a BH-q value (corrected p-value) of q < 0.05 were considered to be statistically significantly regulated. After 4 h the expression of only 36 genes was significantly altered with a fold change cut off value of ±0.5 $\log_2$ (FC), while after 24 h the expression of 324 genes was significantly altered. Treatment with IC_{90} (785 nM) dose of JQ1 had a stronger impact on the expression of genes with 301 genes altered at 4 h, while 2,117 genes were significantly altered after 24 h (Figure 24).

This suggests that there is either a small number of fast responding genes that leads to downstream transcriptional regulation or a number of genes with fast turn-over transcripts and a number of slower turn-over transcripts that are directly regulated by BET bromodomain proteins. Additionally it is possible that the expression of some primary BET target genes can be re-initiated by the cell upon BET inhibitor treatment through alternative transcriptional regulatory mechanisms as described recently (Rathert et al., 2015).

Results
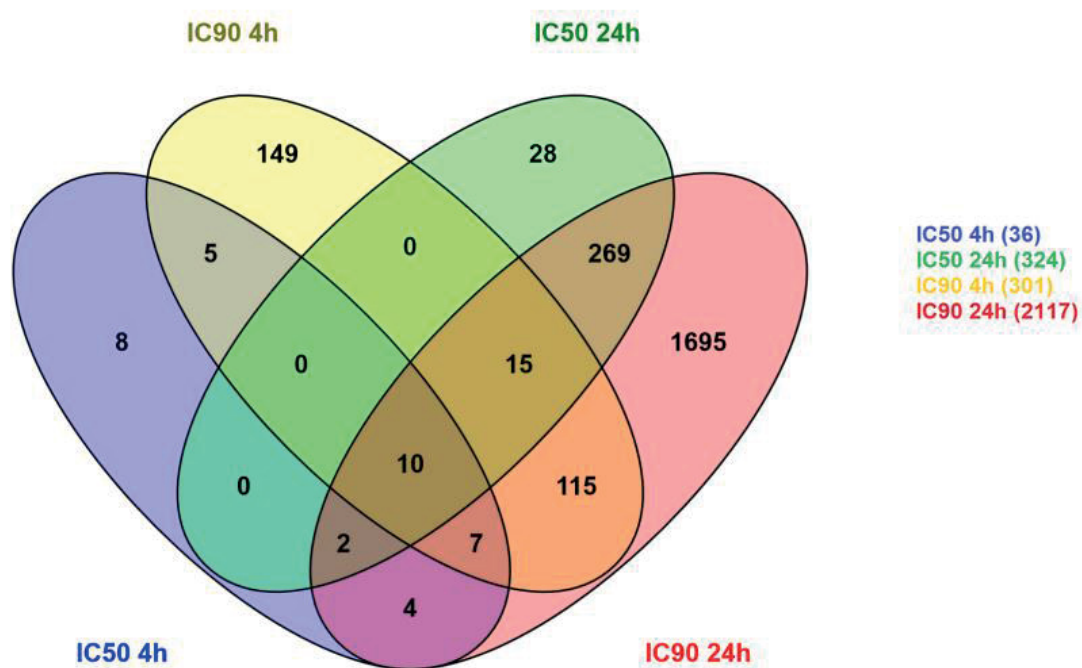
Figure 24: Venn Diagram showing the number of genes with expression changes after treatment of DV90 cells with different doses of JQ1 for 4 h or 24 h: Toggle represents the genes modulated by treatment at IC50 (135 nM) for 4 h (blue) and 24 h (green), and by treatment at IC90 for 4h (yellow) and 24h (red), Overlapping areas indicate common genes within the groups. BH-Q value (corrected p-value) cut off of 0.05 was considered as statistically significant. Numbers in brackets indicate the total number of genes with significantly changed expression level after JQ1 treatment. Diagram was generated using Venny 2.1 software (http://bioinfogp.cnb.csic.es/tools/venny/).

The significantly differentially expressed genes after 4 h treatment with IC_{50} or IC_{90} dose of JQ1 were categorized using the functional annotation tool Database for Annotation, Visualization and Integrated Discovery (DAVID). Gene ontology term annotation (GOTERM_BP_ALL) clustering revealed that the regulated genes were involved in regulation of cellular biosynthetic process, transcriptional and apoptosis (Top three clustered GO terms shown in Table 16 and Table 17).

Among the 10 genes commonly regulated by JQ1 (Figure 24) 4 genes were coding for transcription factors: *GTF2B*, *JUNB*, *ZNF280C* and *MYC*. *GFT2B* codes for a general transcription factor TFIIB, *ZNF280C* for a (C2H2) zinc finger containing protein with yet undescribed function, *JUNB* for the proto-oncogene transcription factor JunB (Eckhoff et al., 2013) and *MYC* for the proto-oncogene transcription factor c-Myc that can largely influence

the malignant state and fate of a cell (Ott, 2014). Among these 4 genes, only *MYC* expression was reduced.

To further look into the transcriptional networks regulated by BET inhibition, gene set enrichment was used to identify significantly altered expression of target gene sets after BET inhibition. The expression profile of the DV90 cells treated for 24 h at IC_{50} was ranked by the difference between the untreated control replicates and the JQ1 treatment replicates. All current gene sets in the molecular signature database (MsigDB) were used for the GSE analysis. Strikingly 4 among the top 8 ranked gene sets were *MYC* target gene sets (Figure 25A). This shows that the genes down-regulated by JQ1 were enriched for *MYC* target genes, implicating an important role of down-regulation of *MYC* expression and its target genes in the response to BET inhibition. Looking at the list of significantly differentially expressed genes additional interesting genes were identified including *FLIP*, *BCL2* and *MCL1*, which are involved in the negative regulation of apoptosis, *HEXIM* which forms the cellular inhibitory complex of transcriptional elongation P-TEFb and *BRD2,* a member of the BET family. Importantly the expression of *BRD3* and *BRD4* remained unchanged (Figure 25B).

Results

Figure 25: Gene set enrichment analysis of DV90 expression profiles after 24 h treatment with JQ1 (IC_{50}) and heatmap of the depicted differentially expressed genes: A: Table showing the top significantly enriched gene sets ranked by normalized enrichment scores (NES). False discovery rate (FDR) and number of genes in the gene set (N) are shown. Below, 2 depicted gene set enrichment plots showing significantly enriched c-Myc target gene sets: MYC_UP.V1_UP and SCHUHMACHER_MYC_TARGETS_UP. Genes of the gene sets are indicated by the black bars and show an enrichment of genes with the DMSO phenotype. B: Heatmap of the $\log_2$ fold change (FC) of all differentially expressed genes which shows the ranking of *MYC*, *FLIP*, *BCL2*, *MCL1*, *HEXIM* and *BRD2* gene after 24 h of treatment with JQ1 (IC_{50}).

4.1.5 Analysis of BET bromodomain gene regulatory function in NSCLC cell lines

4.1.5.1 Characterization of enhancers in DV90 cells

To characterize the putative enhancers in DV90 cells, ChIP-seq experiments using antibodies directed against BRD4 and Mediator (MED1) and histone marks H3K27Ac and H3K4me1 were performed. (Sequencing data were provided by the Target Discovery Department at Bayer Pharma) Peak-calling from Model-based analysis software MACS2 was used to identify statistically enriched regions in the H3K27Ac ChIP-seq dataset. These regions were used to discriminate between typical enhancers and super-enhancers. Super-enhancers are large enhancer sites recently identified to regulate and drive expression of genes defining the identity of a cell (Whyte et al., 2013). Heatmaps and line plots of H3K27Ac, H3K4me1 and BRD4 coverage at regions around ± 5 kb of typical and super-enhancer sites were generated (Figure 26A). Enhancer regions had characteristic H3K4me1 and H3K27Ac peaks. In addition, BRD4 was found to bind to the H3K27Ac+/H3K4me1+ enhancer regions with a

Results

similar profile, in accordance with earlier studies in models of small-cell lung cancer (SCLC) and MM (Loven et al., 2013). The Chem-seq method (Anders et al., 2014) was used to map the interaction sites of the BET inhibitor JQ1 on the genome and showed strong correlation with the BRD4 binding profile.

In contrast, BRD4 occupancy was less pronounced at regions around TSS of gene-coding regions, when compared to H3K27Ac and H3K4me1 marks (Figure 26 B).
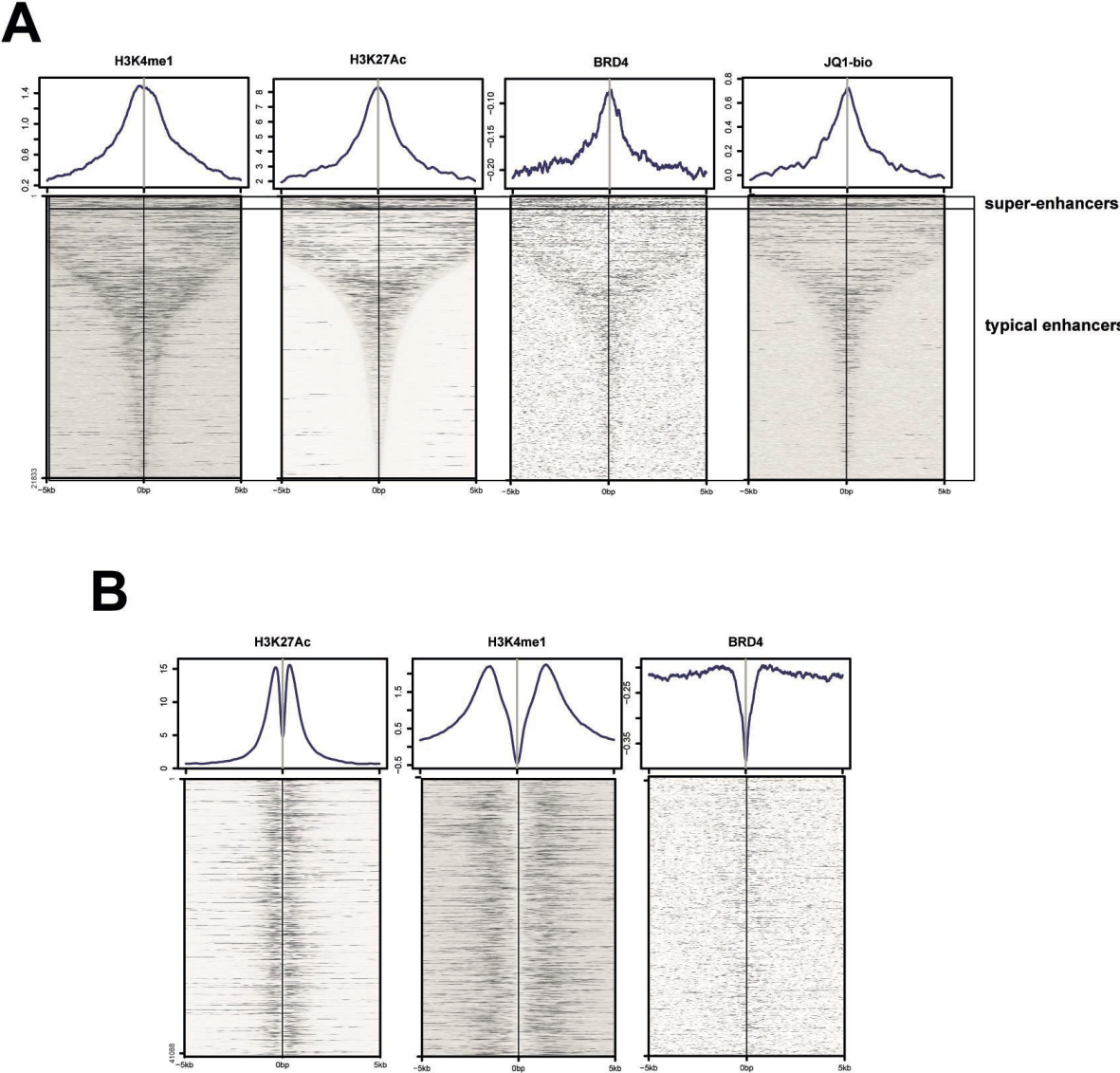
Figure 26: ChIP-seq heatmaps and profiles of H3K27Ac, H3K4me1, BRD4 and JQ1-biotin binding at enhancers and TSS regions. A: Occupancy around ±5 kb of the midpoint of the enhancer regions. Regions were sorted descending by peak weights and characterized super-enhancer and typical enhancers are marked. B: Occupancy around ±5 kb of the midpoint of the TSS regions.

Results

4.1.5.2 BRD4 is bound at *MYC* super-enhancers

The identification of super-enhancers was performed using genome-wide listing of potential enhancer sites marked by H3K27Ac marks followed by analysis of enhancer-binding factors like mediator 1 (MED1) occupancy clustering (Figure 27A). Small nearby clusters not further away than 12.5kb of enhancer binding factors were summarized into large clusters to form a super-enhancer site. The super-enhancers were identified and ranked using the background corrected MED1 signal as reads per million per base pair (rpm/bp) calculated by the ROSE software. This led to the identification of 873 super-enhancers and 20,960 typical enhancers. The nearest coding gene to each super-enhancers was annotated using PeakAnalyzer software. Even though this method is not very accurate in assigning typical enhancers to their genes (Mora et al., 2015) it has been shown to be more accurate in the case of super-enhancer assignment (Whyte et al., 2013). In total 4 super-enhancer regions have been annotated to the *MYC* gene, namely MYC-E1, MYC-E2, MYC-E3 and MYC-E4 (Figure 27A). The H3K27Ac$^+$/H3K4me1$^+$ *MYC* super-enhancers were occupied by the mediator complex together with BRD4 (Figure 27 B). Chem-seq was used to map the interaction sites of the BET inhibitor JQ1 on the genome and the strong binding at *MYC* super-enhancer regions was found to correlate with BRD4 binding (Figure 27B). This leads to the assumption that the *MYC* expression is regulated and dependent on BRD4 occupancy at *MYC* super-enhancers.

Results
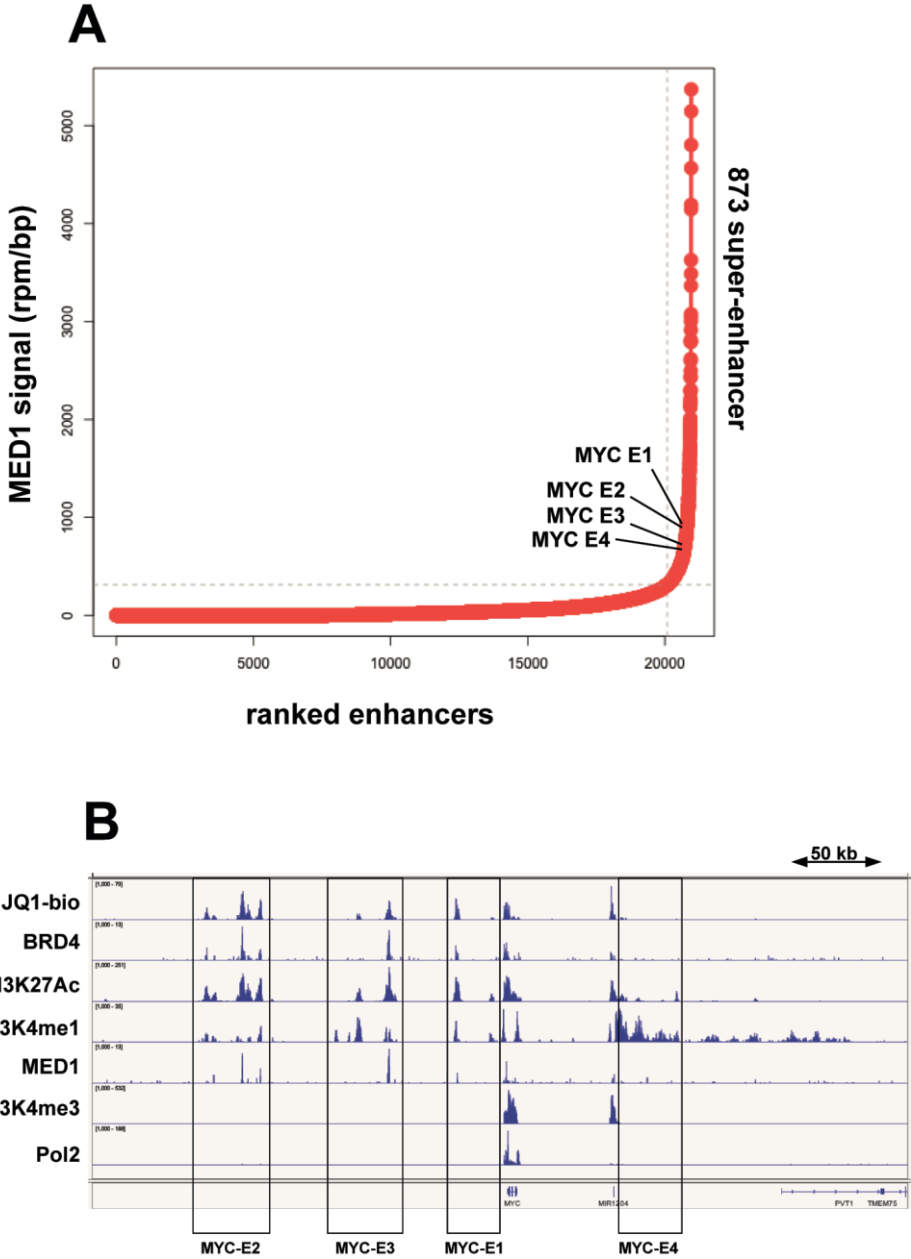
Figure 27: Super-enhancer identification using clustered MED1 signal on putative enhancer regions and ChIP-seq tracks at *MYC* super-enhancers. A: Dot plot showing ranked enhancers normalized by MED1 signal (MED1 signal – input signal in rpm/bp). B: Chem-seq/ChIP-seq tracks of JQ1-biotin (JQ1-bio), BRD4, RNA polymerase 2 (Pol2), mediator complex 1 (MED1) and histone marks H3K27Ac, H3K4me1 and H3K4me3. Enrichment of signal is presented as log likelihood ratio (log LR) over background signal. Tracks are shown as an overlay of two independent ChIP experiments.

4.1.5.3 JQ1 treatment leads to down-regulation of proto-oncogenes

Given the contradictory results of two studies in lung cancer proposing the effects of BET inhibition to be driven by regulation of *FOSL1* (Lockwood et al., 2012) or *MYC* expression

Results

(Shimamura et al., 2013) we looked more closely at both transcription factors. The expression of *MYC* and *FOSL1* was determined 24 h after treatment with 0.1 µM or 1 µM JQ1 in all 12 NSCLC cell lines using qRT-PCR. The relative mRNA levels were normalized to the DMSO-treated control (0.1%). Interestingly the relative mRNA levels of *MYC* were reduced in a dose-dependent manner but only in 5 out of 12 cell lines: DV90, H1373, LCLC97TM1, H441 and H2347, including the 3 most BET inhibitor sensitive cell lines (Figure 28A). The expression of *FOSL1* on the other hand was reduced in most of the cell lines upon BET inhibition except for H1373, H1792 and SKLU-1 (Figure 28B). The basal expression of *MYC* was increased in almost all cell lines, except for LCLC-97TM1, H358 and H2030 compared to normal lung fibroblasts. *FOSL1* expression was only relatively increased in H441 cells (Figure 28C). This leads to the assumption that neither the basal gene expression of *FOSL1* nor the basal expression of *MYC* is predictive of response to BET inhibition. The down-regulation of *MYC* expression on the other hand was seen in the three most sensitive cell lines, while its regulation was largely unaffected in insensitive cell lines.

Results
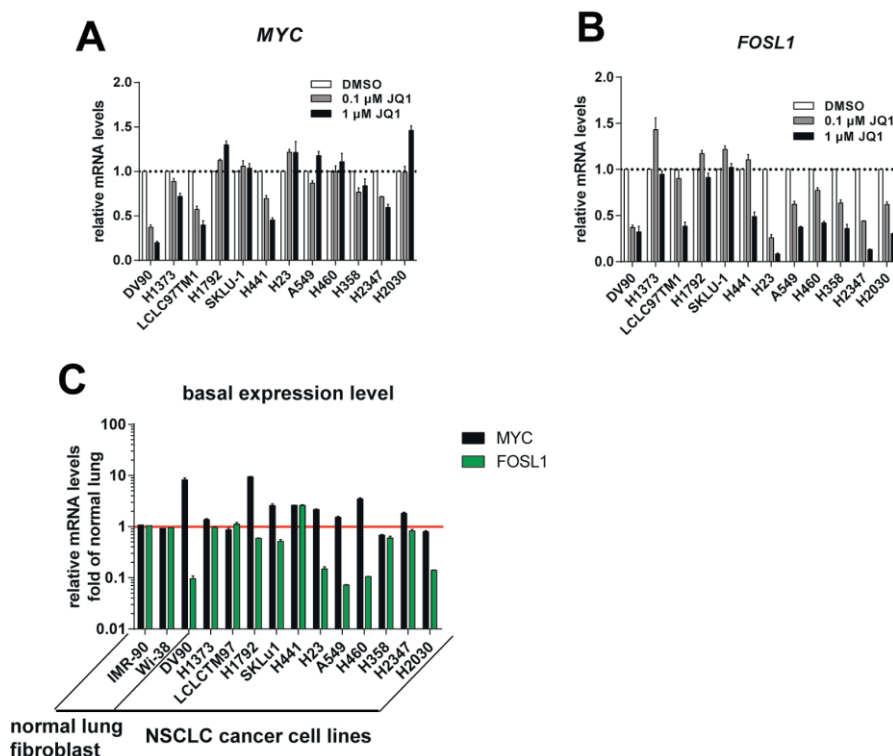
Figure 28: Gene expression analysis of *MYC* and *FOSL1* proto oncogene transcription factor basal expression and change of expression level after JQ1 treatment of all 12 tested NSCLC cell lines. A, B: qRT-PCR analysis of *MYC* and *FOSL1* mRNA expression 24 h after treatment with 0.1 μM or 1 μM of JQ1 normalized to the housekeeping gene human cyclophilin A and DMSO-treated control. Error bars denote SEM (n=3). C: qRT-PCR analysis of basal *MYC* mRNA expression of NSCLC cell lines normalized to the housekeeping gene human cyclophilin A and normal fibroblast cell lines IMR-90 and Wi-38. Error bars denote SEM (n=3)

4.1.5.4 Down-regulation of c-Myc oncoprotein by JQ1

This needed to be confirmed at the protein level, as post-translational modifications could influence the stability and thereby the abundance and turnover rate of c-Myc in the cell. Western blot analysis of 24 h JQ1 treated cells showed that c-Myc protein level was only reduced in DV90, H1373, LCLC97TM1, H441 and H2347 cells, consistent with the reduction of mRNA level, while the c-Myc protein level was largely unaffected in insensitive cell lines (Figure 29A). Time- and dose-dependent down-regulation of c-Myc was confirmed in H1373 cells (Figure 29B), while c-Myc levels were consistently unaffected in insensitive A549 (Figure 29C) and H2030 cells (Figure 29D).The c-Myc protein level in H1373 cells was significantly down-regulated after 6 h of 1 μM JQ1 treatment. A CHX-chase experiment was performed to determine the turnover rate of c-Myc in H1373 cells. Cycloheximide (CHX) is a potent translation inhibitor that can be used to determine the stability of a protein of interest in

the cellular context. It was found that c-Myc had a fast turnover rate in cells with a protein half-life of around 150 min (Figure 30).
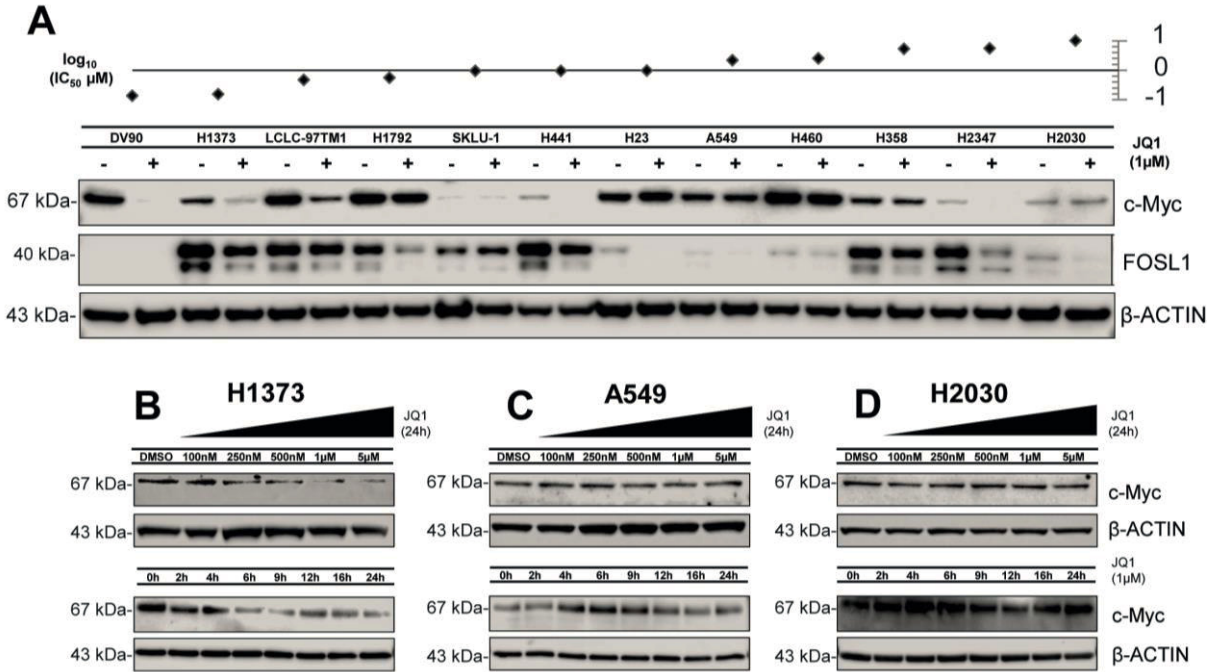
Figure 29: Western blot analysis of c-Myc and FOSL1 protein levels after JQ1 treatment. A: Western blot analysis of c-Myc and FOSL1 expression 24 h after DMSO (-) or 1 µM JQ1 (+) treatment. Sensitivity of cell lines to JQ1 is represented by log (IC50 µM). B-D: Western blot analysis of c-Myc expression in cell lines with different sensitivities to JQ1. H1373 (B) A549 (C) and H2030 (D) cells were treated with different doses of JQ1 for 24 h or 1 µM JQ1 for different times.
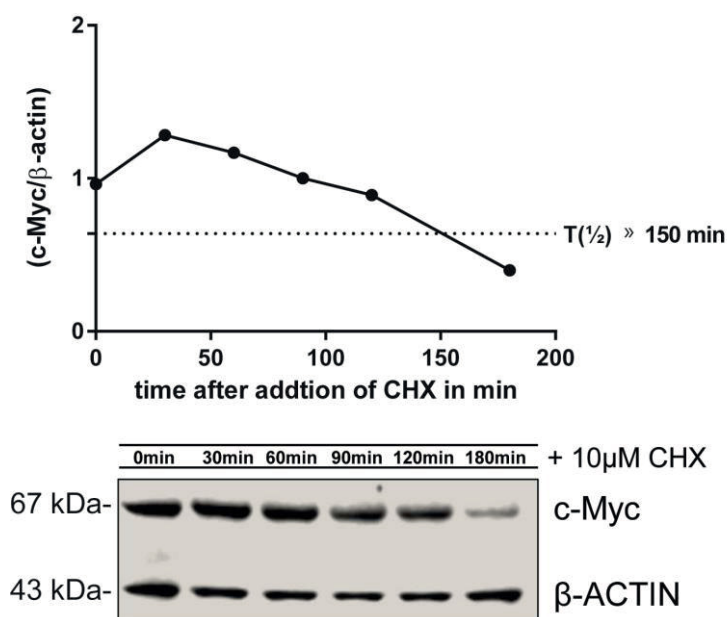
Figure 30: Determination of cellular turnover rate of c-Myc in H1373 cells. H1373 cells were treated with 10 µM cycloheximide (CHX) for a maximum of 3 h. Cells were lysed after indicated treatment times. Western blot analysis of c-Myc was performed and normalized to ß-ACTIN levels using Image Studio software. The time until the half maximal relative level c-Myc was reached was determined and defined as protein half-life.

4.1.6 Anti-tumor efficacy of JQ1 in vivo the subcutaneous H1373 xenograft mouse model

Given the promising anti-proliferative activity of BET inhibitors in H1373 cells, the subcutaneous H1373 xenograft mouse model was chosen to evaluate the anti-tumor activity of JQ1 *in vivo*. FOX chase severe combined immunodeficiency (SCID) mice (CB17/Icr-Prkdc^{scid}/IcrIcoCrl) were inoculated with 3×10^6 cells/mouse (3.2.16.1). Once tumor burden was measurable, mice were randomized into groups of 12 mice and daily *intra peritoneal* (i.p) treatment with vehicle or JQ1 given at 50 mg/kg (10 ml/kg) was performed for 15 days.

JQ1 at 50 mg/kg, was active with a percent treatment vs. control tumor weight ratio (%T/C) of 32% on day 15 after start of treatment (Figure 31A) and was tolerated with a maximal mean body weight loss (BWL) of 5% (Figure 31B). The tumor weight was determined on the final day and showed significant reduction of the tumor (p < 0.01). Down-regulation of c-Myc, as previously shown *in vitro*, was also observed in tumor tissue lysates using western blot analysis, 24 h after JQ1 treatment (Figure 31C).
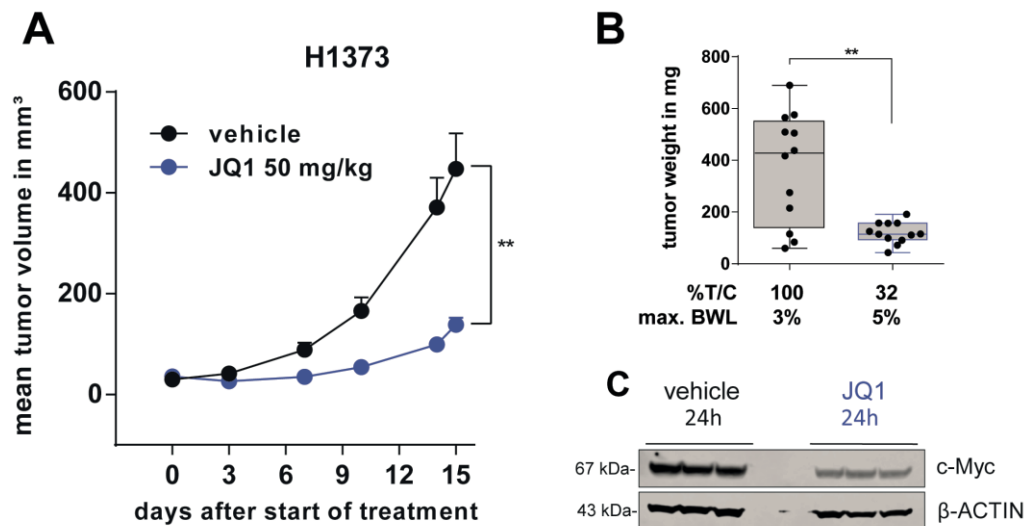
Figure 31: *In vivo* anti-tumor efficacy of JQ1 in the subcutaneous H1373 xenograft mouse model. A: Growth curve of H1373 xenograft treated with vehicle or 50 mg/kg JQ1 i.p. daily. Error bars denote SEM (n=12 mice per group) ** $p < 0.01$ two-tailed unpaired Student's t-test on $\log_{10}$ -transformed tumor volume on day 15 after start of treatment. B, Box and whiskers plot of tumor weight in the H1373 xenograft study on day 15 after start of treatment. Error bars denote SEM (n=12 mice per group). ** $p < 0.01$ two-tailed unpaired Student's t-test on $\log_{10}$ -transformed tumor weight. C, Western blot analysis of c-Myc protein levels in tumor tissue from the H1373 xenograft study treated with vehicle or 50 mg/kg JQ1.

4.1.7 c-Myc overexpression rescues the effects of JQ1

The function of c-Myc in driving proliferation of cancer cells is well established and loss of c-Myc can lead to cell cycle arrest and cell death in tumors (Hydbring et al., 2010; Soucek et al., 2013; Wu et al., 2007). To investigate whether the anti-tumor activity of BET inhibition in H1373 cells was truly mediated by loss of c-Myc oncoprotein, an overexpression rescue experiment was performed. H1373 cells were co-transfected with a GFP expression plasmid and either c-Myc cDNA expression plasmid or empty vector control, followed by treatment with JQ1 (0.5 μM). As JQ1 leads to cell cycle arrest in H1373 cells, a flow cytometry EdU staining assay was used (Figure 32A).

Cells transfected with a c-Myc overexpression vector or with empty vector were compared after selection of the positively transfected (GFP[+]) population. Also, the positively transfected and un-transfected populations in DMSO control and JQ1-treated samples were compared (GFP[+] vs. GFP[-]). Ectopic overexpression of c-Myc significantly increased the EdU[+] population of JQ1-treated cells (60% EdU[+] transfected with c-Myc vector vs. 26% EdU[+]

Results

transfected with empty vector control) (Figure 32B, C), while un-transfected cells were not rescued (GFP⁻ 33% vs GFP⁺ 60%) (Figure 32B, D). Interestingly ectopic expression of c-Myc could not completely rescue the effect of JQ1. This suggests that BET inhibition had additional effects on the apoptotic pathway.
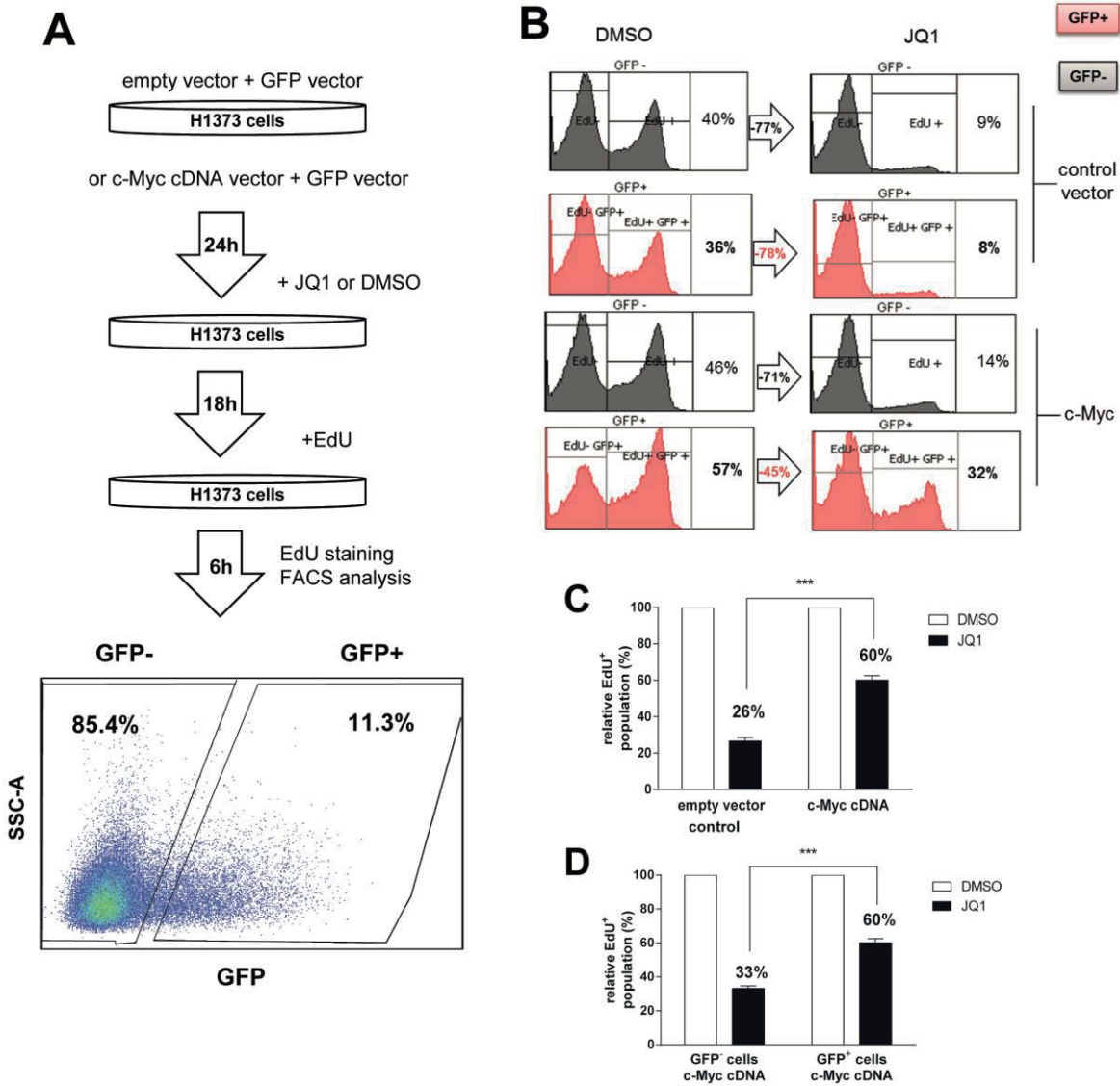
Figure 32: c-Myc overexpression rescues anti-proliferative activity of JQ1 in H1373 cells. A: Workflow of rescue experiment in H1373. Cells were transfected with empty vector or c-Myc expressing vector and GFP vector, and then subsequently treated with JQ1 (0.5 μM) or DMSO and stained using EdU.B: Representative histogram of EdU staining following c-Myc overexpression rescue and JQ1 treatment. The GFP⁺ population is marked in red and the GFP- population is marked in grey. C and D: Results of overexpression rescue experiments comparing empty vector vs c-Myc vector transfected cells (C) and GFP⁻ vs GFP⁺ cells co-expressing c-Myc (D). EdU⁺ population was normalized to DMSO-treated control sample. Error bars denote SEM (n=3). *** $p < 0.001$ two-tailed unpaired Student's t-test.

Results

4.2 Combinatory potential of BET inhibition with pro-apoptotic therapy

The transcriptional regulation of 370 apoptosis-pathway genes was compared in the JQ1-sensitive H1373 cells and the JQ1-resistant H2030 cell lines. Cells were treated with 1 µM JQ1 for 6 h, followed by analysis of gene expression using qRT-PCR. Among the non-overlapping and overlapping expression changes observed, the levels of two cellular caspase inhibitors FLIP and XIAP, which exhibit key regulatory functions in the apoptosis pathway, were strongly reduced in both cell lines (Figure 33). Looking at the extrinsic and intrinsic apoptosis pathways of mammalian cells led to a strong rationale for combining BET inhibition with pro-apoptotic therapy like TRAIL or the standard of care chemotherapy agent cisplatin.

The regulatory effects of JQ1 on gene expression of the BCL-2 and IAP family was analyzed using western blot in sensitive H1373 and insensitive A549 and H2030 cells. The expression of the members of the BCL-2 and of the IAP family remained largely unaffected by BET inhibition in most of the cells tested (Figure 34A, B, C). However c-FLIP and XIAP protein levels were reduced in all of the cell lines in a dose-dependent manner. It was interesting to see whether the expression of these genes was dependent on BET proteins and would be reduced by BET inhibition in all of the tested NSCLC cell lines.

Results
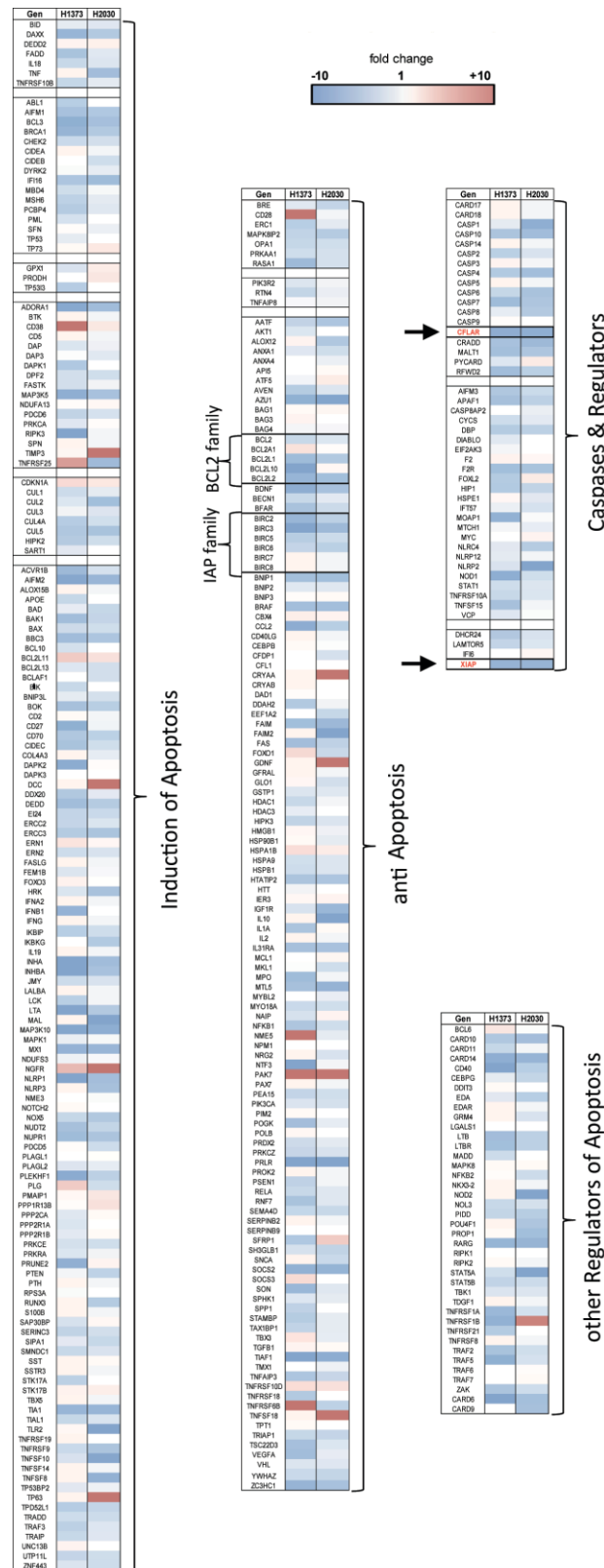
Figure 33: Profiling of 370 apoptosis related genes in relation to BET inhibition. QRT-PCR analysis of 370 genes involved in apoptosis regulation, in JQ1-sensitive H1373 cells (left) and JQ1-resistant H2030 cells (right) after 6 h of treatment with 1 μM JQ1. Data were normalized to housekeeping genes, and the fold-change compared to DMSO treatment was calculated.
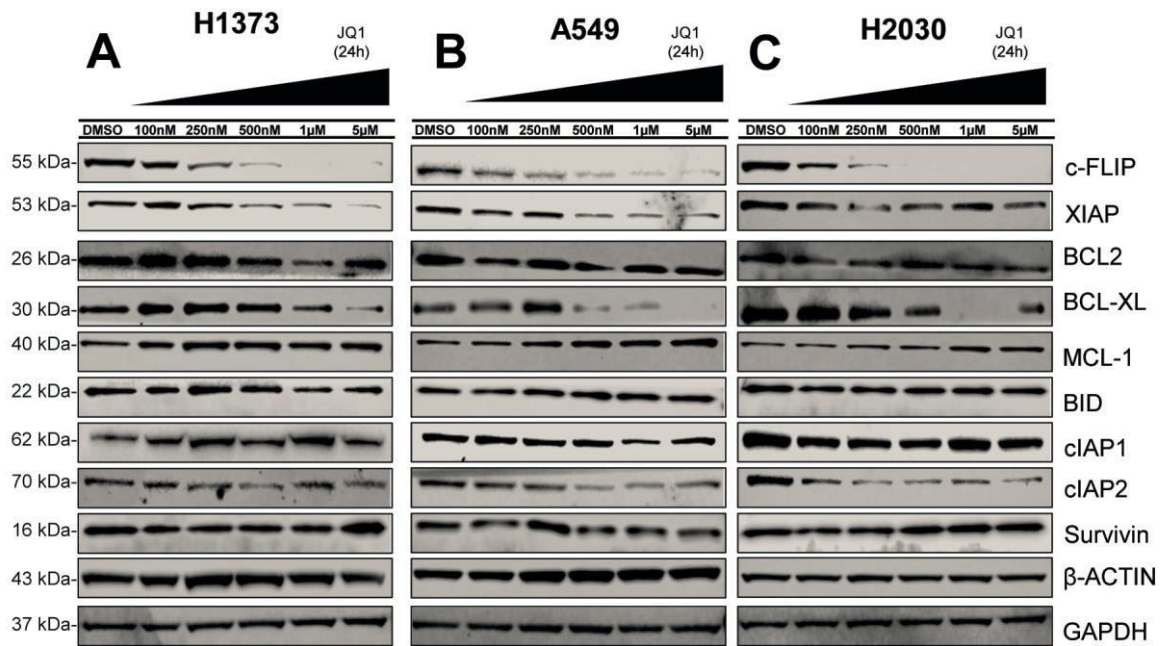
Figure 34: Western blot analysis of BCL-2 and IAP family in cell lines treated with JQ1. A, B and C: Western blot analysis of apoptosis-related genes in cell lines with different sensitivities to JQ1. H1373 (A) A549 (B) and H2030 (C) cells were treated with increasing doses of JQ1 for 24 h.

4.2.1 Expression of the apoptosis regulators c-FLIP and XIAP is dependent on BET proteins

Indeed, JQ1 treatment reduced the mRNA levels of FLIP and XIAP in all 12 NSCLC cell lines tested (Figure 35A, B). Chromatin immunoprecipitation (ChIP) was performed in H1373 cells and showed that BRD4 occupancy at the promoter sites of *FLIP* and *XIAP* was significantly reduced after JQ1 treatment (Figure 35C, D), in line with the reduction of FLIP and XIAP mRNA expression, thus leading to the hypothesis that BRD4 bound to promoter sites of *XIAP* and *FLIP* and thereby drove gene expression.

Results
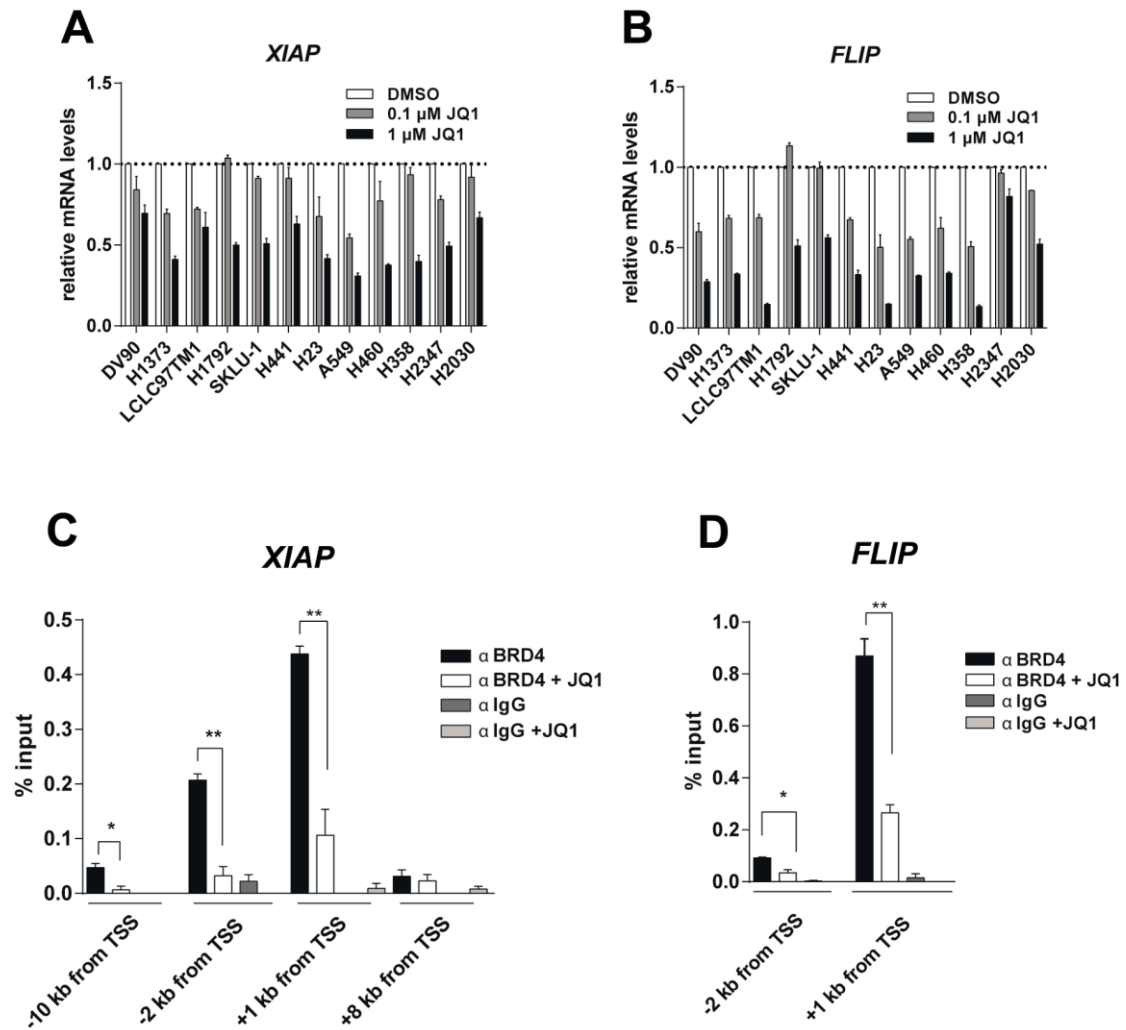
Figure 35: Regulation of the apoptosis regulators c-FLIP and XIAP expression is dependent on BET proteins. A and B: qRT-PCR analysis of XIAP and FLIP mRNA expression 24 h after treatment with 0.1 µM or 1 µM of JQ1 normalized to the expression levels of the housekeeping gene human cyclophilin A and the DMSO-treated control. Error bars denote SEM (n=3). C and D, ChIP-qPCR analysis of BRD4 binding at the *XIAP* and *FLIP* promoters (primer distance from transcription start site (TSS) is indicated) in H1373 cells treated with DMSO or JQ1 (0.5 µM). Error bars denote SEM (n=3). * p < 0.05, ** p < 0.01, two-tailed unpaired Student's t-test.

Reduction of both c-FLIP and XIAP at the protein level was also observed in all NSCLC cell lines tested after addition of 1 µM JQ1 for 24 h (Figure 36A). Time-course and dose-response experiments confirmed the effect of BET inhibition at the protein levels in 3 cell lines with different sensitivities to JQ1 (Figure 36B, C, D). Treatment of H1373, A549 and H2030 with a dose of 0.25 µM to 1 µM JQ1 strongly reduced the protein levels of both c-FLIP and XIAP after 24 h. The time-course experiments revealed that treatment with 1 µM JQ1 led to a strong reduction of c-FLIP and XIAP protein level after 4-6 h.
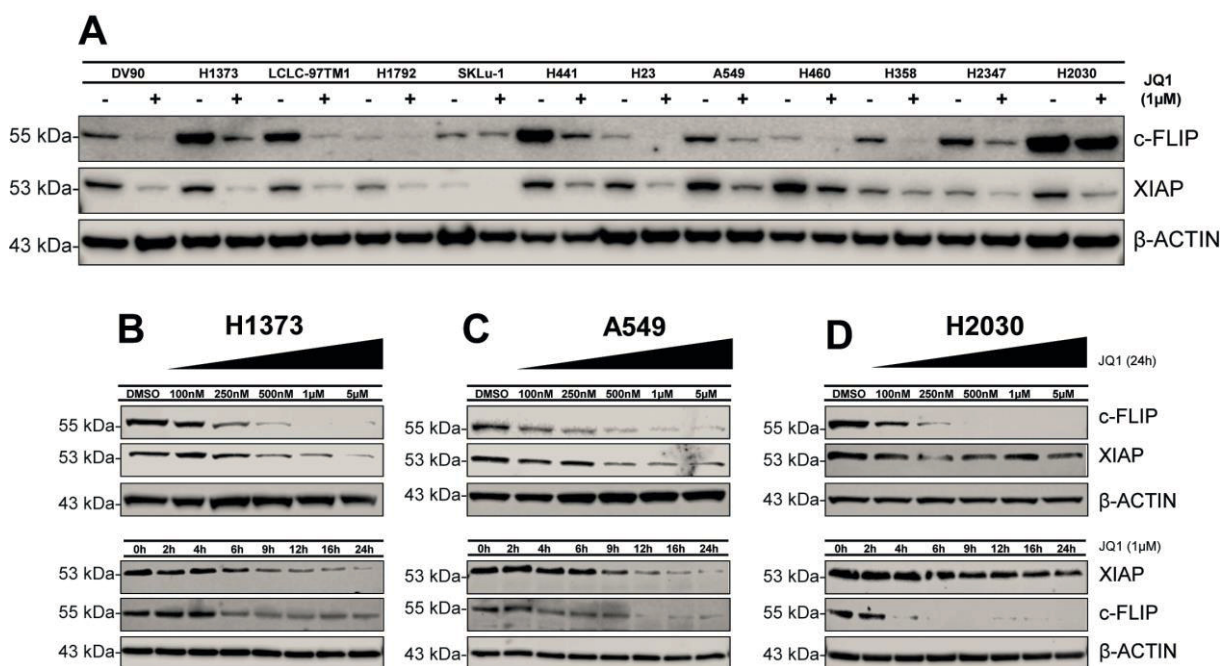
Figure 36: Western blot analysis showing down-regulation of c-FLIP and XIAP protein levels following BET inhibition. A: Western blot analysis of c-FLIP and XIAP 24 h after DMSO (-) or 1 μM JQ1 (+) treatment. B, C and D: Western blot analysis of c-FLIP and XIAP in cell lines with different sensitivities to JQ1. H1373 (B) A549 (C) and H2030 (D) cells were treated with increasing doses of JQ1 for 24 h or with 1 μM for different times.

4.2.2 Loss of XIAP and c-FLIP leads to enhanced TRAIL-induced apoptosis

XIAP and c-FLIP have key inhibitory functions in the extrinsic apoptosis pathway and were reduced in both resistant and sensitive cells treated with JQ1, although their loss did not consistently lead to apoptosis in all cell lines. Therefore JQ1 was combined with the death receptor ligand TRAIL to test whether cell death can be stimulated, especially in the insensitive cell lines. Death receptor binding of TRAIL is known to strongly activate the extrinsic apoptosis pathway through the cleavage of caspase-8/10, leading to downstream activation of caspase 3 and amplifying activation of the intrinsic apoptosis pathway. As the time-course experiments revealed that treatment with 1 μM JQ1 led to a reduction of c-FLIP and XIAP protein level after 4-6 h, H1373 cells were pretreated with 1 μM JQ1 2 h prior to addition of TRAIL (Figure 37A). Significantly enhanced TRAIL-dependent induction of apoptosis was evidenced by Annexin-V staining and PARP-cleavage in H1373 cells (Figure 37B, C). While addition of 1 μM JQ1 and 10 ng/mL TRAIL alone induced apoptosis in a small number of cells, the combination of both strikingly reduced the number of viable cells down to 15.5%.

Results

To further increase the understanding on which components of the apoptotic pathway were affected by JQ1 and to establish whether enhanced TRAIL-induced apoptosis was truly dependent on caspase activity, extended analyses were performed. To investigate the dependency of the JQ1 enhanced TRAIL-induced apoptosis on caspase activity, H1373 cells were treated with pan-caspase inhibitor z-VAD-FMK, caspase-9 inhibitor z-LEHD-FMK or caspase-8 inhibitor z-IETD-FMK (Figure 37D). Impressively the addition of the pan-caspase inhibitor z-VAD-FMK completely rescued H1373 cells from induction of apoptosis, while the caspase-9 inhibitor z-LEHD-FMK and the caspase-8 inhibitor z-IETD-FMK did only partially rescue the effect.
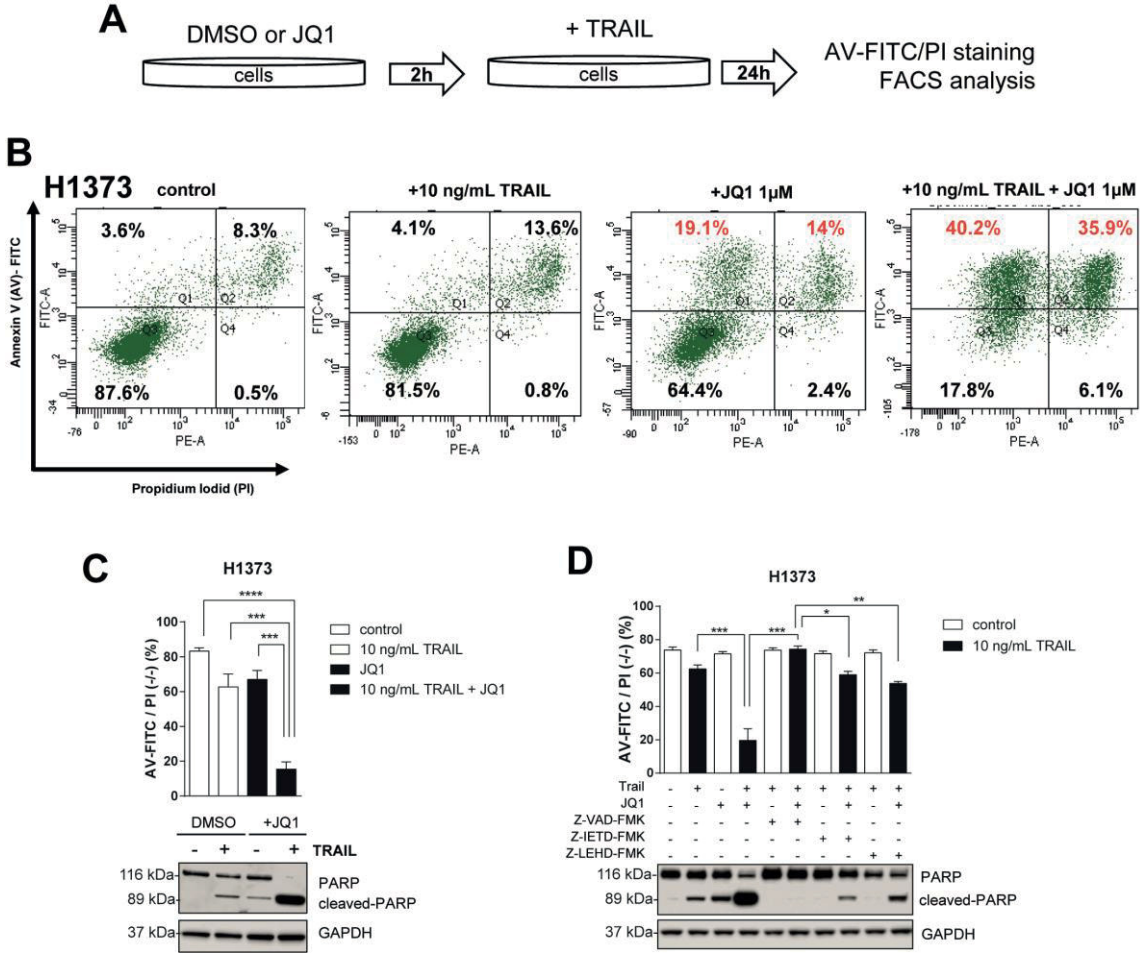
Figure 37: Combination of JQ1 and TNF related apoptosis inducing ligand (TRAIL) in H1373 cells. A: Workflow of combination treatment using JQ1 and TRAIL: Cells were pre-treated with JQ1, subsequently treated with TRAIL, and stained using AV-FITC/PI for analysis of apoptosis by flow cytometry (results showing the percentage of viable population (% AV-FITC / PI negative (-/-)) are reported in top of panels C and D; western blot results showing PARP cleavage are on the bottom of panels C and D). B: Representative plot of flow cytometry analysis showing Annexin-V, propidium iodide stained H1373 cells following TRAIL treatment for 24 h. C: treatment of H1373 cells with TRAIL (10 ng/mL) and JQ1 (1 µM) alone or in combination. D: as in panel B but with 20 µM of the caspase inhibitors Z-VAD-FMK (pan-caspase inhibitor), Z-IETD-FMK (caspase-8 inhibitor), or Z-LEHD-FMK (caspase-9 inhibitor). Error bars denote SEM (n=3-5). * $p < 0.05$, ** $p < 0.01$, *** $p < 0.001$, non-parametric one-way ANOVA with Sidak's correction for multiple comparisons.

Results

The pro-apoptotic proteins BAX and BAK are essential to induce outer mitochondrial membrane permeabilization (MOMP) leading to activation of the intrinsic apoptosis pathway and apoptosome formation (1.5.1.1). BAX and BAK have redundant functions (Lindsten et al., 2000), they induce apoptosis with preference towards specific BH3 only proteins (Figure 11A). However a recent study reported chemotherapy and TRAIL-induced apoptosis to be dependent on the pro-apoptotic proteins BAX and BAK, while TRAIL-induced apoptosis was rather dependent on BAK (Sarosiek et al., 2013). To further investigate whether the combination of JQ1 and TRAIL was dependent on either BAX or BAK, H1373 cells depleted of BAX or BAK were produced using the CRISPR-Cas9 technology (1.4.3). Interestingly the enhanced TRAIL-induced apoptosis was independent of pro-apoptotic proteins BAX or BAK, as knockout did not significantly affect the combination potential of JQ1 and TRAIL (Figure 38A). However knockout of BAX or BAK also did not block the apoptosis induction of TRAIL alone compared to wild-type cells. In order to confirm that the enhancing effect of JQ1 was linked to the down-regulation of XIAP and c-FLIP, siRNA knockdown experiments were performed. Simultaneous knockdown of c-FLIP and XIAP in H1373 cells using pooled targeted siRNAs nearly completely recapitulated the enhancing effects of JQ1 when combined with TRAIL (37% viability) (Figure 38 A, B). This suggested that the enhancing effect of JQ1 was largely dependent on loss of c-FLIP and XIAP. Knock-down efficiency of siRNA treatment was confirmed by western blot analysis.

Results
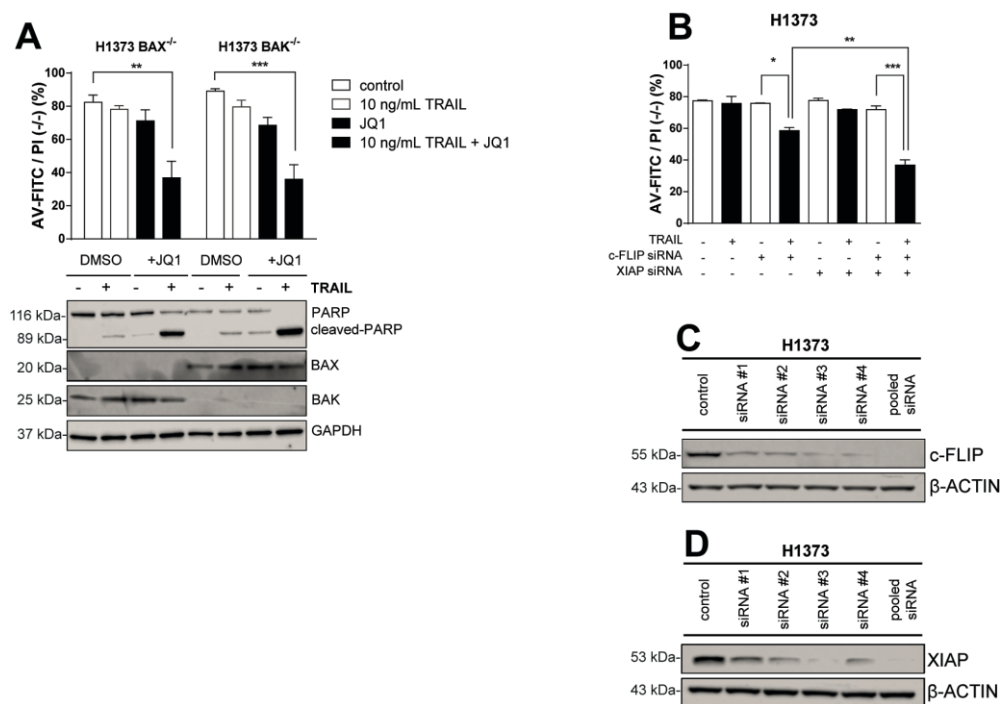
Figure 38: Combined treatment with JQ1 and TRAIL in H1373 BAX or BAK knockout cells. A: results of the rescue experiment after treatment of H1373 BAX or BAK knockout cells with TRAIL (10 ng/mL) and JQ1 (1 µM) alone or in combination. B: Flow cytometry results plotting percentage of viable population (% AV-FITC / PI negative (-/-)) of H1373 cells treated with TRAIL (10 ng/mL) 24 h after siRNA knockdown of c-FLIP or XIAP. Error bars denote SEM (n=3). * $p < 0.05$, ** $p < 0.01$, *** $p < 0.01$, non-parametric one-way ANOVA with Sidak's correction for multiple comparison. C and D: Western blot analysis of knockdown efficiency using single or pooled siRNAs targeting FLIP or XIAP transcripts.

It was furthermore interesting to see whether JQ1 treatment did also increase TRAIL-induced apoptosis in JQ1-insensitive cell lines, and enabled the combination treatment to overcome resistance. H2030 and A459 cells were treated with JQ1 and 2 h later TRAIL was added as described before (Figure 37A). Even though A549 cells were less sensitive to TRAIL, the combination of JQ1 and TRAIL reduced the viability of A549 cells to 57% at 100 ng/mL TRAIL (Figure 39A). In the case of H2030 cells, the combination also enhanced the effect of TRAIL and reduced the viability to 68% using a 10 ng/mL TRAIL dose (Figure 39B). These results were confirmed in 5 NSCLC models with different sensitivities to BET inhibition which were treated either with JQ1 alone or in combination with TRAIL (Figure 39C). Importantly, combination of TRAIL and JQ1 did limit the viability of all 5 NSCLC models tested (Figure 39D-H), while the combination did not reduce the viability of normal fibroblast HFF-1 cells (Figure 39I).

Results
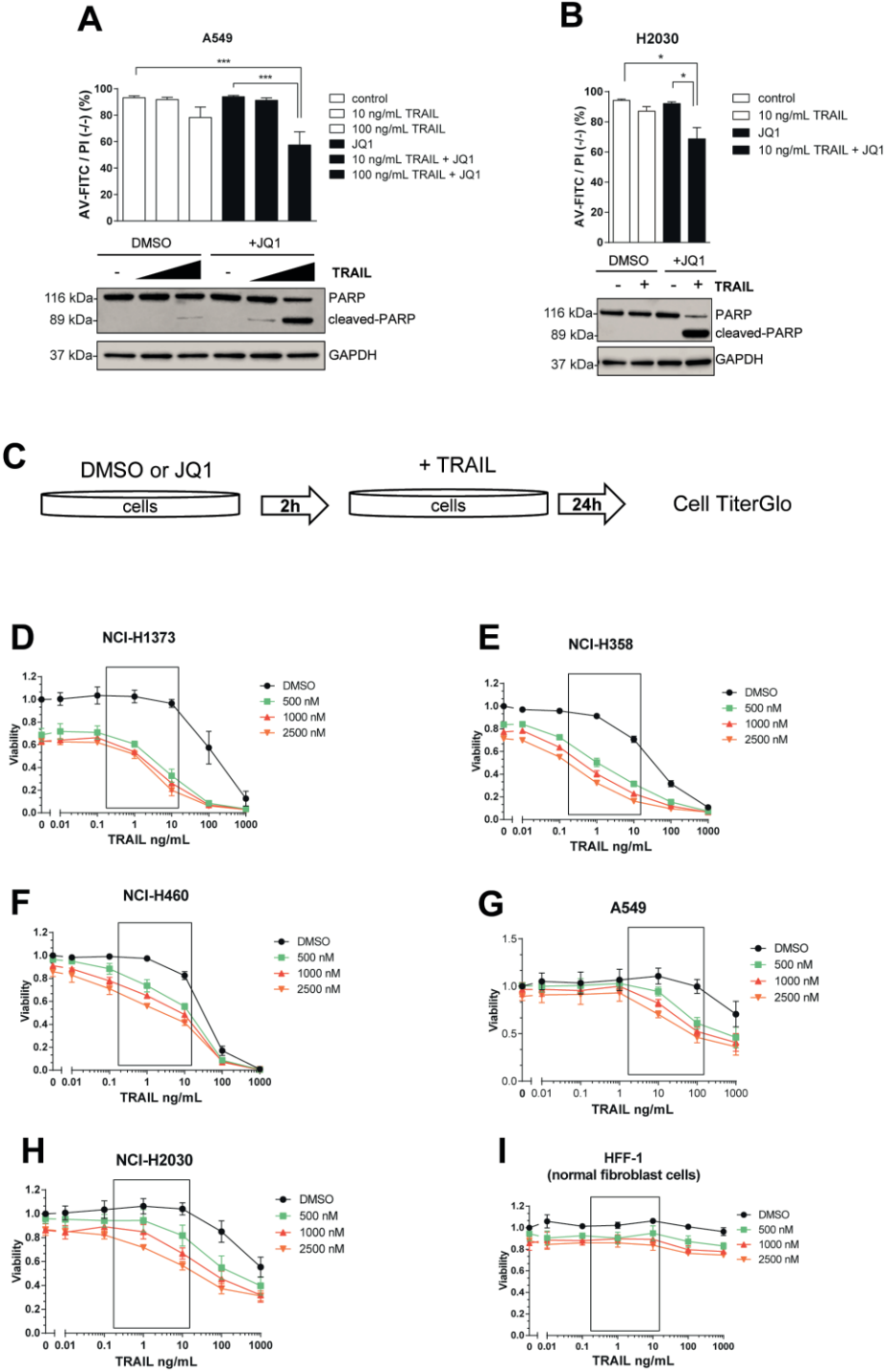
Figure 39: Combination of JQ1 and TRAIL in NSCLC cells. A and B: H2030 or A549 cells after treatment with TRAIL (10 ng/mL or 100ng/mL) and JQ1 (1 µM) alone or in combination. C: Workflow of combination treatment with JQ1 and TRAIL. Cells were pretreated with 1 µM JQ1 and subsequently treated with TRAIL, followed by assessment of cell viability using Cell TiterGlo. Five NSCLC cell lines with different sensitivities to JQ1 were treated with different doses of JQ1 prior to treatment and with increasing doses of TRAIL. D: H1373, E: H358, F: H460, G: A549, H: H2030, NSCLC cells ; I: HFF-1 normal fibroblast cells. Data were normalized to DMSO-treated cells. Error bars denote SEM (n=3-5). * p < 0.05, ** p < 0.01, *** p < 0.01, non-parametric one-way ANOVA with Sidak's correction for multiple comparison.

Results

4.2.3 *In vitro* combination of JQ1 and cisplatin synergistically reduces cell viability and overcomes resistance in the A549 cell line

The sensitizing effect of BET inhibition towards pro-apoptotic agents through down-regulation of c-FLIP and XIAP led to explore the combination of JQ1 with pro-apoptotic chemotherapy such as cisplatin, which is frequently used as a single agent to treat NSCLC patients. Combination of JQ1 and cisplatin significantly increased apoptosis in all 3 cell lines tested, as measured by Annexin-V staining and PARP cleavage (Figure 40A, B). To determine a potential synergistic effect of JQ1 and cisplatin a drug combination assay was performed (3.2.4.1) combining JQ1 and cisplatin in various ratios and treating A549 cells with ranging doses of these ratios (Figure 40C). The resulting IC_{50} values were used to calculate a potential synergy of the two agents using the Chou-Talalay method which considers a combinatory index below 1 (CI < 1) to be synergistic (3.2.4.1). Indeed cisplatin and JQ1 synergistically reduced viability of A549 cells when combined with JQ1, with a combination index (CI) of 0.34-0.54 (Figure 40C). In order to confirm that the enhancing effect of JQ1 was linked to the down-regulation of XIAP and c-FLIP, siRNA knockdown experiment was performed. Interestingly knockdown of c-FLIP alone using pooled targeted siRNAs recapitulated the enhancing effects of JQ1 when combined with cisplatin in A549 cells (54.2% viability) (Figure 40E). This suggested that the enhancing effect of JQ1 was largely dependent on the loss of c-FLIP.
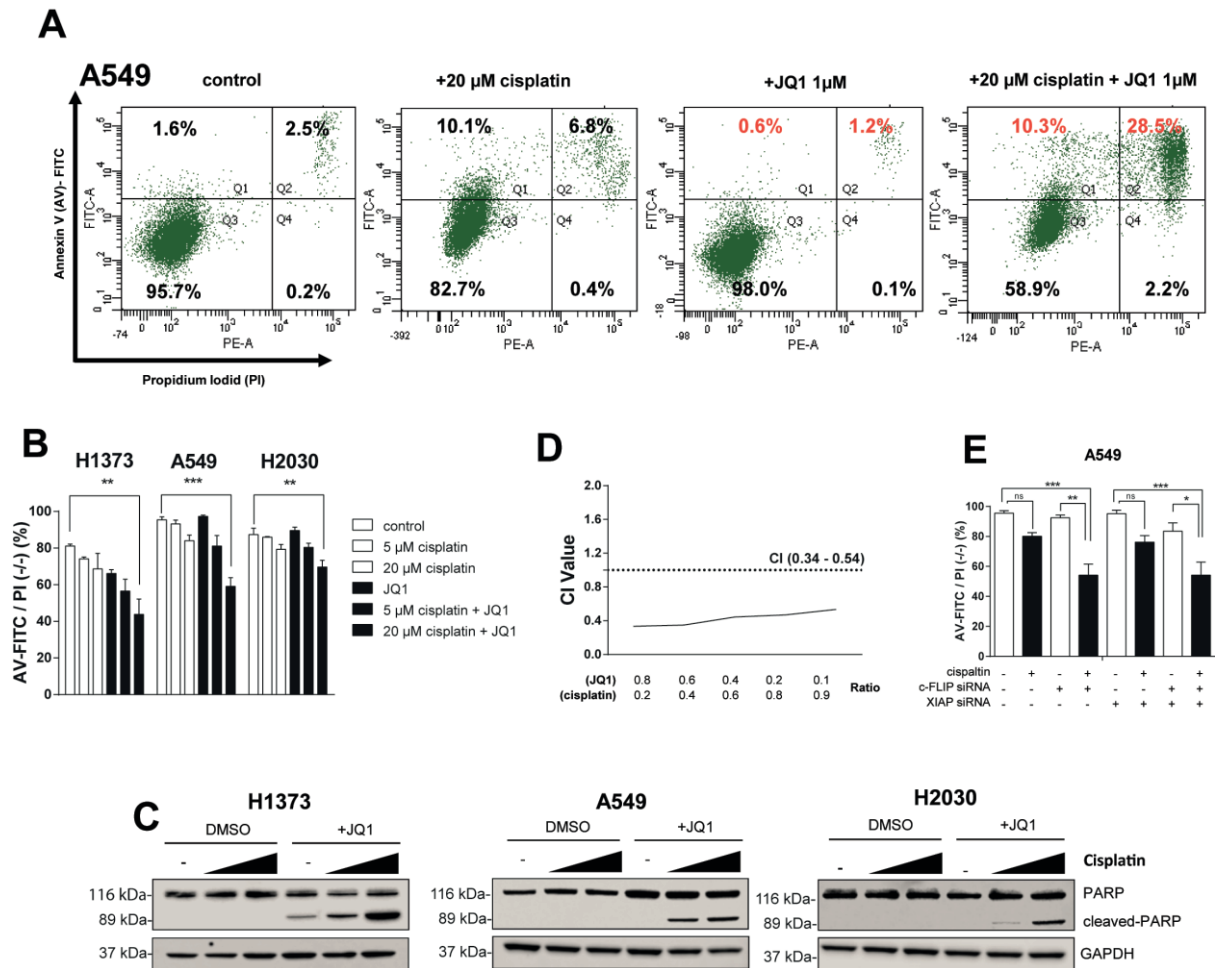
Figure 40: Combination of JQ1 and cisplatin in NSCLC cells. A: Representative plots of flow cytometry analysis showing Annexin-V, propidium iodide stained A549 cells following cisplatin treatment for 48 h. B: Flow cytometry results showing the percentage of viable population (% AV-FITC / PI negative (-/-)) after treatment of H1373, A549 and H2030 cells with cisplatin and JQ1 (1 µM) alone or in combination. Error bars denote SEM (n=3). ** $p < 0.01$, *** $p < 0.001$, non-parametric one-way ANOVA with Sidak's correction for multiple comparison. C: Western blot analyses of PARP cleavage following treatment with cisplatin and JQ1 (1 µM) alone or in combination. D: Assessment of the degree of synergy between cisplatin and JQ1 in A549 cells using the Chou Talalay method. Calculated CI is plotted against drug ratios. Results are shown as the mean (n=2). The cutoff point for synergy is defined by CI < 1.0. E: Flow cytometry results plotting percentage of viable population (% AV-FITC / PI negative (-/-)) of A549 cells treated with cisplatin (20 µM) 4 h after siRNA knockdown of c-FLIP or XIAP. Error bars denote SEM (n=3). * $p < 0.05$, ** $p < 0.01$, *** $p < 0.01$, non-parametric one-way ANOVA with Sidak's correction for multiple comparison.

Results

4.2.4 *In vivo* combination of JQ1 and cisplatin overcomes resistance in the A549 xenograft model

Given the strong synergy of the combination of cisplatin and BET inhibition in A549 cells *in vitro*, the subcutaneous A549 xenograft mouse model was chosen to evaluate the anti-tumor activity of the combination of cisplatin and JQ1 *in vivo*. FOX chase severe combined immunodeficiency (SCID) mice were inoculated with 3 x 10^6 cells/mouse (3.2.16.1). After tumor burden was established mice were randomized into groups of 10 mice and *intraperitoneal* (i.p) treatment was initiated with vehicle or JQ1 given at 50 mg/kg or 80 mg/kg (maximal tolerated dose) (10 ml/kg) or cisplatin 1.2 mg/kg injected *intravenous* (i.v.) as a bolus (10 ml/kg) (Figure 41A).Vehicle and JQ1 were given for 28 days and cisplatin was administered at its optimal schedule, for 5 days (i.v.).The combination of JQ1 and cisplatin was given for 5 days within the first week of treatment, followed by JQ1 maintenance from day 14 until the end of the study on day 28.

Cisplatin and JQ1 were well tolerated as single agents with a maximum mean BWL of 6% for cisplatin, and 5% and 7% for JQ1 at 50 mg/kg and 80 mg/kg, respectively. Combination of cisplatin and JQ1 led to slightly increased mean BWL of 10%. The mice were therefore given 1 week drug holiday before starting the JQ1 maintenance. The activity of the treatment was evaluated on day 28 after start of treatment comparing the mean tumor weights of the control group and treated groups (%T/C) (3.2.16.2).

The activity of cisplatin and JQ1 alone in this study was classified as not active according to standard National Cancer Institute criteria (active treatment: %T/C < 42%) with a %T/C of 88% for cisplatin, and 79% and 60% for JQ1 at 50 mg/kg and 80 mg/kg, respectively (Figure 41B). The combination of cisplatin and JQ1 followed by JQ1 maintenance however, was active with a %T/C of 41% on day 28, and resulted in a statistically significant lower tumor weight and tumor volume, compared with either agent alone (Figure 41 A, B).
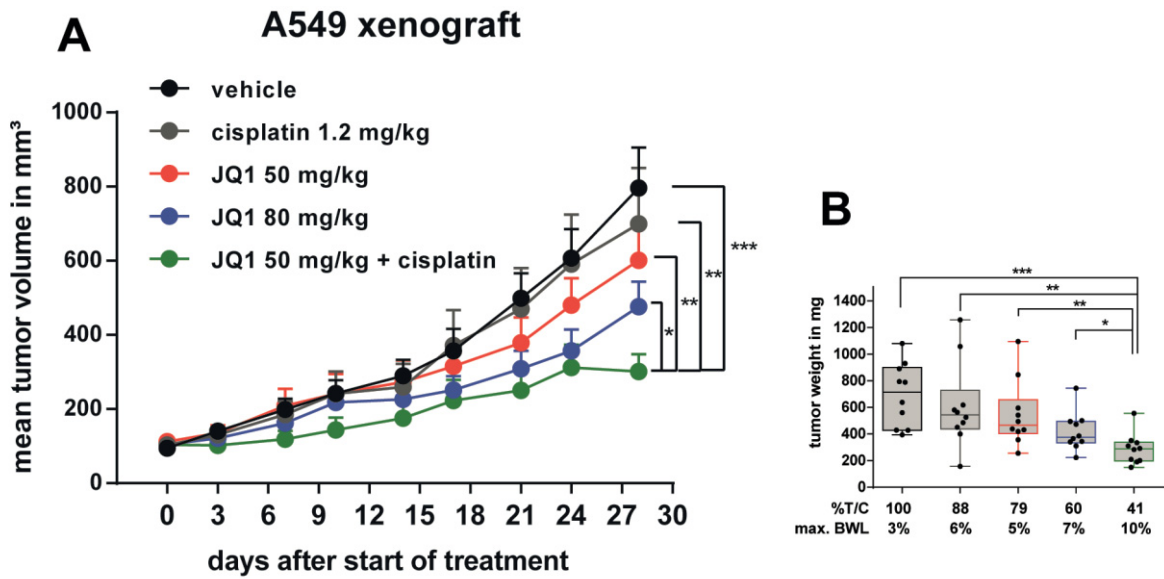
Figure 41: Combination of JQ1 and cisplatin in the subcutaneous A549 xenograft mouse model. A, Growth curve of A549 xenograft treated with vehicle, JQ1 (50 mg/kg, 80 mg/kg) i.p. QDx28, cisplatin 1.2 mg/kg i.v. QDx5 or in combination (50 mg/kg JQ1 + 1.2. mg/kg QDx5 cisplatin followed by 7 days off and JQ1 maintenance). Error bars denote SEM (n=10 mice per group) * $p < 0.05$, ** $p < 0.01$, *** $p < 0.001$ two-tailed unpaired Student's t-test on $\log_{10}$ transformed tumor volume on day 28 after start of treatment. B, Box and whiskers plot of tumor weight on day 28 after start of treatment. Error bars denote SEM (n=10 mice per group). * $p < 0.05$, ** $p < 0.01$, *** $p < 0.001$ two-tailed unpaired Student's t-test on $\log_{10}$-transformed tumor weight.

5. Discussion

In recent years epigenetic regulators have become attractive targets for therapy of complex diseases like cancer, in which both genetic and epigenetic alterations play essential roles. Since the approval of the first-generation epigenetic therapies targeting DNA methyltransferases and histone deacetylases for the treatment of hematological malignancies, the field has expanded to several other protein families such as bromodomain proteins, histone methyltransferases, and histone demethylases (Valdespino and Valdespino, 2015). Understanding and defining the roles of these epigenetic regulators at the cellular level is an important part of pre-clinical drug development. BET (BRD2, BRD3, BRD4 and BRDT) inhibitors block the interaction between members of the BET family and acetylated lysine residues of histone tails (Filippakopoulos et al., 2010). Anti-tumor activity of potent and selective inhibitors of BET proteins like JQ1, I-BET762 and OTX015 has been shown in a large number of pre-clinical models of hematological and solid tumors (Table 2). However the anti-tumor activity of BET inhibitors can be quite diverse among cell lines. Given the potential of BET bromodomain proteins in cancer therapy, a detailed understanding of their functional activity becomes more and more important.

5.1 Functional effects of BET inhibition in NSCLC

5.1.1 Activity of BET inhibitors in *KRAS*-mutated NSCLC cell lines

The activity of BET inhibitors has been linked to a reduction of gene expression for a number of oncogene drivers such as members of the *MYC* family, *GLI* and *FOSL1* transcription factors (Delmore et al., 2011; Kandela et al., 2015; Lockwood et al., 2012; Tang et al., 2014). A recent study (Soucek et al., 2013) has shown that the *MYC* proto-oncogene is essential for *KRAS*-driven tumors. The expression profiles of tumors from patients diagnosed with lung adenocarcinoma comparing the *KRAS* wild-type and mutant populations identified *MYC* expression together with an enrichment of the *MYC* transcriptional profile as characteristic of the *KRAS* mutant cohort.

BET inhibitors potently reduce the growth of *MYC*-dependent malignancies like MM and AML (Delmore et al., 2011; Zuber et al., 2011).They were already tested on a number of *KRAS* mutant NSCLC cell lines but their activity could not always be linked to transcriptional

Discussion

suppression of *MYC* (Lockwood et al., 2012). In the present work, the activity of JQ1 was characterized using a viability assay in a panel of 12 *KRAS* mutant NSCLC cell lines. Strong effects leading to a reduction of cell growth and viability were observed in a sub-population of cell lines, defining them as particularly sensitive to BET bromodomain inhibition. This subset of 3 out of 12 cell lines accounted for 25% of the tested cell lines.

5.1.2 Mutation status, cell doubling time of the NSCLC cell lines and basal expression of BET family members

The mutational status of the 12 NSCLC cell lines revealed that the tumor suppressor p53 and Liver kinase B1 (LKB1) were frequently mutated and that LKB1 mutation was enriched in the BET inhibitor insensitive cell lines population. P53 mutation has a high incidence in all cancer types and can lead to loss of wild-type p53 or gain of function p53 supporting the malignant state of a cancer cell (Muller and Vousden, 2014). Co-occurring genetic alterations of *KRAS* and *LKB1* on the other hand lead to a more aggressive type of lung cancer with lower levels of immune markers, and define a major subgroup (18-32%) of *KRAS*-mutated NSCLC (Ji et al., 2007; Skoulidis et al., 2015).

Additionally LKB1 knockdown was described to reduce the sensitivity of *KRAS*-driven lung tumors to the BET inhibitor JQ1 (Shimamura et al., 2013) but the underlying mechanism remains unclear. Basal levels of BRD2, BRD3 and BRD4 were determined using qRT-PCR and showed that their expression did not predict the activity of BET inhibitors. Also, the doubling time of the cells did not influence the activity of BET inhibitors either.

5.1.3 Effect of BET inhibitors on cell cycle and apoptosis induction

To further characterize the effect of BET inhibitors on the cellular phenotype, cell cycle distribution and apoptosis assays were performed. Using a flow cytometry based EdU staining assay, DV90 and H1373 cells treated for 24 h with BET inhibitors showed a dose-dependent reduction of the S phase population, while the G1/G0 phase population increased. Exposure of DV90 and H1373 cells with BET inhibitors for 48 h lead to increased induction of apoptosis in a dose-dependent manner, while being independently of the p53 mutation status of the cells. Neither cell cycle arrest nor induction of apoptosis was seen in the BET inhibitor insensitive A549 and H460 cells.

Discussion

This suggested that induction of cell cycle arrest was a sign of early response, while induction of apoptosis only took place at a later stage and that the two effects were induced by BET inhibitor treatment. Also the data revealed that insensitive cell lines showed no change in cell cycle distribution or cellular viability when exposed to BET inhibitors.

5.1.4 BET inhibitor effect on BRD4 function in sensitive and insensitive cell lines

It was interesting to see whether JQ1 might still be functionally active in the insensitive cell line, as some tumors have been described to develop multi-drug resistance by up-regulation of exporter proteins such as P-glycoprotein or Multidrug-Resistance-Protein-1 (MDR-1), thereby acquiring resistance to chemotherapy. These exporters actively pump the small molecules out of the cytosol, leading to reduced drug concentrations inside the cell and acquired drug resistance.

BET inhibition was shown before to efficiently block BRD4 chromatin interaction. Therefore the activity of JQ1 was determined in the cellular context. Detergent washout of BRD4-GFP fusion protein overexpressed in H1373 cells showed that BRD4 was unable to bind to chromatin anymore after cells were treated with JQ1. Immunocytochemistry confirmed that JQ1 was functionally active in the sensitive H1373 cells but also in the insensitive A549 cells. Additionally, western blot analysis showed that JQ1 treatment led to increased chromatin-unbound fraction of BRD4 in a dose-dependent manner, independently of the anti-tumor activity of JQ1 in the cell line.

Altogether this confirmed that BET inhibitors were functionally active in sensitive and resistant cell lines. This led to the hypothesis that the anti-tumor activity of BET inhibition is linked to changes in gene regulation following functional inhibition of BET-chromatin interactions.

5.1.5 BET bromodomain gene regulatory functions

Microarray-based whole transcript analysis was used to identify the global changes induced by BET inhibition in the sensitive DV90 cells. The early (4 h) significant change of gene expression induced by JQ1 treatment at IC_{50} were quite limited and revealed *MYC* as one of the early response genes.

Discussion

The protein half life time of c-Myc is quite fast with 150 min. Accordingly, *MYC* transcriptional programs were among the top enriched gene sets after 24 h of JQ1 treatment. Even though *MYC* down-regulation was reported in a number of indications following BET inhibition (Delmore et al., 2011; Kandela et al., 2015; Zuber et al., 2011), its regulation was not a common feature of BET inhibition in NSCLC. However, the most sensitive cell lines showed strong down-regulation of c-Myc confirmed by western blot, while insensitive cell lines were largely unaffected. The H2347 cell line shown not to be not very sensitive to BET inhibition, also showed down-regulation of c-Myc. A possible explanation for this might be that the growth of these cells is dependent on other oncogenic drivers unaffected by c-Myc, as suggested by its low expression level in this cell line. On the other hand, BET inhibition showed anti-proliferative activity in H1792 cells even though c-Myc expression was not altered, suggesting that additional effects of BET inhibition, independent of c-Myc down-regulation can lead to anti-proliferative activity.

The members of the BET family and in particular BRD4 bind genome-wide to chromatin and exhibit regulatory functions, however the number of gene with expression changes found by micro array analysis was rather limited. A possible explanation is that only a limited number of genes and enhancers would be sensitive to loss of occupancy by BRD4. Recent studies described large enhancer sites called super-enhancers that regulate and drive expression of genes defining the identity of a cell were recently identified (Whyte et al., 2013). Here the identification of super-enhancers was made possible by genome-wide listing of potential enhancer sites marked by H3K27Ac marks followed by analysis of enhancer binding factors like mediator 1 (MED1) occupancy clustering. Small nearby clusters of enhancer binding factors are concentrated in large clusters forming a super-enhancer site. In the DV90 cells 873 super-enhancers were identified. The nearest coding gene of those super-enhancers was annotated. Among these there were 4 super-enhancers in close proximity to the *MYC* TSS, called MYC E1-4. BRD4 was found to occupy a large number of super-enhancers and loss of BRD4 at those sites ultimately led to strong loss of expression of the target genes (Loven et al., 2013). It is assumed that absence of BRD4 can destabilize protein complexes that bind to these enhancers, strongly reducing the activity of these complexes and the expression of downstream genes. Among the NSCLC models tested, the differential down-regulation of *MYC* upon JQ1 treatment may be explained by the occurrence of different enhancer landscapes with variable dependencies on BRD4 occupancy.

Discussion

In AML a distant super-enhancer was identified that drives *MYC* expression in a BRD4-dependent manner (Roe et al., 2015; Shi et al., 2013). Also, the enhancer landscapes of initially sensitive cancer cells can change under the pressure of BET inhibitors, as recently described in *in vitro* and *in vivo* in models of AML (Fong et al., 2015; Rathert et al., 2015). The cells acquired resistance to BET inhibition by changing the enhancer landscape nearby the promoter of *MYC* leading to a rebound of *MYC* expression. Constant expression of c-Myc in spite of treatment with BET inhibitors may therefore play a role in inherent JQ1 resistance.

As *in vitro* assays are unable to completely recapitulate the pharmacological properties of a compound which will ultimately determine its applicability in cancer treatment, the anti-tumor activity of BET inhibition was evaluated in an *in vivo* setting. H1373-xenografted SCID mice were treated with 50 mg/kg JQ1 daily. The treatment with JQ1 significantly reduced tumor growth *in vivo* with a %T/C value of 32%, in agreement with recent findings describing the efficacy of BET inhibitors in a *KRAS*-driven NSCLC mouse model (Shimamura et al., 2013). In addition, western blot analysis of the tumor tissue showed a down-regulation of c-Myc protein level 24 h after treatment with JQ1.

Loss of c-Myc can lead to cell cycle arrest and cell death in tumors (Hydbring et al., 2010; Soucek et al., 2013; Wu et al., 2007), however whether the overexpression of c-Myc could rescue the cells from the BET inhibitory effect had not been evaluated so far. A rescue experiment showed that the proliferation inhibition induced by JQ1 in H1373 cell, as evidenced by EdU staining, could be at least partially rescued by c-Myc overexpression thus establishing a link between reduced NSCLC cell proliferation and c-Myc protein levels. However the only partial rescue indicates that there are probably additional effects induced by JQ1, in line with the finding that some cells are sensitive to BET inhibitor without changes in c-Myc protein levels.

Overall these results support the role of BET inhibition in the suppression of oncogene expression such as *MYC*. They also show that the differential gene regulatory role of BET proteins depends on the enhancer landscape of the cell.

Discussion

5.2 Combinatory potential of BET inhibition

Even though depletion of the *MYC* oncogene can strongly reduce the growth of *KRAS* mutant NSCLC, only a distinct sub-group of NSCLC was affected in this way by JQ1 treatment. Beyond the regulation of the *MYC* oncogene, the transcriptional changes of 370 genes in sensitive H1373 and insensitive H2030 cells were evidenced using qRT-PCR and showed that two key negative regulators of apoptosis, c-FLIP and XIAP, were both strongly down-regulated in the two cell lines after JQ1 treatment. Western blotting showed that in contrast to *MYC*, the expression of these two genes was reduced in all NSCLC cell lines tested.

ChIP-qPCR revealed that BRD4 indeed occupies the promoter site of *FLIP* and *XIAP* and can be effectively removed by BET inhibitors, leading to strong down-regulation of the two genes. Cellular FLICE-like inhibitory protein (c-FLIP) is one of the key anti-apoptotic regulators overexpressed in NSCLC. It binds to pro-caspase-8 and thereby regulates its activation by FADD (Fas-associated death domain protein) bound to death receptors such as Fas, DR4, DR5 and TNF-R1 (Hughes et al., 2016; Shirley and Micheau, 2013). Additionally, cytoplasmic overexpression of c-FLIP has been linked to poor overall survival in NSCLC patients (Riley et al., 2013). Because of its structural similarity with caspase-8, direct targeting of c-FLIP with small-molecules has been challenging. Another frequently overexpressed anti-apoptotic regulator is X-linked inhibitor of apoptosis (XIAP), a member of the inhibitor of apoptosis protein (IAP) family, which blocks the activity of caspase-3, -7 and -9. Endogenous inhibitors of XIAP function such as second mitochondria-derived activator of caspases (SMAC) released from the mitochondria have been described and molecules that mimics SMAC are already in clinical development as apoptosis inducers or drug-sensitizers (Obexer and Ausserlechner, 2014).

This observation of reduced c-FLIP and XIAP levels led to the rationale of combining the BET inhibitor JQ1 with a pro-apoptotic agent such as TRAIL. Death receptor targeting agents inducing extrinsic apoptosis are currently in clinical development (Lemke et al., 2014b) and down-regulation of two key anti-apoptotic proteins MCL1 and c-FLIP by CDK9 inhibition was recently identified to have enhanced effects in NSCLC when combined with death-receptor ligand TRAIL (Lemke et al., 2014a). While finishing these studies, another group also proposed that JQ1 enhances TRAIL-induced apoptosis (Yao et al., 2015), although the molecular mechanism was not described. In this work, the combination of JQ1 with TRAIL

Discussion

treatment showed potent induction of apoptosis in the treated H1373 cells (sensitive to BET inhibition) as well as in the A549 and H2030 cells (not sensitive to BET inhibition). Enhanced TRAIL-induced apoptosis was shown to be generally caspase dependent, and not depending solely on either initiator caspase-8 or -9. TRAIL induces the apoptotic extrinsic pathway by binding the death receptor at the extra cellular matrix, inducing activation of caspase-8. The apoptotic signal can then be amplified by mitochondria outer-membrane permeabilization (MOMP) and caspase-9 activation. MOMP-dependent apoptosis is mediated by the pro-apoptotic proteins BAX and BAK which interact with BH3-only proteins such as BID and BIM. BAX and BAK possess redundant functions in releasing cytochrome C from mitochondria in mice. Recently the pro-apoptotic activity of BET inhibitors was described to be dependent on BAX and BAK function (Xu et al., 2016), while TRAIL was shown to preferentially induce BID-BAK dependent apoptosis (Sarosiek et al., 2013).

In this study, JQ1-enhanced TRAIL-induced apoptosis was shown to be largely unaffected by loss of either BAX or BAK, in agreement with previous observations showing that XIAP down-regulation enhances TRAIL activity in a BAX/BAK-independent manner (Gillissen et al., 2013). Using siRNA knockdown, the simultaneous loss of expression of the key apoptotic proteins XIAP and c-FLIP was identified as the major driver of caspase-8 and -9-dependent TRAIL-induced cell death by JQ1. Interestingly, BET inhibition led to down-regulation of XIAP and c-FLIP in all the NSCLC cell lines tested and accordingly, JQ1 treatment showed enhancing effects on TRAIL-induced apoptosis induction in all cell lines tested. Importantly combination of JQ1 and TRAIL did not affect the viability of normal HFF-1 fibroblast cells. Interestingly, combination of JQ1 with the pro-apoptotic agent cisplatin synergistically induced apoptosis as well as cell viability, independently of the sensitivity of the cell line to JQ1 as a single agent. Experiments with siRNAs showed that although the combination of JQ1 and cisplatin may result in broad effects on transcriptional programs and signaling pathways, down-regulation of the anti-apoptotic protein c-FLIP is a key driver for the enhanced cell death induction.

The increased anti-proliferative effect also translated *in vivo* in the A549 xenograft model, where treatment with either cisplatin or JQ1 alone showed limited activity.

Discussion

Promising first results of the clinical phase I trials with BET inhibitors have been reported (Amorim et al., 2016; Berthon et al., 2016; Stathis et al., 2016), and the present results show that characterization of the effect of BET inhibition on apoptosis-related genes can be valuable for the identification of attractive combination partners. The results also suggest that epigenetic therapy targeting BET proteins may be a useful approach to improve outcomes and overcome resistance compared to current standard-of-care treatments for NSCLC patients.

5.3   Final conclusion

This work contributes to a better understanding of BET bromodomain inhibition in cancer and should help to increase both the knowledge of the biology of the BET protein family and of the mode of action of BET inhibitors such as JQ1 or early clinical candidates such as I-BET762 and OTX-015. Initially the *MYC* oncogene was identified as the driving gene responding to BET inhibition in a subpopulation of *KRAS*-mutated NSCLC cell lines, which were particularly sensitive to BET inhibition.

Additionally two key negative regulators of apoptosis XIAP and c-FLIP were identified to be expressed in a BET-dependent manner. The loss of XIAP and c-FLIP increases the cellular susceptibility to caspase-dependent induction of apoptosis. Accordingly the effect of pro-apoptotic agents like TRAIL and the chemotherapeutic agent cisplatin was significantly enhanced in combination with the BET inhibitor JQ1. These combinations were able to re-sensitize cell lines resistant to BET inhibition alone.

5.4   Outlook

NSCLC has the highest incidence of cancer-related death worldwide and a high medical need for more effective therapies. About 80 percent of lung cancers can be histologically classified as NSCLC (VanderMeer et al., 2015), of which 30% harbor an activating oncogenic mutation in the GTPase domain of the KRAS signaling protein (Pylayeva-Gupta et al., 2011). A number of driving gene mutations have been identified and are characteristic of more than 50% of NSCLC cases (Figure 13). While a number of therapies are in clinical development and EGFR inhibitors are already on the market, no therapy for mutant *KRAS* is available.

Discussion

Anti-tumor activity of the potent and selective inhibitors of BET proteins like JQ1, I-BET762 and OTX015 has been shown in a large number of pre-clinical models of hematological and solid tumors (Table 2). However the anti-tumor activity of BET inhibitors can be quite diverse in pre-clinical models, which is consistent with the first results from the clinic. This work showed that BET inhibitor treatment could potentially become an attractive therapeutic option for the treatment for patients with malignant aggressive *KRAS*-mutated NSCLC.

Summary

Non-small cell lung cancer (NSCLC) has the highest incidence of cancer-related death worldwide and a high medical need for more effective therapies. Small molecule inhibitors of the bromodomain and extra terminal domain (BET) family such as JQ1, I-BET762 and OTX-015 are active in a wide range of different cancer types, including lung cancer. While their activity on oncogene expression such as c-Myc has been addressed by many studies, the effects of BET inhibition on the apoptotic pathway remain largely unknown. This work evaluates the activity of BET bromodomain inhibitors on cell cycle distribution and on components of the apoptotic response. Genome-wide transcriptional analyses together with chromatin immunoprecipitation followed by sequencing helped to identify the *MYC* gene and associated super-enhancers as a primary target of JQ1. Using a panel of twelve *KRAS*-mutated NSCLC models, it was found that cell lines responsive to BET inhibitors underwent apoptosis and reduced their S-phase population, concomitant with down-regulation of c-Myc expression. Conversely, ectopic c-Myc overexpression rescued the anti-proliferative effect of JQ1. In the H1373 xenograft model, treatment with JQ1 significantly reduced tumor growth and down-regulated the expression of c-Myc. The effects of BET inhibition on the expression of 370 genes involved in apoptosis were compared in sensitive and resistant cells and the expression of the two key apoptosis regulators *FLIP* and *XIAP* was found to be highly BET-dependent. Consistent with this, combination treatment of JQ1 with the tumor necrosis factor-related apoptosis-inducing ligand (TRAIL) or the pro-apoptotic chemotherapeutic agent cisplatin enhanced induction of apoptosis in both BET inhibitor sensitive and resistant cells. Furthermore the combination of JQ1 with cisplatin led to significantly improved anti-tumor efficacy in A549 tumor-bearing mice. Altogether these results show that the identification of BET-dependent genes provides guidance for the choice of drug combinations in cancer treatment. They also demonstrate that BET inhibition primes NSCLC cells for induction of apoptosis and that a combination with pro-apoptotic compounds represents a valuable strategy to overcome treatment resistance.

Zusammenfassung

Nicht-kleinzelliger Lungenkrebs (NSCLC) hat die höchste Inzidenz an krebsbedingten Todesfällen weltweit und gleichzeitig einen hohen medizinischen Bedarf an effektiveren Therapien. Molekulare Inhibitoren der Bromodomain and extra-terminal domain (BET) Familie wie JQ1, IBET-762 und OTX-015 wirken in einem breiten Spektrum von verschiedenen Krebsarten, einschließlich Lungenkrebs. Während ihre Aktivität auf die Expression von Onkogenen wie c-Myc in vielen Studien untersucht wurde, bleibt der Effekt von BET-Inhibition auf den Apoptose Signalweg weitgehend unbekannt. In dieser Arbeit wurde die Aktivität von BET Bromodomain-Inhibitoren auf den Zellzyklus und auf Komponenten der Apoptose-Antwort der Zelle untersucht. Genomweite Transkriptionsanalysen haben zusammen mit Chromatin Immunpräzipitation und anschließender Sequenzierung geholfen das *MYC* Gen und dessen assoziierte Super-enhancer als primäres Ziel des BET-Inhibitors JQ1 zu identifizieren. Mittels einer Gruppe von 12 NSCLC Modellen mit *KRAS* Mutation belegt diese Arbeit, dass Zelllinien die auf die BET-Inhibitoren reagieren in Apoptose gehen und eine Reduktion der S-Phasen Population zusammen mit gleichzeitiger Herunterregulation der c-Myc Expression aufwiesen. Andererseits konnte die ektopische Überexpression von c-Myc der anti-proliferativen Wirkung entgegenwirken. In dem H1373-Xenograft Modell reduzierte die Behandlung mit JQ1 das Tumorwachstum und die Expression von c-Myc signifikant. Die Auswirkung von BET-Inhibition auf die Expression von 370 Genen, die in der Apoptose Regulation involviert sind, wurde in sensitiven und resistenten Zellen verglichen und dabei wurde die starke BET-Abhängigkeit der Expression von zwei Schlüsselgenen der Apoptose *FLIP* und *XIAP* festgestellt. Damit übereinstimmend verstärkte die Kombination von JQ1 mit dem *tumor necrosis factor-related apoptosis-inducing ligand* (TRAIL) oder dem pro-apoptotischen Chemotherapeutikums Cisplatin die Induktion von Apoptose in sowohl BET-Inhibitor sensitiven als auch in resistenten Zellen. Des Weiteren zeigte die Kombination einen signifikant verbesserten Antitumor-Effekte in A549 tumortragenden Mäusen. Insgesamt zeigen diese Ergebnisse, dass die Identifizierung von BET-abhängigen Genen unterstützend für die Wahl von therapeutischen Kombinationspartnern in der Krebsbehandlung sein kann. Sie zeigen auch, dass die Inhibition von BET Proteinen, NSCLC Zellen für die Induktion von Apoptose sensibilisiert und dass eine Kombination mit pro-apoptotischen Verbindungen eine wertvolle Behandlungsstrategie, um Resistenzen zu überwinden, bieten kann.

References

(2012). An integrated encyclopedia of DNA elements in the human genome. Nature *489*, 57-74.

Adelman, K., and Lis, J.T. (2012). Promoter-proximal pausing of RNA polymerase II: emerging roles in metazoans. Nat Rev Genet *13*, 720-731.

Ahnesorg, P., and Jackson, S.P. (2007). The non-homologous end-joining protein Nej1p is a target of the DNA damage checkpoint. DNA Repair (Amst) *6*, 190-201.

Alekseyenko, A.A., Walsh, E.M., Wang, X., Grayson, A.R., Hsi, P.T., Kharchenko, P.V., Kuroda, M.I., and French, C.A. (2015). The oncogenic BRD4-NUT chromatin regulator drives aberrant transcription within large topological domains. Genes Dev *29*, 1507-1523.

Allfrey, V.G., Faulkner, R., and Mirsky, A.E. (1964). Acetylation and Methylation of Histones and Their Possible Role in the Regulation of Rna Synthesis. Proc Natl Acad Sci U S A *51*, 786-794.

Ambrosini, G., Sawle, A.D., Musi, E., and Schwartz, G.K. (2015). BRD4-targeted therapy induces Myc-independent cytotoxicity in Gnaq/11-mutatant uveal melanoma cells. Oncotarget *6*, 33397-33409.

Amorim, S., Stathis, A., Gleeson, M., Iyengar, S., Magarotto, V., Leleu, X., Morschhauser, F., Karlin, L., Broussais, F., Rezai, K.*, et al.* (2016). Bromodomain inhibitor OTX015 in patients with lymphoma or multiple myeloma: a dose-escalation, open-label, pharmacokinetic, phase 1 study. Lancet Haematol *3*, e196-204.

Anders, L., Guenther, M.G., Qi, J., Fan, Z.P., Marineau, J.J., Rahl, P.B., Loven, J., Sigova, A.A., Smith, W.B., Lee, T.I.*, et al.* (2014). Genome-wide localization of small molecules. Nat Biotechnol *32*, 92-96.

Andrews, F.H., Shanle, E.K., Strahl, B.D., and Kutateladze, T.G. (2016). The essential role of acetyllysine binding by the YEATS domain in transcriptional regulation. Transcription *7*, 14-20.

Arner, E., Daub, C.O., Vitting-Seerup, K., Andersson, R., Lilje, B., Drablos, F., Lennartsson, A., Ronnerblad, M., Hrydziuszko, O., Vitezic, M.*, et al.* (2015). Transcribed enhancers lead waves of coordinated transcription in transitioning mammalian cells. Science *347*, 1010-1014.

Arrowsmith, C.H., Bountra, C., Fish, P.V., Lee, K., and Schapira, M. (2012). Epigenetic protein families: a new frontier for drug discovery. Nat Rev Drug Discov *11*, 384-400.

Asangani, I.A., Dommeti, V.L., Wang, X., Malik, R., Cieslik, M., Yang, R., Escara-Wilke, J., Wilder-Romans, K., Dhanireddy, S., Engelke, C.*, et al.* (2014). Therapeutic targeting of BET bromodomain proteins in castration-resistant prostate cancer. Nature *510*, 278-282.

References

Ausio, J., and Abbott, D.W. (2002). The many tales of a tail: carboxyl-terminal tail heterogeneity specializes histone H2A variants for defined chromatin function. Biochemistry *41*, 5945-5949.

Baker, E.K., Taylor, S., Gupte, A., Sharp, P.P., Walia, M., Walsh, N.C., Zannettino, A.C., Chalk, A.M., Burns, C.J., and Walkley, C.R. (2015). BET inhibitors induce apoptosis through a MYC independent mechanism and synergise with CDK inhibitors to kill osteosarcoma cells. Sci Rep *5*, 10120.

Bandopadhayay, P., Bergthold, G., Nguyen, B., Schubert, S., Gholamin, S., Tang, Y., Bolin, S., Schumacher, S.E., Zeid, R., Masoud, S.*, et al.* (2014). BET bromodomain inhibition of MYC-amplified medulloblastoma. Clin Cancer Res *20*, 912-925.

Bannister, A.J., and Kouzarides, T. (2011). Regulation of chromatin by histone modifications. Cell Res *21*, 381-395.

Baratta, M.G., Schinzel, A.C., Zwang, Y., Bandopadhayay, P., Bowman-Colin, C., Kutt, J., Curtis, J., Piao, H., Wong, L.C., Kung, A.L.*, et al.* (2015). An in-tumor genetic screen reveals that the BET bromodomain protein, BRD4, is a potential therapeutic target in ovarian carcinoma. Proc Natl Acad Sci U S A *112*, 232-237.

Barneda-Zahonero, B., and Parra, M. (2012). Histone deacetylases and cancer. Mol Oncol *6*, 579-589.

Barrangou, R., Fremaux, C., Deveau, H., Richards, M., Boyaval, P., Moineau, S., Romero, D.A., and Horvath, P. (2007). CRISPR provides acquired resistance against viruses in prokaryotes. Science *315*, 1709-1712.

Bartke, T., Vermeulen, M., Xhemalce, B., Robson, S.C., Mann, M., and Kouzarides, T. (2010). Nucleosome-interacting proteins regulated by DNA and histone methylation. Cell *143*, 470-484.

Bedford, M.T., and Clarke, S.G. (2009). Protein arginine methylation in mammals: who, what, and why. Mol Cell *33*, 1-13.

Belkina, A.C., and Denis, G.V. (2012). BET domain co-regulators in obesity, inflammation and cancer. Nat Rev Cancer *12*, 465-477.

Bentley, D.L. (2014). Coupling mRNA processing with transcription in time and space. Nat Rev Genet *15*, 163-175.

Berg, J.M., Tymoczko, J.L., and Stryer, L. (2007). Biochemistry, 6th edn (New York, W.H. Freeman).

Berkovits, B.D., and Wolgemuth, D.J. (2013). The role of the double bromodomain-containing BET genes during mammalian spermatogenesis. Curr Top Dev Biol *102*, 293-326.

Bernstein, B.E., and Schreiber, S.L. (2002). Global approaches to chromatin. Chem Biol *9*, 1167-1173.

References

Berthon, C., Raffoux, E., Thomas, X., Vey, N., Gomez-Roca, C., Yee, K., Taussig, D.C., Rezai, K., Roumier, C., Herait, P.*, et al.* (2016). Bromodomain inhibitor OTX015 in patients with acute leukaemia: a dose-escalation, phase 1 study. Lancet Haematol *3*, e186-195.

Bhagwat, A.S., Roe, J.S., Mok, B.Y., Hohmann, A.F., Shi, J., and Vakoc, C.R. (2016). BET Bromodomain Inhibition Releases the Mediator Complex from Select cis-Regulatory Elements. Cell Rep *15*, 519-530.

Bienroth, S., Keller, W., and Wahle, E. (1993). Assembly of a processive messenger RNA polyadenylation complex. EMBO J *12*, 585-594.

Birney, E., Stamatoyannopoulos, J.A., Dutta, A., Guigo, R., Gingeras, T.R., Margulies, E.H., Weng, Z., Snyder, M., Dermitzakis, E.T., Thurman, R.E.*, et al.* (2007). Identification and analysis of functional elements in 1% of the human genome by the ENCODE pilot project. Nature *447*, 799-816.

Boi, M., Gaudio, E., Bonetti, P., Kwee, I., Bernasconi, E., Tarantelli, C., Rinaldi, A., Testoni, M., Cascione, L., Ponzoni, M.*, et al.* (2015). The BET Bromodomain Inhibitor OTX015 Affects Pathogenetic Pathways in Preclinical B-cell Tumor Models and Synergizes with Targeted Drugs. Clin Cancer Res *21*, 1628-1638.

Bolden, J.E., Peart, M.J., and Johnstone, R.W. (2006). Anticancer activities of histone deacetylase inhibitors. Nat Rev Drug Discov *5*, 769-784.

Bosch, A., and Suau, P. (1995). Changes in core histone variant composition in differentiating neurons: the roles of differential turnover and synthesis rates. Eur J Cell Biol *68*, 220-225.

Buratowski, S. (2009). Progression through the RNA polymerase II CTD cycle. Mol Cell *36*, 541-546.

Chaidos, A., Caputo, V., Gouvedenou, K., Liu, B., Marigo, I., Chaudhry, M.S., Rotolo, A., Tough, D.F., Smithers, N.N., Bassil, A.K.*, et al.* (2014). Potent antimyeloma activity of the novel bromodomain inhibitors I-BET151 and I-BET762. Blood *123*, 697-705.

Chang, B., Chen, Y., Zhao, Y., and Bruick, R.K. (2007). JMJD6 is a histone arginine demethylase. Science *318*, 444-447.

Chen, Z.A., Jawhari, A., Fischer, L., Buchen, C., Tahir, S., Kamenski, T., Rasmussen, M., Lariviere, L., Bukowski-Wills, J.C., Nilges, M.*, et al.* (2010). Architecture of the RNA polymerase II-TFIIF complex revealed by cross-linking and mass spectrometry. EMBO J *29*, 717-726.

Cheng, J., Blum, R., Bowman, C., Hu, D., Shilatifard, A., Shen, S., and Dynlacht, B.D. (2014). A role for H3K4 monomethylation in gene repression and partitioning of chromatin readers. Mol Cell *53*, 979-992.

Cheng, X., Collins, R.E., and Zhang, X. (2005). Structural and sequence motifs of protein (histone) methylation enzymes. Annu Rev Biophys Biomol Struct *34*, 267-294.

References

Cheng, Z., Gong, Y., Ma, Y., Lu, K., Lu, X., Pierce, L.A., Thompson, R.C., Muller, S., Knapp, S., and Wang, J. (2013). Inhibition of BET bromodomain targets genetically diverse glioblastoma. Clin Cancer Res *19*, 1748-1759.

Ciceri, P., Muller, S., O'Mahony, A., Fedorov, O., Filippakopoulos, P., Hunt, J.P., Lasater, E.A., Pallares, G., Picaud, S., Wells, C.*, et al.* (2014). Dual kinase-bromodomain inhibitors for rationally designed polypharmacology. Nat Chem Biol *10*, 305-312.

Cong, L., Ran, F.A., Cox, D., Lin, S., Barretto, R., Habib, N., Hsu, P.D., Wu, X., Jiang, W., Marraffini, L.A.*, et al.* (2013). Multiplex genome engineering using CRISPR/Cas systems. Science *339*, 819-823.

Corden, J.L. (2013). RNA polymerase II C-terminal domain: Tethering transcription to transcript and template. Chem Rev *113*, 8423-8455.

Crick, F. (1970). Central dogma of molecular biology. Nature *227*, 561-563.

Crick, F.H. (1958). On protein synthesis. Symp Soc Exp Biol *12*, 138-163.

Cuthbert, G.L., Daujat, S., Snowden, A.W., Erdjument-Bromage, H., Hagiwara, T., Yamada, M., Schneider, R., Gregory, P.D., Tempst, P., Bannister, A.J.*, et al.* (2004). Histone deimination antagonizes arginine methylation. Cell *118*, 545-553.

Da Costa, D., Agathanggelou, A., Perry, T., Weston, V., Petermann, E., Zlatanou, A., Oldreive, C., Wei, W., Stewart, G., Longman, J.*, et al.* (2013). BET inhibition as a single or combined therapeutic approach in primary paediatric B-precursor acute lymphoblastic leukaemia. Blood Cancer J *3*, e126.

de Castro Carpeno, J., and Belda-Iniesta, C. (2013). KRAS mutant NSCLC, a new opportunity for the synthetic lethality therapeutic approach. Transl Lung Cancer Res *2*, 142-151.

Delmore, J.E., Issa, G.C., Lemieux, M.E., Rahl, P.B., Shi, J., Jacobs, H.M., Kastritis, E., Gilpatrick, T., Paranal, R.M., Qi, J.*, et al.* (2011). BET bromodomain inhibition as a therapeutic strategy to target c-Myc. Cell *146*, 904-917.

Dhalluin, C., Carlson, J.E., Zeng, L., He, C., Aggarwal, A.K., and Zhou, M.M. (1999). Structure and ligand of a histone acetyltransferase bromodomain. Nature *399*, 491-496.

Dias, J.D., Rito, T., Torlai Triglia, E., Kukalev, A., Ferrai, C., Chotalia, M., Brookes, E., Kimura, H., and Pombo, A. (2015). Methylation of RNA polymerase II non-consensus Lysine residues marks early transcription in mammalian cells. Elife *4*.

Eckhoff, K., Flurschutz, R., Trillsch, F., Mahner, S., Janicke, F., and Milde-Langosch, K. (2013). The prognostic significance of Jun transcription factors in ovarian cancer. J Cancer Res Clin Oncol *139*, 1673-1680.

Eichner, J., Chen, H.T., Warfield, L., and Hahn, S. (2010). Position of the general transcription factor TFIIF within the RNA polymerase II transcription preinitiation complex. EMBO J *29*, 706-716.

References

Ember, S.W., Zhu, J.Y., Olesen, S.H., Martin, M.P., Becker, A., Berndt, N., Georg, G.I., and Schonbrunn, E. (2014). Acetyl-lysine binding site of bromodomain-containing protein 4 (BRD4) interacts with diverse kinase inhibitors. ACS Chem Biol *9*, 1160-1171.

Ernst, J., Kheradpour, P., Mikkelsen, T.S., Shoresh, N., Ward, L.D., Epstein, C.B., Zhang, X., Wang, L., Issner, R., Coyne, M.*, et al.* (2011). Mapping and analysis of chromatin state dynamics in nine human cell types. Nature *473*, 43-49.

Filippakopoulos, P., and Knapp, S. (2014). Targeting bromodomains: epigenetic readers of lysine acetylation. Nat Rev Drug Discov *13*, 337-356.

Filippakopoulos, P., Picaud, S., Mangos, M., Keates, T., Lambert, J.P., Barsyte-Lovejoy, D., Felletar, I., Volkmer, R., Muller, S., Pawson, T.*, et al.* (2012). Histone recognition and large-scale structural analysis of the human bromodomain family. Cell *149*, 214-231.

Filippakopoulos, P., Qi, J., Picaud, S., Shen, Y., Smith, W.B., Fedorov, O., Morse, E.M., Keates, T., Hickman, T.T., Felletar, I.*, et al.* (2010). Selective inhibition of BET bromodomains. Nature *468*, 1067-1073.

Fong, C.Y., Gilan, O., Lam, E.Y., Rubin, A.F., Ftouni, S., Tyler, D., Stanley, K., Sinha, D., Yeh, P., Morison, J.*, et al.* (2015). BET inhibitor resistance emerges from leukaemia stem cells. Nature *525*, 538-542.

French, C. (2014). NUT midline carcinoma. Nat Rev Cancer *14*, 149-150.

Frye, R.A. (2000). Phylogenetic classification of prokaryotic and eukaryotic Sir2-like proteins. Biochem Biophys Res Commun *273*, 793-798.

Garber, K. (2007). HDAC inhibitors overcome first hurdle. Nat Biotechnol *25*, 17-19.

Gaucher, J., Boussouar, F., Montellier, E., Curtet, S., Buchou, T., Bertrand, S., Hery, P., Jounier, S., Depaux, A., Vitte, A.L.*, et al.* (2012). Bromodomain-dependent stage-specific male genome programming by Brdt. EMBO J *31*, 3809-3820.

Gelato, K.A., Shaikhibrahim, Z., Ocker, M., and Haendler, B. (2016). Targeting epigenetic regulators for cancer therapy: modulation of bromodomain proteins, methyltransferases, demethylases, and microRNAs. Expert Opin Ther Targets *20*, 783-799.

Gillissen, B., Richter, A., Overkamp, T., Essmann, F., Hemmati, P.G., Preissner, R., Belka, C., and Daniel, P.T. (2013). Targeted therapy of the XIAP/proteasome pathway overcomes TRAIL-resistance in carcinoma by switching apoptosis signaling to a Bax/Bak-independent 'type I' mode. Cell Death Dis *4*, e643.

Gyuris, A., Donovan, D.J., Seymour, K.A., Lovasco, L.A., Smilowitz, N.R., Halperin, A.L., Klysik, J.E., and Freiman, R.N. (2009). The chromatin-targeting protein Brd2 is required for neural tube closure and embryogenesis. Biochim Biophys Acta *1789*, 413-421.

Hakim, O., and Misteli, T. (2012). SnapShot: Chromosome confirmation capture. Cell *148*, 1068 e1061-1062.

References

Hanahan, D., and Weinberg, R.A. (2000). The hallmarks of cancer. Cell *100*, 57-70.

Hanahan, D., and Weinberg, R.A. (2011). Hallmarks of cancer: the next generation. Cell *144*, 646-674.

He, Y., Fang, J., Taatjes, D.J., and Nogales, E. (2013). Structural visualization of key steps in human transcription initiation. Nature *495*, 481-486.

Heintzman, N.D., Stuart, R.K., Hon, G., Fu, Y., Ching, C.W., Hawkins, R.D., Barrera, L.O., Van Calcar, S., Qu, C., Ching, K.A.*, et al.* (2007). Distinct and predictive chromatin signatures of transcriptional promoters and enhancers in the human genome. Nat Genet *39*, 311-318.

Heinz, S., Romanoski, C.E., Benner, C., and Glass, C.K. (2015). The selection and function of cell type-specific enhancers. Nat Rev Mol Cell Biol *16*, 144-154.

Hensel, T., Giorgi, C., Schmidt, O., Calzada-Wack, J., Neff, F., Buch, T., Niggli, F.K., Schafer, B.W., Burdach, S., and Richter, G.H. (2016). Targeting the EWS-ETS transcriptional program by BET bromodomain inhibition in Ewing sarcoma. Oncotarget *7*, 1451-1463.

Henssen, A., Althoff, K., Odersky, A., Beckers, A., Koche, R., Speleman, F., Schafers, S., Bell, E., Nortmeyer, M., Westermann, F.*, et al.* (2016). Targeting MYCN-Driven Transcription By BET-Bromodomain Inhibition. Clin Cancer Res *22*, 2470-2481.

Henssen, A., Thor, T., Odersky, A., Heukamp, L., El-Hindy, N., Beckers, A., Speleman, F., Althoff, K., Schafers, S., Schramm, A.*, et al.* (2013). BET bromodomain protein inhibition is a therapeutic option for medulloblastoma. Oncotarget *4*, 2080-2095.

Hernando, H., Gelato, K.A., Lesche, R., Beckmann, G., Koehr, S., Otto, S., Steigemann, P., and Stresemann, C. (2016). EZH2 Inhibition Blocks Multiple Myeloma Cell Growth through Upregulation of Epithelial Tumor Suppressor Genes. Mol Cancer Ther *15*, 287-298.

Heyn, H., and Esteller, M. (2012). DNA methylation profiling in the clinic: applications and challenges. Nat Rev Genet *13*, 679-692.

Hodawadekar, S.C., and Marmorstein, R. (2007). Chemistry of acetyl transfer by histone modifying enzymes: structure, mechanism and implications for effector design. Oncogene *26*, 5528-5540.

Holliday, R., and Pugh, J.E. (1975). DNA modification mechanisms and gene activity during development. Science *187*, 226-232.

Houzelstein, D., Bullock, S.L., Lynch, D.E., Grigorieva, E.F., Wilson, V.A., and Beddington, R.S. (2002). Growth and early postimplantation defects in mice deficient for the bromodomain-containing protein Brd4. Mol Cell Biol *22*, 3794-3802.

Hu, S., Xie, Z., Onishi, A., Yu, X., Jiang, L., Lin, J., Rho, H.S., Woodard, C., Wang, H., Jeong, J.S.*, et al.* (2009). Profiling the human protein-DNA interactome reveals ERK2 as a transcriptional repressor of interferon signaling. Cell *139*, 610-622.

References

Hughes, M.A., Powley, I.R., Jukes-Jones, R., Horn, S., Feoktistova, M., Fairall, L., Schwabe, J.W., Leverkus, M., Cain, K., and MacFarlane, M. (2016). Co-operative and Hierarchical Binding of c-FLIP and Caspase-8: A Unified Model Defines How c-FLIP Isoforms Differentially Control Cell Fate. Mol Cell *61*, 834-849.

Hydbring, P., Bahram, F., Su, Y., Tronnersjo, S., Hogstrand, K., von der Lehr, N., Sharifi, H.R., Lilischkis, R., Hein, N., Wu, S.*, et al.* (2010). Phosphorylation by Cdk2 is required for Myc to repress Ras-induced senescence in cotransformation. Proc Natl Acad Sci U S A *107*, 58-63.

Imai, S., Johnson, F.B., Marciniak, R.A., McVey, M., Park, P.U., and Guarente, L. (2000). Sir2: an NAD-dependent histone deacetylase that connects chromatin silencing, metabolism, and aging. Cold Spring Harb Symp Quant Biol *65*, 297-302.

Jenuwein, T., and Allis, C.D. (2001). Translating the histone code. Science *293*, 1074-1080.

Jesenberger, V., and Jentsch, S. (2002). Deadly encounter: ubiquitin meets apoptosis. Nat Rev Mol Cell Biol *3*, 112-121.

Ji, H., Ramsey, M.R., Hayes, D.N., Fan, C., McNamara, K., Kozlowski, P., Torrice, C., Wu, M.C., Shimamura, T., Perera, S.A.*, et al.* (2007). LKB1 modulates lung cancer differentiation and metastasis. Nature *448*, 807-810.

Jiang, Y.W., Veschambre, P., Erdjument-Bromage, H., Tempst, P., Conaway, J.W., Conaway, R.C., and Kornberg, R.D. (1998). Mammalian mediator of transcriptional regulation and its possible role as an end-point of signal transduction pathways. Proc Natl Acad Sci U S A *95*, 8538-8543.

Jinek, M., Chylinski, K., Fonfara, I., Hauer, M., Doudna, J.A., and Charpentier, E. (2012). A programmable dual-RNA-guided DNA endonuclease in adaptive bacterial immunity. Science *337*, 816-821.

Jonkers, I., and Lis, J.T. (2015). Getting up to speed with transcription elongation by RNA polymerase II. Nat Rev Mol Cell Biol *16*, 167-177.

Jung, M., Gelato, K.A., Fernandez-Montalvan, A., Siegel, S., and Haendler, B. (2015). Targeting BET bromodomains for cancer treatment. Epigenomics *7*, 487-501.

Kallenberger, S.M., Beaudouin, J., Claus, J., Fischer, C., Sorger, P.K., Legewie, S., and Eils, R. (2014). Intra- and interdimeric caspase-8 self-cleavage controls strength and timing of CD95-induced apoptosis. Sci Signal *7*, ra23.

Kamakaka, R.T., and Biggins, S. (2005). Histone variants: deviants? Genes Dev *19*, 295-310.

Kandela, I., Jin, H.Y., and Owen, K. (2015). Registered report: BET bromodomain inhibition as a therapeutic strategy to target c-Myc. Elife *4*, e07072.

Kanno, T., Kanno, Y., LeRoy, G., Campos, E., Sun, H.W., Brooks, S.R., Vahedi, G., Heightman, T.D., Garcia, B.A., Reinberg, D.*, et al.* (2014). BRD4 assists elongation of both

References

coding and enhancer RNAs by interacting with acetylated histones. Nat Struct Mol Biol *21*, 1047-1057.

Khorasanizadeh, S. (2004). The nucleosome: from genomic organization to genomic regulation. Cell *116*, 259-272.

Kim, J., Daniel, J., Espejo, A., Lake, A., Krishna, M., Xia, L., Zhang, Y., and Bedford, M.T. (2006). Tudor, MBT and chromo domains gauge the degree of lysine methylation. EMBO Rep *7*, 397-403.

Kim, J.L., and Burley, S.K. (1994). 1.9 A resolution refined structure of TBP recognizing the minor groove of TATAAAAG. Nat Struct Biol *1*, 638-653.

Kim, J.L., Nikolov, D.B., and Burley, S.K. (1993a). Co-crystal structure of TBP recognizing the minor groove of a TATA element. Nature *365*, 520-527.

Kim, Y., Geiger, J.H., Hahn, S., and Sigler, P.B. (1993b). Crystal structure of a yeast TBP/TATA-box complex. Nature *365*, 512-520.

Kim, Y.G., Cha, J., and Chandrasegaran, S. (1996). Hybrid restriction enzymes: zinc finger fusions to Fok I cleavage domain. Proc Natl Acad Sci U S A *93*, 1156-1160.

Kouzarides, T. (2007). Chromatin modifications and their function. Cell *128*, 693-705.

Kulaeva, O.I., Hsieh, F.K., Chang, H.W., Luse, D.S., and Studitsky, V.M. (2013). Mechanism of transcription through a nucleosome by RNA polymerase II. Biochim Biophys Acta *1829*, 76-83.

Kumar, K., Raza, S.S., Knab, L.M., Chow, C.R., Kwok, B., Bentrem, D.J., Popovic, R., Ebine, K., Licht, J.D., and Munshi, H.G. (2015). GLI2-dependent c-MYC upregulation mediates resistance of pancreatic cancer cells to the BET bromodomain inhibitor JQ1. Sci Rep *5*, 9489.

Kwak, H., and Lis, J.T. (2013). Control of transcriptional elongation. Annu Rev Genet *47*, 483-508.

Lan, F., and Shi, Y. (2009). Epigenetic regulation: methylation of histone and non-histone proteins. Sci China C Life Sci *52*, 311-322.

Larsson, L.G., and Henriksson, M.A. (2010). The Yin and Yang functions of the Myc oncoprotein in cancer development and as targets for therapy. Exp Cell Res *316*, 1429-1437.

Lee, J.H., Choy, M.L., and Marks, P.A. (2012). Mechanisms of resistance to histone deacetylase inhibitors. Adv Cancer Res *116*, 39-86.

Lemke, J., von Karstedt, S., Abd El Hay, M., Conti, A., Arce, F., Montinaro, A., Papenfuss, K., El-Bahrawy, M.A., and Walczak, H. (2014a). Selective CDK9 inhibition overcomes TRAIL resistance by concomitant suppression of cFlip and Mcl-1. Cell Death Differ *21*, 491-502.

References

Lemke, J., von Karstedt, S., Zinngrebe, J., and Walczak, H. (2014b). Getting TRAIL back on track for cancer therapy. Cell Death Differ *21*, 1350-1364.

Lenhart, R., Kirov, S., Desilva, H., Cao, J., Lei, M., Johnston, K., Peterson, R., Schweizer, L., Purandare, A., Ross-Macdonald, P*., et al.* (2015). Sensitivity of Small Cell Lung Cancer to BET Inhibition Is Mediated by Regulation of ASCL1 Gene Expression. Mol Cancer Ther *14*, 2167-2174.

Lindsten, T., Ross, A.J., King, A., Zong, W.X., Rathmell, J.C., Shiels, H.A., Ulrich, E., Waymire, K.G., Mahar, P., Frauwirth, K*., et al.* (2000). The combined functions of proapoptotic Bcl-2 family members bak and bax are essential for normal development of multiple tissues. Mol Cell *6*, 1389-1399.

Liu, W., Ma, Q., Wong, K., Li, W., Ohgi, K., Zhang, J., Aggarwal, A.K., and Rosenfeld, M.G. (2013). Brd4 and JMJD6-associated anti-pause enhancers in regulation of transcriptional pause release. Cell *155*, 1581-1595.

Lockwood, W.W., Zejnullahu, K., Bradner, J.E., and Varmus, H. (2012). Sensitivity of human lung adenocarcinoma cell lines to targeted inhibition of BET epigenetic signaling proteins. Proc Natl Acad Sci U S A *109*, 19408-19413.

Loosveld, M., Castellano, R., Gon, S., Goubard, A., Crouzet, T., Pouyet, L., Prebet, T., Vey, N., Nadel, B., Collette, Y*., et al.* (2014). Therapeutic targeting of c-Myc in T-cell acute lymphoblastic leukemia, T-ALL. Oncotarget *5*, 3168-3172.

Loven, J., Hoke, H.A., Lin, C.Y., Lau, A., Orlando, D.A., Vakoc, C.R., Bradner, J.E., Lee, T.I., and Young, R.A. (2013). Selective inhibition of tumor oncogenes by disruption of super-enhancers. Cell *153*, 320-334.

Magnaghi-Jaulin, L., Groisman, R., Naguibneva, I., Robin, P., Lorain, S., Le Villain, J.P., Troalen, F., Trouche, D., and Harel-Bellan, A. (1998). Retinoblastoma protein represses transcription by recruiting a histone deacetylase. Nature *391*, 601-605.

Marmorstein, R. (2001). Structure and function of histone acetyltransferases. Cell Mol Life Sci *58*, 693-703.

Marraffini, L.A., and Sontheimer, E.J. (2008). CRISPR interference limits horizontal gene transfer in staphylococci by targeting DNA. Science *322*, 1843-1845.

Marraffini, L.A., and Sontheimer, E.J. (2010). CRISPR interference: RNA-directed adaptive immunity in bacteria and archaea. Nat Rev Genet *11*, 181-190.

Mertz, J.A., Conery, A.R., Bryant, B.M., Sandy, P., Balasubramanian, S., Mele, D.A., Bergeron, L., and Sims, R.J., 3rd (2011). Targeting MYC dependence in cancer by inhibiting BET bromodomains. Proc Natl Acad Sci U S A *108*, 16669-16674.

Mio, C., Lavarone, E., Conzatti, K., Baldan, F., Toffoletto, B., Puppin, C., Filetti, S., Durante, C., Russo, D., Orlacchio, A*., et al.* (2016). MCM5 as a target of BET inhibitors in thyroid cancer cells. Endocr Relat Cancer *23*, 335-347.

References

Moore, J.K., and Haber, J.E. (1996). Cell cycle and genetic requirements of two pathways of nonhomologous end-joining repair of double-strand breaks in Saccharomyces cerevisiae. Mol Cell Biol *16*, 2164-2173.

Mora, A., Sandve, G.K., Gabrielsen, O.S., and Eskeland, R. (2015). In the loop: promoter-enhancer interactions and bioinformatics. Brief Bioinform.

Muller, P.A., and Vousden, K.H. (2014). Mutant p53 in cancer: new functions and therapeutic opportunities. Cancer Cell *25*, 304-317.

Ng, S.S., Yue, W.W., Oppermann, U., and Klose, R.J. (2009). Dynamic protein methylation in chromatin biology. Cell Mol Life Sci *66*, 407-422.

Nowak, S.J., and Corces, V.G. (2004). Phosphorylation of histone H3: a balancing act between chromosome condensation and transcriptional activation. Trends Genet *20*, 214-220.

Obexer, P., and Ausserlechner, M.J. (2014). X-linked inhibitor of apoptosis protein - a critical death resistance regulator and therapeutic target for personalized cancer therapy. Front Oncol *4*, 197.

Oki, M., Aihara, H., and Ito, T. (2007). Role of histone phosphorylation in chromatin dynamics and its implications in diseases. Subcell Biochem *41*, 319-336.

Orlando, V. (2000). Mapping chromosomal proteins in vivo by formaldehyde-crosslinked-chromatin immunoprecipitation. Trends Biochem Sci *25*, 99-104.

Ott, C.J., Kopp, N., Bird, L., Paranal, R.M., Qi, J., Bowman, T., Rodig, S.J., Kung, A.L., Bradner, J.E., and Weinstock, D.M. (2012). BET bromodomain inhibition targets both c-Myc and IL7R in high-risk acute lymphoblastic leukemia. Blood *120*, 2843-2852.

Ott, G. (2014). Impact of MYC on malignant behavior. Hematology Am Soc Hematol Educ Program *2014*, 100-106.

Pao, W., and Girard, N. (2011). New driver mutations in non-small-cell lung cancer. Lancet Oncol *12*, 175-180.

Pardo, B., Gomez-Gonzalez, B., and Aguilera, A. (2009). DNA repair in mammalian cells: DNA double-strand break repair: how to fix a broken relationship. Cell Mol Life Sci *66*, 1039-1056.

Parseghian, M.H., and Hamkalo, B.A. (2001). A compendium of the histone H1 family of somatic subtypes: an elusive cast of characters and their characteristics. Biochem Cell Biol *79*, 289-304.

Parthun, M.R. (2007). Hat1: the emerging cellular roles of a type B histone acetyltransferase. Oncogene *26*, 5319-5328.

Peterlin, B.M., and Price, D.H. (2006). Controlling the elongation phase of transcription with P-TEFb. Mol Cell *23*, 297-305.

References

Pina, B., and Suau, P. (1987). Changes in histones H2A and H3 variant composition in differentiating and mature rat brain cortical neurons. Dev Biol *123*, 51-58.

Pollard, T.D., Earnshaw, W.C., and Lippincott-Schwartz, J. (2008). Cell biology, 2nd edn (Philadelphia, Saunders/Elsevier).

Prior, I.A., Lewis, P.D., and Mattos, C. (2012). A comprehensive survey of Ras mutations in cancer. Cancer Res *72*, 2457-2467.

Puissant, A., Frumm, S.M., Alexe, G., Bassil, C.F., Qi, J., Chanthery, Y.H., Nekritz, E.A., Zeid, R., Gustafson, W.C., Greninger, P.*, et al.* (2013). Targeting MYCN in neuroblastoma by BET bromodomain inhibition. Cancer Discov *3*, 308-323.

Pylayeva-Gupta, Y., Grabocka, E., and Bar-Sagi, D. (2011). RAS oncogenes: weaving a tumorigenic web. Nat Rev Cancer *11*, 761-774.

Ran, F.A., Hsu, P.D., Wright, J., Agarwala, V., Scott, D.A., and Zhang, F. (2013). Genome engineering using the CRISPR-Cas9 system. Nat Protoc *8*, 2281-2308.

Rathert, P., Roth, M., Neumann, T., Muerdter, F., Roe, J.S., Muhar, M., Deswal, S., Cerny-Reiterer, S., Peter, B., Jude, J.*, et al.* (2015). Transcriptional plasticity promotes primary and acquired resistance to BET inhibition. Nature *525*, 543-547.

Rawluszko-Wieczorek, A.A., Siera, A., and Jagodzinski, P.P. (2015). TET proteins in cancer: Current 'state of the art'. Crit Rev Oncol Hematol *96*, 425-436.

Rea, S., Eisenhaber, F., O'Carroll, D., Strahl, B.D., Sun, Z.W., Schmid, M., Opravil, S., Mechtler, K., Ponting, C.P., Allis, C.D.*, et al.* (2000). Regulation of chromatin structure by site-specific histone H3 methyltransferases. Nature *406*, 593-599.

Redon, C., Pilch, D., Rogakou, E., Sedelnikova, O., Newrock, K., and Bonner, W. (2002). Histone H2A variants H2AX and H2AZ. Curr Opin Genet Dev *12*, 162-169.

Riggs, A.D. (1975). X inactivation, differentiation, and DNA methylation. Cytogenet Cell Genet *14*, 9-25.

Riley, J.S., Hutchinson, R., McArt, D.G., Crawford, N., Holohan, C., Paul, I., Van Schaeybroeck, S., Salto-Tellez, M., Johnston, P.G., Fennell, D.A.*, et al.* (2013). Prognostic and therapeutic relevance of FLIP and procaspase-8 overexpression in non-small cell lung cancer. Cell Death Dis *4*, e951.

Robinson, C., Lowe, M., Schwartz, A., and Kikyo, N. (2016). Mechanisms and Developmental Roles of Promoter-proximal Pausing of RNA Polymerase II. J Stem Cell Res Ther *6*.

Roche, J., Gorka, C., Goeltz, P., and Lawrence, J.J. (1985). Association of histone H1(0) with a gene repressed during liver development. Nature *314*, 197-198.

References

Roe, J.S., Mercan, F., Rivera, K., Pappin, D.J., and Vakoc, C.R. (2015). BET Bromodomain Inhibition Suppresses the Function of Hematopoietic Transcription Factors in Acute Myeloid Leukemia. Mol Cell *58*, 1028-1039.

Roeder, R.G., and Rutter, W.J. (1969). Multiple forms of DNA-dependent RNA polymerase in eukaryotic organisms. Nature *224*, 234-237.

Roeder, R.G., and Rutter, W.J. (1970). Specific nucleolar and nucleoplasmic RNA polymerases. Proc Natl Acad Sci U S A *65*, 675-682.

Rogakou, E.P., Pilch, D.R., Orr, A.H., Ivanova, V.S., and Bonner, W.M. (1998). DNA double-stranded breaks induce histone H2AX phosphorylation on serine 139. J Biol Chem *273*, 5858-5868.

Sahai, V., Kumar, K., Knab, L.M., Chow, C.R., Raza, S.S., Bentrem, D.J., Ebine, K., and Munshi, H.G. (2014). BET bromodomain inhibitors block growth of pancreatic cancer cells in three-dimensional collagen. Mol Cancer Ther *13*, 1907-1917.

Sainsbury, S., Bernecky, C., and Cramer, P. (2015). Structural basis of transcription initiation by RNA polymerase II. Nat Rev Mol Cell Biol *16*, 129-143.

Sarosiek, K.A., Chi, X., Bachman, J.A., Sims, J.J., Montero, J., Patel, L., Flanagan, A., Andrews, D.W., Sorger, P., and Letai, A. (2013). BID preferentially activates BAK while BIM preferentially activates BAX, affecting chemotherapy response. Mol Cell *51*, 751-765.

Segura, M.F., Fontanals-Cirera, B., Gaziel-Sovran, A., Guijarro, M.V., Hanniford, D., Zhang, G., Gonzalez-Gomez, P., Morante, M., Jubierre, L., Zhang, W.*, et al.* (2013). BRD4 sustains melanoma proliferation and represents a new target for epigenetic therapy. Cancer Res *73*, 6264-6276.

Selamat, S.A., Chung, B.S., Girard, L., Zhang, W., Zhang, Y., Campan, M., Siegmund, K.D., Koss, M.N., Hagen, J.A., Lam, W.L.*, et al.* (2012). Genome-scale analysis of DNA methylation in lung adenocarcinoma and integration with mRNA expression. Genome Res *22*, 1197-1211.

Sengupta, D., Kannan, A., Kern, M., Moreno, M.A., Vural, E., Stack, B., Jr., Suen, J.Y., Tackett, A.J., and Gao, L. (2015a). Disruption of BRD4 at H3K27Ac-enriched enhancer region correlates with decreased c-Myc expression in Merkel cell carcinoma. Epigenetics *10*, 460-466.

Sengupta, S., Biarnes, M.C., Clarke, R., and Jordan, V.C. (2015b). Inhibition of BET proteins impairs estrogen-mediated growth and transcription in breast cancers by pausing RNA polymerase advancement. Breast Cancer Res Treat *150*, 265-278.

Shalem, O., Sanjana, N.E., Hartenian, E., Shi, X., Scott, D.A., Mikkelsen, T.S., Heckl, D., Ebert, B.L., Root, D.E., Doench, J.G.*, et al.* (2014). Genome-scale CRISPR-Cas9 knockout screening in human cells. Science *343*, 84-87.

References

Shang, E., Wang, X., Wen, D., Greenberg, D.A., and Wolgemuth, D.J. (2009). Double bromodomain-containing gene Brd2 is essential for embryonic development in mouse. Dev Dyn *238*, 908-917.

Shao, Q., Kannan, A., Lin, Z., Stack, B.C., Jr., Suen, J.Y., and Gao, L. (2014). BET protein inhibitor JQ1 attenuates Myc-amplified MCC tumor growth in vivo. Cancer Res *74*, 7090-7102.

Shen, C., Ipsaro, J.J., Shi, J., Milazzo, J.P., Wang, E., Roe, J.S., Suzuki, Y., Pappin, D.J., Joshua-Tor, L., and Vakoc, C.R. (2015). NSD3-Short Is an Adaptor Protein that Couples BRD4 to the CHD8 Chromatin Remodeler. Mol Cell *60*, 847-859.

Shi, J., Wang, E., Milazzo, J.P., Wang, Z., Kinney, J.B., and Vakoc, C.R. (2015). Discovery of cancer drug targets by CRISPR-Cas9 screening of protein domains. Nat Biotechnol *33*, 661-667.

Shi, J., Whyte, W.A., Zepeda-Mendoza, C.J., Milazzo, J.P., Shen, C., Roe, J.S., Minder, J.L., Mercan, F., Wang, E., Eckersley-Maslin, M.A.*, et al.* (2013). Role of SWI/SNF in acute leukemia maintenance and enhancer-mediated Myc regulation. Genes Dev *27*, 2648-2662.

Shi, Y., Lan, F., Matson, C., Mulligan, P., Whetstine, J.R., Cole, P.A., and Casero, R.A. (2004). Histone demethylation mediated by the nuclear amine oxidase homolog LSD1. Cell *119*, 941-953.

Shilatifard, A. (2006). Chromatin modifications by methylation and ubiquitination: implications in the regulation of gene expression. Annu Rev Biochem *75*, 243-269.

Shimamura, T., Chen, Z., Soucheray, M., Carretero, J., Kikuchi, E., Tchaicha, J.H., Gao, Y., Cheng, K.A., Cohoon, T.J., Qi, J.*, et al.* (2013). Efficacy of BET bromodomain inhibition in Kras-mutant non-small cell lung cancer. Clin Cancer Res *19*, 6183-6192.

Shirley, S., and Micheau, O. (2013). Targeting c-FLIP in cancer. Cancer Lett *332*, 141-150.

Skoulidis, F., Byers, L.A., Diao, L., Papadimitrakopoulou, V.A., Tong, P., Izzo, J., Behrens, C., Kadara, H., Parra, E.R., Canales, J.R.*, et al.* (2015). Co-occurring genomic alterations define major subsets of KRAS-mutant lung adenocarcinoma with distinct biology, immune profiles, and therapeutic vulnerabilities. Cancer Discov *5*, 860-877.

Smith, E., Lin, C., and Shilatifard, A. (2011). The super elongation complex (SEC) and MLL in development and disease. Genes Dev *25*, 661-672.

Solomon, M.J., Larsen, P.L., and Varshavsky, A. (1988). Mapping protein-DNA interactions in vivo with formaldehyde: evidence that histone H4 is retained on a highly transcribed gene. Cell *53*, 937-947.

Soucek, L., Whitfield, J.R., Sodir, N.M., Masso-Valles, D., Serrano, E., Karnezis, A.N., Swigart, L.B., and Evan, G.I. (2013). Inhibition of Myc family proteins eradicates KRas-driven lung cancer in mice. Genes Dev *27*, 504-513.

References

Stathis, A., Zucca, E., Bekradda, M., Gomez-Roca, C., Delord, J.P., de La Motte Rouge, T., Uro-Coste, E., de Braud, F., Pelosi, G., and French, C.A. (2016). Clinical Response of Carcinomas Harboring the BRD4-NUT Oncoprotein to the Targeted Bromodomain Inhibitor OTX015/MK-8628. Cancer Discov *6*, 492-500.

Sterner, D.E., and Berger, S.L. (2000). Acetylation of histones and transcription-related factors. Microbiol Mol Biol Rev *64*, 435-459.

Strahl, B.D., and Allis, C.D. (2000). The language of covalent histone modifications. Nature *403*, 41-45.

Stucki, M., Clapperton, J.A., Mohammad, D., Yaffe, M.B., Smerdon, S.J., and Jackson, S.P. (2005). MDC1 directly binds phosphorylated histone H2AX to regulate cellular responses to DNA double-strand breaks. Cell *123*, 1213-1226.

Sun, B., Shah, B., Fiskus, W., Qi, J., Rajapakshe, K., Coarfa, C., Li, L., Devaraj, S.G., Sharma, S., Zhang, L.*, et al.* (2015). Synergistic activity of BET protein antagonist-based combinations in mantle cell lymphoma cells sensitive or resistant to ibrutinib. Blood *126*, 1565-1574.

Tang, Y., Gholamin, S., Schubert, S., Willardson, M.I., Lee, A., Bandopadhayay, P., Bergthold, G., Masoud, S., Nguyen, B., Vue, N.*, et al.* (2014). Epigenetic targeting of Hedgehog pathway transcriptional output through BET bromodomain inhibition. Nat Med *20*, 732-740.

Tessarz, P., and Kouzarides, T. (2014). Histone core modifications regulating nucleosome structure and dynamics. Nat Rev Mol Cell Biol *15*, 703-708.

Tjeertes, J.V., Miller, K.M., and Jackson, S.P. (2009). Screen for DNA-damage-responsive histone modifications identifies H3K9Ac and H3K56Ac in human cells. EMBO J *28*, 1878-1889.

Tolani, B., Gopalakrishnan, R., Punj, V., Matta, H., and Chaudhary, P.M. (2014). Targeting Myc in KSHV-associated primary effusion lymphoma with BET bromodomain inhibitors. Oncogene *33*, 2928-2937.

Trabucco, S.E., Gerstein, R.M., Evens, A.M., Bradner, J.E., Shultz, L.D., Greiner, D.L., and Zhang, H. (2015). Inhibition of bromodomain proteins for the treatment of human diffuse large B-cell lymphoma. Clin Cancer Res *21*, 113-122.

Tsukada, Y., Fang, J., Erdjument-Bromage, H., Warren, M.E., Borchers, C.H., Tempst, P., and Zhang, Y. (2006). Histone demethylation by a family of JmjC domain-containing proteins. Nature *439*, 811-816.

Valdespino, V., and Valdespino, P.M. (2015). Potential of epigenetic therapies in the management of solid tumors. Cancer Manag Res *7*, 241-251.

van Leeuwen, F., Gafken, P.R., and Gottschling, D.E. (2002). Dot1p modulates silencing in yeast by methylation of the nucleosome core. Cell *109*, 745-756.

References

van Nimwegen, E. (2003). Scaling laws in the functional content of genomes. Trends Genet *19*, 479-484.

VanderMeer, R., Chambers, S., Van Dam, A., Cutz, J.C., Goffin, J.R., and Ellis, P.M. (2015). Diagnosing lung cancer in the 21st century: are we ready to meet the challenge of individualized care? Curr Oncol *22*, 272-278.

Vannini, A., and Cramer, P. (2012). Conservation between the RNA polymerase I, II, and III transcription initiation machineries. Mol Cell *45*, 439-446.

Venkataraman, S., Alimova, I., Balakrishnan, I., Harris, P., Birks, D.K., Griesinger, A., Amani, V., Cristiano, B., Remke, M., Taylor, M.D*., et al.* (2014). Inhibition of BRD4 attenuates tumor cell self-renewal and suppresses stem cell signaling in MYC driven medulloblastoma. Oncotarget *5*, 2355-2371.

Vermeulen, M., Eberl, H.C., Matarese, F., Marks, H., Denissov, S., Butter, F., Lee, K.K., Olsen, J.V., Hyman, A.A., Stunnenberg, H.G*., et al.* (2010). Quantitative interaction proteomics and genome-wide profiling of epigenetic histone marks and their readers. Cell *142*, 967-980.

Wang, H., Yang, H., Shivalila, C.S., Dawlaty, M.M., Cheng, A.W., Zhang, F., and Jaenisch, R. (2013). One-step generation of mice carrying mutations in multiple genes by CRISPR/Cas-mediated genome engineering. Cell *153*, 910-918.

Wang, R., Li, Q., Helfer, C.M., Jiao, J., and You, J. (2012). Bromodomain protein Brd4 associated with acetylated chromatin is important for maintenance of higher-order chromatin structure. J Biol Chem *287*, 10738-10752.

Wang, T., Wei, J.J., Sabatini, D.M., and Lander, E.S. (2014). Genetic screens in human cells using the CRISPR-Cas9 system. Science *343*, 80-84.

Wang, Y., Wysocka, J., Sayegh, J., Lee, Y.H., Perlin, J.R., Leonelli, L., Sonbuchner, L.S., McDonald, C.H., Cook, R.G., Dou, Y*., et al.* (2004). Human PAD4 regulates histone arginine methylation levels via demethylimination. Science *306*, 279-283.

Watson, J.D., and Crick, F.H. (1953). Molecular structure of nucleic acids; a structure for deoxyribose nucleic acid. Nature *171*, 737-738.

Weinberg, R.A. (2014). The biology of cancer, Second edition. edn (New York, Garland Science, Taylor & Francis Group).

Whetstine, J.R., Nottke, A., Lan, F., Huarte, M., Smolikov, S., Chen, Z., Spooner, E., Li, E., Zhang, G., Colaiacovo, M*., et al.* (2006). Reversal of histone lysine trimethylation by the JMJD2 family of histone demethylases. Cell *125*, 467-481.

Whyte, W.A., Orlando, D.A., Hnisz, D., Abraham, B.J., Lin, C.Y., Kagey, M.H., Rahl, P.B., Lee, T.I., and Young, R.A. (2013). Master transcription factors and mediator establish super-enhancers at key cell identity genes. Cell *153*, 307-319.

References

Winston, F. (2001). Control of eukaryotic transcription elongation. Genome Biol *2*, REVIEWS1006.

Wolf, S.S. (2009). The protein arginine methyltransferase family: an update about function, new perspectives and the physiological role in humans. Cell Mol Life Sci *66*, 2109-2121.

Wu, C.H., van Riggelen, J., Yetil, A., Fan, A.C., Bachireddy, P., and Felsher, D.W. (2007). Cellular senescence is an important mechanism of tumor regression upon c-Myc inactivation. Proc Natl Acad Sci U S A *104*, 13028-13033.

Wu, S.Y., and Chiang, C.M. (2007). The double bromodomain-containing chromatin adaptor Brd4 and transcriptional regulation. J Biol Chem *282*, 13141-13145.

Wyce, A., Degenhardt, Y., Bai, Y., Le, B., Korenchuk, S., Crouthame, M.C., McHugh, C.F., Vessella, R., Creasy, C.L., Tummino, P.J.*, et al.* (2013). Inhibition of BET bromodomain proteins as a therapeutic approach in prostate cancer. Oncotarget *4*, 2419-2429.

Xiong, J.S., Ding, J., and Li, Y. (2015). Genome-editing technologies and their potential application in horticultural crop breeding. Hortic Res *2*, 15019.

Xu, Z., Sharp, P.P., Yao, Y., Segal, D., Ang, C.H., Khaw, S.L., Aubrey, B.J., Gong, J., Kelly, G.L., Herold, M.J.*, et al.* (2016). BET inhibition represses miR17-92 to drive BIM-initiated apoptosis of normal and transformed hematopoietic cells. Leukemia *30*, 1531-1541.

Yang, X.J., and Seto, E. (2007). HATs and HDACs: from structure, function and regulation to novel strategies for therapy and prevention. Oncogene *26*, 5310-5318.

Yao, W., Yue, P., Khuri, F.R., and Sun, S.Y. (2015). The BET bromodomain inhibitor, JQ1, facilitates c-FLIP degradation and enhances TRAIL-induced apoptosis independent of BRD4 and c-Myc inhibition. Oncotarget *6*, 34669-34679.

Zeng, L., Zhang, Q., Li, S., Plotnikov, A.N., Walsh, M.J., and Zhou, M.M. (2010). Mechanism and regulation of acetylated histone binding by the tandem PHD finger of DPF3b. Nature *466*, 258-262.

Zhang, X., Yang, Z., Khan, S.I., Horton, J.R., Tamaru, H., Selker, E.U., and Cheng, X. (2003). Structural basis for the product specificity of histone lysine methyltransferases. Mol Cell *12*, 177-185.

Zhang, Y., and Reinberg, D. (2001). Transcription regulation by histone methylation: interplay between different covalent modifications of the core histone tails. Genes Dev *15*, 2343-2360.

Zhao, R., Nakamura, T., Fu, Y., Lazar, Z., and Spector, D.L. (2011). Gene bookmarking accelerates the kinetics of post-mitotic transcriptional re-activation. Nat Cell Biol *13*, 1295-1304.

Zhuang, D., Mannava, S., Grachtchouk, V., Tang, W.H., Patil, S., Wawrzyniak, J.A., Berman, A.E., Giordano, T.J., Prochownik, E.V., Soengas, M.S.*, et al.* (2008). C-MYC overexpression is required for continuous suppression of oncogene-induced senescence in melanoma cells. Oncogene *27*, 6623-6634.

References

Zuber, J., Shi, J., Wang, E., Rappaport, A.R., Herrmann, H., Sison, E.A., Magoon, D., Qi, J., Blatt, K., Wunderlich, M.*, et al.* (2011). RNAi screen identifies Brd4 as a therapeutic target in acute myeloid leukaemia. Nature *478*, 524-528.

Publications

Publications

O. Klingbeil, R. Lesche, K. A. Gelato, B. Haendler, P. Lejeune. Inhibition of BET bromodomain-dependent *XIAP* and *FLIP* expression sensitizes *KRAS*-mutated NSCLC to pro-apoptotic agents. Accepted for publication in *Nature Cell Death and Disease*.

K.A. Gelato*, L. Schöckel*, **O. Klingbeil***, T. Rückert, E. Kalfon, M. Héroult, P. Lejeune, Dr. U. Mönning, A. Fernández-Montalván, S. Bäurle, S. Siegel, B. Haendler. Super-enhancers define a proliferative PGC-1α-expressing melanoma subgroup sensitive to BET inhibition. In review. * shared co-first author.

Conference Presentations

O. Klingbeil, B. Haendler, P. Lejeune. BET inhibition efficiently blocks growth of lung cancer in vitro and in vivo. Abstracts of the European Association of Cancer Research Conference on Basic Epigenetic Mechanisms in Cancer 2015. Abstract 17.

O.Klingbeil, B. Haendler, A. Stresemann, C. Merz, A. Walter, A. E. Fernández-Montalván, M. Ocker, S. Siegel, P. Lejeune. *In vivo* efficacy of BET inhibitor BAY 1238097 in preclinical models of melanoma and lung cancer. Abstracts of the American Association of Cancer Research Annual Meeting 2016. Abstract # 988.

K. A. Gelato, L. Schöckel, **O. Klingbeil**, E. Kalfon, M. Héroult, P.Lejeune, B. Haendler. OXPHOS and Epigenetics: Paths to BET inhibitor Sensitivity in Melanoma. Keystone Symposia Q7 New Frontiers in Understanding Tumor Metabolism 2016. Abstract #1046.

Curriculum vitae

Der Lebenslauf ist in der Online-Version aus Gründen des Datenschutzes nicht enthalten.

Abbreviations

Name	Abbreviation
Chromosome conformation capture	3C
Acetyl coenzyme A	acetyl-CoA
Adaptive Focused Acoustics	AFA
V-akt murine thymoma viral oncogene homolog 1	AKT1
Apoptotic protease activating factor 1	Apaf-1
Adenosine triphosphate	ATP
BCL-2-antagonist/killer	BAK
BCL-2-assoociated X protein	BAX
Bromodomain 1	BD1
Bromodomain 2	BD2
Bromodomain and extra terminal domain	BET
BCL-2 homology domains	BH
V-Raf murine sarcoma viral oncogene homolog B	BRAF
Carboxy-terminal domain of a breast cancer susceptibility protein	BRCT
Bromodomain-containing protein 2	BRD2
Bromodomain-containing protein 3	BRD3
Bromodomain-containing protein 4	BRD4
Bromodomain-containing protein in testis	BRDT
Bovine serum albumin	BSA
Cancer Cell Line Encyclopedia	CCLE
Cyclin-dependent kinas 9	CDK9
Cleavage factor	CF
Chromatin immunoprecipitation	ChIP
Chromatin immunoprecipitation sequencing	ChIP-seq
Catalogue of Somatic Mutations in Cancer	COSMIC
Cleavage of polyadenylation factor	CPF
Cleavage of polyadenylation factor and cleavage factor	CPF-CF
Cleavage/polyadenylation specificity factor	CPSF
Clustered regularly interspersed short palindromic repeats	CRISPR
CRISPR RNA	cr-RNA
Carboxy-terminal domain	CTD
Database for Annotation Visualization and Integrated Discovery	DAVID
Death domain	DD
DNA damage response	DDR
Death effector domain	DED
DNase I hypersensitivty sites	DHSs
Demethylases	DMTs
Deoxyribonucleic acid	DNA
De novo methyltransferase	DNMT
DNA methyltransferases	DNMTs

Abbreviations

Name	Abbreviation
Dulbecco's Phosphate-Buffered Saline	DPBS
Double strand brake	DSB
DRB-sensitivity-induced factor	DSIF
Dithiothreitol	DTT
Escherichia coli	E. coli
Ethylenediaminetetraacetic acid	EDTA
Epidermal growth factor receptor	EGFR
Eleven-nineteen lysine-rich leukemia	ELL
Enhancer of zeste homolog 2	EZH2
Flavin adenine dinucleotide	FAD
Fas-associated death domain protein	FADD
Fetal calf serum	FCS
Food and drug administration	FDA
FLICE like inhibitor protein	FLIP
Earth gravity	g
Guanosine diphosphate	GDP
Genetically engineered mouse model	GEMM
Guanosine triphosphate	GTP
Histone acetyltransferaces	HATs
Histone deacetylases	HDACs
Homology directed repair	HDR
Human epidermal growth factor receptor 2	HER2
Histone lysine demethylase	HKDM
Histone lysine methyltransferase	HKMT
Histone methyltransferase	HMT
Horseradish peroxidase	HRP
Inhibitor of apoptosis family	IAP
Immunocytochemistry	ICC
Immunofluorescence	IF
Jumonji, AT rich interactive domain 2	JARID2
Jumonji C-domain-containing protein 6	JMJD6
Lysine	K
Kilo base pairs	kb
Kinesin family member 5B - rearranged during transfection (receptor tyrosine kinase)	KIF5B-RET
V-Ki-RAS Kirsten rat sarcoma viral oncogene	KRAS
Mitogen-activated protein kinase 1	MAP2K1
Malignant brain tumour domains	MBTs
Microhomology-mediated end joining	MMEJ
Messenger-RNA	mRNA
Nicotinamide adenine dinucleotide	NAD+
Negative elongation factor	NELF
Next generation sequencing	NGS
Next generation sequencing	NGS
Non-homologous end joining	NHEJ
NUT middle line carcinoma	NMC

Abbreviations

Name	Abbreviation
Nrd1-Nab3-Sen1	NNS
Nucleotide	nt
Amino terminal ends of about 30 amino acids	N-terminal tails
Polyadenylate polymerase	PAB
Protospacer adjacent motif	PAM
Phosphate-Buffered Saline	PBS
PBS or TBS with 0.1% tween 20	PBS-T/TBS-T
Plant homeodomain	PHD
Phosphatidylinositol-4,5-bisphosphate 3-kinase catalytic subunit alpha	PI3KCA
PCR	polmerase chain reaction
Peptidylprolyl isomerase A	PPIA
Precursor crRNA	pre-crRNA
Pre mature messenger-RNA	pre-mRNA
Protein arginine methyltransferases	PRMT
Post-translational modification	PTM
Pro-Trp-Trp-Pro domain	PWWP
quantitative real time-PCR	qRT-PCR
Arginine	R
Radioimmunoprecipitation assay	RIPA
Ribonucleic acid	RNA
Pol II	RNA polymerase II
V-ros avian UR2 sarcoma virus oncogene homolog 1	ROS1
Rounds per minute	rpm
Robust Spline normalization	RSN
Room temperature	RT
Serine	S
Synthesis Phase	S phase
S-adenosylmethionine	SAM
Standard deviation	SD
Sodium dodecyl sulfate	SDS
Super elongation complex	SEC
Standard error of the mean	SEM
Stable Isotype Labeling by Amino acids in Cell culture	SILAC
Mitochondria-derived activator of caspases	SMAC
Threonine	T
Culture flask with 75 cm² surface	T75
Transcription activator-like effector-based nucleases	TALENs
TATA box-binding protein	TBP
Tris-buffered saline	TBS
Positive transcription elongation factor-b	TEFb
Ten-eleven translocation	TET
Transcription factors	TFs
Trans-activating crRNA	tracrRNA
Transcription start site	TSS
X-linked inhibitor of apoptosis protein	XIAP

Abbreviations

Name	Abbreviation
Tyrosine	Y
Zinc finger nucleases	ZFNs

Tyrosine	Y
Zinc finger nucleases	ZFNs

Appendix

Table 16: Gene Ontology terms of significantly differentially regulated genes upon 4 h IC$_{50}$ JQ1 treatment

IC50 JQ1 treated DV90 cells

Annotation Cluster 1 Enrichment Score: 1.17 n = 23

Term	Count	%	PValue	Fold Enrichment
GO:0045449~regulation of transcription	9	32	0.036	2.124
GO:0019219~regulation of nucleobase, nucleoside, nucleotide and nucleic acid metabolic process	9	32	0.055	1.963
GO:0010556~regulation of macromolecule biosynthetic process	9	32	0.057	1.952
GO:0051171~regulation of nitrogen compound metabolic process	9	32	0.058	1.946
GO:0010468~regulation of gene expression	9	32	0.059	1.934
GO:0031326~regulation of cellular biosynthetic process	9	32	0.070	1.874
GO:0009889~regulation of biosynthetic process	9	32	0.072	1.862
GO:0060255~regulation of macromolecule metabolic process	9	32	0.113	1.695
GO:0080090~regulation of primary metabolic process	9	32	0.118	1.678

Annotation Cluster 2 Enrichment Score: 1.05 n = 23

Term	Count	%	PValue	Fold Enrichment
GO:0006350~transcription	9	32	0.011	2.629
GO:0034645~cellular macromolecule biosynthetic process	9	32	0.055	1.964
GO:0009059~macromolecule biosynthetic process	9	32	0.057	1.950
GO:0010467~gene expression	9	32	0.076	1.842
GO:0006139~nucleobase, nucleoside, nucleotide and nucleic acid metabolic process	9	32	0.139	1.620
GO:0044249~cellular biosynthetic process	9	32	0.145	1.605
GO:0009058~biosynthetic process	9	32	0.164	1.559
GO:0034641~cellular nitrogen compound metabolic process	9	32	0.190	1.505
GO:0006807~nitrogen compound metabolic process	9	32	0.214	1.462

Annotation Cluster 3 Enrichment Score: 0.95 n = 23

Term	Count	%	PValue	Fold Enrichment
GO:0051173~positive regulation of nitrogen compound metabolic process	4	14	0.076	3.812
GO:0031328~positive regulation of cellular biosynthetic process	4	14	0.088	3.584
GO:0009891~positive regulation of biosynthetic process	4	14	0.091	3.532
GO:0031325~positive regulation of cellular metabolic process	4	14	0.155	2.790
GO:0009893~positive regulation of metabolic process	4	14	0.170	2.666

Appendix

Table 17: Gene Ontology terms of significantly differentially regulated genes upon 4 h IC_{90} JQ1 treatment

IC90 JQ1 treated DV90 cells

Annotation Cluster 1	Enrichment Score: 4.40			n = 234
Term	Count	%	PValue	Fold Enrichment
GO:0010556~regulation of macromolecule biosynthetic process	75	24	0.000	1.599
GO:0031326~regulation of cellular biosynthetic process	75	24	0.000	1.535
GO:0009889~regulation of biosynthetic process	75	24	0.000	1.525

Annotation Cluster 2	Enrichment Score: 2.39			n = 234
Term	Count	%	PValue	Fold Enrichment
GO:0042981~regulation of apoptosis	25	8	0.004	1.876
GO:0043067~regulation of programmed cell death	25	8	0.004	1.857
GO:0010941~regulation of cell death	25	8	0.004	1.850

Annotation Cluster 3	Enrichment Score: 1.55			n = 234
Term	Count	%	PValue	Fold Enrichment
GO:0043065~positive regulation of apoptosis	14	4	0.027	1.964
GO:0043068~positive regulation of programmed cell death	14	4	0.028	1.950
GO:0010942~positive regulation of cell death	14	4	0.029	1.941

Table 18: List of significantly (q < 0.05) differentially expressed genes (cut off $\pm$ 0.5 $\log_2$ fold change) after treatment of DV90 cells with IC_{50} JQ1 for 24h

gene symbol	$\log_2$ fold change
ACTBL2	-2.999
AGR3	-2.452
SPINK6	-2.209
FER1L6	-2.194
FGFBP1	-1.921
GPR110	-1.493
MUC2	-1.464
MLKL	-1.380
PSCA	-1.332
CEACAM6	-1.328
MIR4738 : H3F3A : H3F3B : UNK	-1.298
RASA4 : RASA4CP : LOC102725198 : RASA4B : RP11-514P8.6 : RP11-514P8.8	-1.244
INHBA	-1.237
EDAR	-1.208
C1orf143	-1.198
PDE8B	-1.192
EREG	-1.141
TRIB3	-1.110

Appendix

gene symbol	log$_2$ fold change
NR1D1	-1.084
MGLL	-1.083
CCL26	-1.080
DUSP27	-0.993
KRT17P1	-0.989
MYC	-0.986
SLC35G6	-0.966
LIPC	-0.961
PHLDA3	-0.934
SULT1C2	-0.870
PDE9A	-0.860
MPST	-0.851
ANO1	-0.840
GLYCTK	-0.825
RP11-121A14.3 : NEK6	-0.824
AEN	-0.823
SDCBP2 : FKBP1A-SDCBP2	-0.803
SCARB1	-0.790
FAM182B : FAM27C : FAM27B	-0.754
GDF15	-0.738
FSTL4	-0.734
LOC389602 : AC021218.2	-0.731
EPB41L1	-0.723
RGS14	-0.717
ANAPC1 : LOC730268 : AC083899.3	-0.706
POMZP3	-0.678
PPFIA3	-0.669
JPH4	-0.668
PKP1	-0.667
CAPN8	-0.666
AIM1L	-0.666
SNORA4 : EIF4A2 : SNORA63 : SNORD2 : SNORA81 : MIR1248	-0.666
ADRA2C	-0.650
NDUFC2-KCTD14 : KCTD14 : NDUFC2	-0.649
SLC25A45	-0.631
ABLIM1	-0.630
RARA : BCOR	-0.628
PLEKHG6	-0.622
SPINK4	-0.618
TRIP13	-0.614
CES2	-0.613
RP11-9B6.1	-0.608
FAM136A : LOC100287852	-0.604

Appendix

gene symbol	log$_2$ fold change
SERPINB5	-0.600
TCTEX1D4 : RP11-269F19.9	-0.599
RAPGEFL1	-0.596
ANKMY1	-0.584
TUBD1	-0.574
PVRL4	-0.569
LOC101928102 : RP11-160N1.10	-0.568
GCNT3	-0.563
CPN2	-0.563
TBX15	-0.562
DCTD	-0.560
NETO1	-0.556
MIS18BP1	-0.553
RP11-293M10.1	-0.533
CD68 : SNORA67 : LOC101928634 : RP11-186B7.4	-0.528
CAPN2	-0.527
SH3RF2	-0.521
DOT1L	-0.520
SLC35G5 : SLC35G4P : SLC35G6	-0.519
ZBTB7C	-0.517
QRSL1	-0.517
FLNB	-0.514
PTK6	-0.512
LBR	-0.510
RASA4 : RASA4B : RASA4CP : LOC102725198 : RASA4DP : RP11-514P8.6 : RP11-514P8.8	-0.507
ANKRD33	-0.503
CDH17	-0.501
HNF1B	0.501
CD2AP	0.502
CD28	0.503
PERP	0.503
ITGA3	0.506
H3F3A : H3F3AP4 : H3F3B : H3F3AP6 : RP11-349N19.2	0.506
REEP3	0.506
IRS2	0.508
DUSP18	0.512
DAPK1	0.514
TFAP2A	0.514
FBXO8	0.516
FOXP4	0.516
KRT19	0.518
MIDN	0.520
GATA4	0.521

Appendix

gene symbol	log$_2$ fold change
MKLN1	0.524
GNAI2	0.530
ITPKC	0.533
UBE2H	0.535
EHF	0.536
SELL	0.539
CROCCP2 : CROCC : CROCCP3	0.542
C6orf203	0.544
H3F3B : H3F3A : MIR4738	0.547
GPRC5C	0.553
ITFG3	0.554
AHR	0.557
RHOV	0.558
FOSB	0.569
RHPN2	0.569
IER2	0.571
HIST4H4 : HIST1H4I : HIST1H4A : HIST1H4D : HIST1H4F : HIST1H4K : HIST1H4J : HIST1H4C : HIST1H4H : HIST1H4B : HIST1H4E : HIST1H4L : HIST2H4A : HIST2H4B	0.572
RASA4B : RASA4	0.574
ABHD11	0.575
COQ2	0.581
CREB3L1	0.583
ERBB3	0.585
SSH3	0.587
LRP11	0.587
S100P	0.592
CXCL2	0.597
CAPN5	0.602
ATP2B4	0.606
EIF4A2 : SNORA63 : SNORD2 : SNORA4 : SNORA81 : MIR1248	0.606
MAPRE3	0.608
POU5F1B	0.609
RHOB	0.610
C6orf132	0.610
ARPC5	0.612
KLF14	0.620
LOC100130691 : AC074286.1 : NFE2L2	0.624
VDR	0.627
ZKSCAN1	0.641
TNRC18 : TNRC18P3	0.645
MIR4640 : DDR1	0.648
PPP1R1B	0.652

Appendix

gene symbol	log$_2$ fold change
FXYD3	0.656
RFX2	0.661
WWC1	0.662
ARHGEF37	0.669
HOXA13	0.671
UNC5B	0.679
RASA4 : RASA4B : RP11-514P8.6 : RP11-514P8.8	0.681
TNRC18	0.683
LGALS3	0.689
MACROD2	0.691
SH2D3A	0.702
NR4A2	0.703
TMEM45B	0.731
HIST1H2BJ	0.733
HOXB3	0.733
TMSB4X	0.743
LINC00998 : AC073346.2	0.743
LOC101930595 : RP11-326C3.2 : ATHL1	0.749
ZFP36	0.755
JUND	0.758
ID1	0.772
DAOA	0.773
PIK3C2B	0.775
SIRT4	0.791
CTH	0.794
DRD1	0.802
MIR21 : VMP1	0.816
OGDH	0.824
FOXA1	0.832
PHLDA1	0.837
DUSP6	0.840
LY86	0.843
ITGB4	0.844
CTNND1 : TMX2 : TMX2-CTNND1	0.847
TRIB1	0.847
TJP3	0.863
JUN	0.868
OR4N4 : LOC101927079 : LOC727924 : RP11-69H14.6 : LOC102723532	0.870
IL1RAPL1	0.880
MALL	0.882
MYH14	0.904
PPP1R15A	0.914
UPK2	0.930

Appendix

gene symbol	log$_2$ fold change
ATF3	0.935
CIRBP	0.948
HIST1H4B : HIST1H4I : HIST1H4A : HIST1H4D : HIST1H4F : HIST1H4K : HIST1H4J : HIST1H4C : HIST1H4H : HIST1H4E : HIST1H4L : HIST2H4A : HIST4H4 : HIST2H4B	0.973
CSRNP1	1.017
IRF1	1.017
SOX9	1.034
MAP3K8	1.035
MLPH	1.069
HIST1H2BG : HIST1H2BF : HIST1H2BE : HIST1H2BI : HIST1H2BC	1.080
NR4A1	1.087
NUAK2	1.115
HIST1H2BF	1.123
HIST2H4B : HIST2H4A : HIST1H4I : HIST1H4A : HIST1H4D : HIST1H4F : HIST1H4K : HIST1H4J : HIST1H4C : HIST1H4H : HIST1H4B : HIST1H4E : HIST1H4L : HIST4H4	1.148
PCDH11Y : PCDH11X	1.170
OR4N3P : OR4N2 : LOC102723532 : RP11-2F9.2 : OR4N4 : LOC101927079 : RP11-69H14.6 : LOC727924	1.193
ELF3	1.198
SPIRE2	1.218
HHLA3	1.271
GPX2	1.357
MMP24-AS1 : EDEM2 : RP4-614O4.11	1.382
HEXIM1	1.385
ABCC3	1.530
DHRS2	1.712
PDK4	1.730
ARHGDIG	1.862
CXCL8 : IL8	1.898
RCAN1	2.041
HIST1H2BG : HIST1H2BJ	2.166
HIST1H2BD	2.627